DEVELOPMENT OF A RAPID PROTOTYPE BASED ANKLE FOOT ORTHOSIS FOR NON-SURGICAL CORRECTION OF CLUBFOOT DEFORMITY IN NEWBORN BABIES

A Thesis Submitted
in Partial Fulfilment of the Requirements
for the Degree of
Doctor of Philosophy

by

Manak Lal Jain

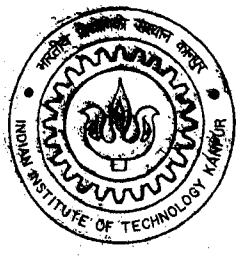

to the

DEPARTMENT OF MECHANICAL ENGINEERING
INDIAN INSTITUTE OF TECHNOLOGY KANPUR

June, 2004

Dedicated to all the children of the world

born with clubfeet

and to the Parents who care for them

CERTIFICATE

It is certified that the work contained in the thesis, "**Development of a Rapid Prototype based Ankle Foot Orthosis for non-surgical correction of clubfoot deformity in newborn babies**" by Manak Lal Jain, has been carried out under our supervision and that this work has not been submitted elsewhere for a degree.

N. S. Vyas
Professor
Departement of ME
Indian Institute of Technology Kanpur
Kanpur. 208016, India

Sanjay G. Dhande
Professor
Department of ME & CSE
Indian Institute of Technology Kanpur
Kanpur. 208016 India

June, 2004

SYNOPSIS

Development of a Rapid Prototype based Ankle Foot Orthosis for non-surgical correction of clubfoot deformity in newborn babies

A Thesis Submitted in Partial Fulfillment of the Requirements for the Degree of

Doctor of Philosophy

by

Manak Lal Jain

Roll no. Y010567

Thesis Supervisors: Dr. Sanjay G. Dhande and Dr. N. S. Vyas

to the

Department of Mechanical Engineering

Indian Institute of Technology Kanpur, India

June, 2004

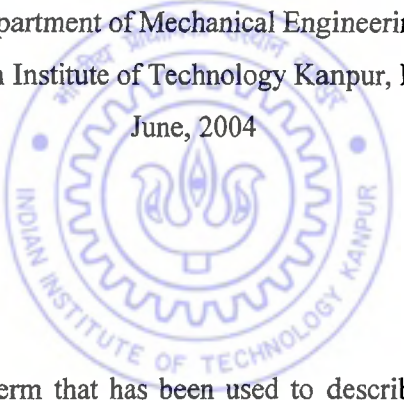

Rapid Prototyping (RP) is a term that has been used to describe the production of physical model from Computer Aided Design (CAD) data. RP produces objects by the addition of layers of material (layer manufacturing process), rather than by material removal (e.g. Milling). During last few years, rapid prototyping has been widely used in medical fields. Now, the use of RP technology for most of the medical applications is well demonstrated. It has become an accepted technique for visualization, surgery simulation and prosthesis generation. This technology has been demonstrated to minimize patient discomfort, improve the speed of patient recovery and ultimately to save lives of people.

In orthopaedics, plain X-ray has been a traditional method for understanding bone geometry. However, due to the limitation of a two dimensional (2D) image, sometimes it is very difficult to visualize complicated bone shapes three-dimensionally. By integrating medical scanning

modality with rapid prototyping, it is possible to build a realistic three dimensional (3D) human anatomical model. The model can then be used for studying deformity, designing implants, and even carrying out a trial surgery.

Medical literature review reveals that, some infants born with an orthopaedic foot deformity which is known as clubfoot and defined as the "Structural deformity of the foot, occurs at birth or during childhood". It has abnormal posturing of the foot, which causes him/her to turn the ankle inward and walk along the outside edges of the foot. Medically, it is also known as "Congenital talipes equino varus (CTEV)". When it is occurred in one foot it is known as unilateral clubfoot and in case if it occurred in both the feet it is called bilateral clubfoot. The literature review also reveals a detailed study of clubfoot from anatomy point of view along with its surgical and non-surgical correction techniques. The non-surgical correction technique presently used is quite a traditional one and much approximation is assumed in it. The technique is found to be only partially successful when applied by skilled orthopaedic surgeons. In any case the technique is highly discomfortable for the baby patients and they are restricted to perform their normal routine activity and exercise.

The engineering literature review particularly from rapid prototyping journal reveals that, RP is successfully used for medical model making and for surgical rehearsal of complicated clinical cases. These models are then used for prosthesis generation and implants fabrication. The review also shows successful application of RP in the surgery of twins' separation, hip implant fabrication and socket fabrication of the above - knee amputee. The technique is quite new. As the application increases gradually, more and more medical professionals will come to know about it. Till date, the literature does not record the application of RP in the area of Orthosis development. Orthosis is a general medical term mostly used for an external device, used for the correction, support or protection of a part of the human body. The actual name differs from time to time to the corresponding body part where it is applied. Considering all these literature reviews and available infrastructure of laboratory, it was decided to propound a new concept of research, using RP for clubfoot correction.

A meeting of the orthopaedic surgeons was called in the laboratory for discussing application of RP in biomedical engineering. The issues of literature review related to clubfoot and RP was discussed. It was concluded that the clubfoot was a burning issue in medical science since

long; and till date there is no standard, scientific or engineering non-surgical correction technique existing. Hence a problem for this dissertation is defined and it stated as follows:

"Development of a custom Ankle Foot Orthosis for non-surgical correction of clubfoot deformity in newborn babies".

As discussed above, the actual name of the orthosis corresponds to the body part where it is actually applied, in this case the orthosis is applied at foot and ankle, hence, it is known as 'Ankle Foot Orthosis' (AFO) and could be more precisely defined as a "device for correction, support or protection of the ankle and foot of human body".
For solving the defined problem, the dissertation consists of the following chapters.

Chapter 1 of the thesis gives an overview of the clubfoot and its corrective measures. It also emphasized the need of AFO and briefly deals about various modeling and simulation tools used for this dissertation. The review of the available literature from medical and engineering journals is presented. The objective as well as the scope of the present work is explained.

Chapter 2 describes the biomechanics of foot along with foot anatomy. It also briefly outlines the walking Gait cycle of normal healthy subject, pathological anatomy and functional anatomy of clubfoot. An approach based on biomechanics study and consultation with orthopaedic surgeon for the clubfoot correction is proposed at the end of the chapter.

The proposed methodology for RP and Silicone clubfoot modeling is explained in chapter 3. A brief overview of the Computed Tomography (CT) and Magnetic Resonance Imaging (MRI) scan data acquisition of patients' feet is also presented in this chapter. Medical image processing and 3D model making of patient's foot is explained. Geometrical modeling that includes solid modeling along with RP and its process sequences is also explained.

Chapter 4 deals with designing of AFO along with mechanical design considerations including proposed mechanism for correction procedure. The chapter deals conventional manufacturing of designed AFO. The chapter also presents the CAD approach for AFO design along with proposed strategies for surface and solid modeling. The chapter schematically explained the approach for designing an equivalent ankle joint of ball and socket type joint, in AFO. It represent the block / flow diagram for the design strategies.

Although RP is relatively a new technology, case studies and application of developed AFO will prove the potential and importance of this dissertation. To determine the possibility of success on human baby patients, case studies were performed in the Laboratory. Chapter 5 consists of finite element case study of clubfoot, experimental case study of silicone clubfoot, visual case study of RP clubfoot model and a clinical case study of a clubfoot patient. These case studies were performed in consultation with noted orthopaedic surgeons of Kanpur city of India.

Chapter 6 deals with the conclusions of the present research, which include technical summery and consideration of the scope for future work.

A significant contribution of this dissertation is the evolution of a realized clubfoot model and the product realization i.e. AFO for this long-standing problem of correcting the clubfoot deformity by non-surgical methods.

List of Publications

1. Jain, Manak, L., Dhande, Sanjay, G., Vyas, Nalinaksh, S., 2004, "CT – based biomodelling of human foot", International conference on mathematical biology, February 19 to 21, 2004, IIT Kanpur, India.

2. Jain, Manak, L., Dhande, Sanjay, G., Vyas, Nalinaksh, S., 2004, "Integration of CT and Rapid Prototyping to build biomodel of lower extremities, Workshop on computerized tomography for scientists and engineers, CT2004, Feb 13-15, 2004, IIT Kanpur, India.

3. Jain, Manak, L., Dhande, Sanjay, G., Vyas, Nalinaksh, S., 2003, "Biomodeling and finite element analysis of clubfoot corrective procedures in new born babies", International conference on rapid prototyping and tooling, RPSI 2003, 6th and 7th June 2003, Bangalore, India.

4. Jain, Manak, L., Dhande, Sanjay, G., Vyas, Nalinaksh, S. Ambekar, Ashok, G., 2003, "Finite element analysis of clubfoot deformity in newborn baby", 3D modeling 2003, 8th International conference, April 23 – 24, 2003, Paris, France.

5. Jain, Manak. L., Dhande, Sanjay, G., Kumar, Saravana, G., Rastogi, Sanjay, Shukla, Mukul, Gupta, T. V. K., 2002, "Preliminary study of clubfoot deformity in new born babies using rapid prototype models." International Congress of Medical and Biological engineering, 2002, Singapore.

Acknowledgements

I am sincerely thankful with my heart and soul to my ever loving, Prof. S. G. Dhande who was and continues to be a model of dedication, discipline and hard work, which was a great inspiration to me. I enjoyed the care and affection he shown on me. Whenever I was in trouble, he was there to help me; on certain occasion he went out of the way to help me. He is more than a Director and Thesis Supervisor to me. My experience with him tempts me to pursue my remaining carrier with him. I also highly indebted to his wife Mrs. Medha Dhande who extended her support to my wife and children. Support of Dr. Dhande and his family to me is unforgettable. I am paying my great regards, respect and love to him. I along with my family wish him, all the success in his endeavors.

I would like to place on records my thanks to Prof. N. S. Vyas for discussion, I had with him. He always extended a helping hand in times of need. Thanks to his wife Dr. Mrs. Mamta Vyas, who helped us, particularly to my wife during her critical time when she was admitted to Gurunanak Hospital Kanpur.

I sincerely appreciate the co-operation of senior orthopaedic surgeons Dr. P. M. Gadre and Dr. Sanjay Rastogi during the research work. I am very much thankful of them. I would also like to thanks Prof. B. Sahay, Prof. V. K. Jain, Dr. Bhaskar Dasgupta, Dr. Annupam Saxena, and Prof. N. N. Kishore who did their best to help me during my programme. I am truly grateful to them.

I wish to express my thanks to Mr. Sarvana kumar for his help during my thesis write-up. He gave me many interesting discussion during my research work. He helped me a lot at the time of my research publication, which I presented at Paris France on April 2003. I have a deep love in my heart for him. I am thankful to Mr. Mukul Shukla who assisted me during my research activities. I appreciate him for improving my presentations and research publication in many international conferences. I am thankful to Mr. T. V. K. Gupta and Mr. Yugandar who helped me during my working on different CAD-software. I never forget Guptaji support extended to me during my participation in Paris, France conference.

Good friends make the life enjoyable. Shivaji, Sanatji, Puneetji, Dharmendraji, Rahulji, Anilji, Sidharthji, Bhanuji, Kiranji, Jeevanji, Dalirajuji, Suryaji, Vaibhavji, who helped me in one way

or other during my stay at IIT Kanpur. I will not forget the memorable days spent with them in the dinner party at Dhaba. They shared and stand with me during days of happiness as well as difficulties, I am thankful for them.

I also thankful to shri A. Chatterjee for providing the necessary support and facilities in the Lab, on certain occasion he really helped me for continuing my smooth research. I always remember his cooperation given to me in some odd time. His wife Dr. Mrs. Sarvari Chatterjee has shared me the knowledge of radiology and the prospectus of the current research in future. Thanks to them as it increases my interest in this research. I sincerely appreciate the co-operation of CAD-P Lab staff, shri Ravindar, shri Shalendra and late shri C. P. Singh who helped me in several ways during the course of my research work. I also owe special thanks to shri Babulalji and shri Sarju Prasadji for their regular supply of tea.

Off the Lab, I thank my wife Anita, daughter Barkha and son Tanmay (who born and followed his footsteps at IITK) for their understanding and refreshingly different atmosphere presented in the home. They happily gave me time that had been theirs. They always extended me a sweet smile even if I returned home in late hours. I am really proud of them. A-6 SBRA will always be memorable one with fond memories of the family of Mr. Vinod Yadav and Mr. Sanjay Kumar who made my stay comfortable at SBRA. I am thankful of them. I am also thankful to CT/MRI technician Mr. A. Ledgy, without him it was difficult for me to scan the baby foot and getting the data in appropriate format. I also like to thanks Mrs. Josephine Siew of Materialise Inc. for assisting me during working in MIMICS software. I also thank to Mr. Satyamurty for his helps during my thesis writing. I would also like to thank the members of Jain Munch for extending the helping hand to me. I immensely grateful to my beloved mother. I express my sincere regards to my brothers for their helps to me from Indore. I would also like to thank my nephew Gaurav Jain and niece Nidhi Jain for their support to me during my visit to Indore. I am thankful to shri T. N. Singh sahab and madam Hemlata Gupta of Indore, for assisting me to focus on the research. Finally, I would also like to thank one and all, who have assisted me in the last four years stay at IITK. May I be forgiven if I have missed out, any of the names.

M Jain 28/06/04

Manak Lal Jain

Contents

List of Figure

List of Tables

Nomenclature

T_c	Talocrural or upper ankle joint across which flexion-extension occurs
XT_c	Flexion-extension along X – axis
YT_c	Flexion-extension along Y – axis
ZT_c	Flexion-extension along Z – axis
T_{cn}	Talocalcaneonavicular or lower ankle joint across which inversion-eversion occurs.
XT_{cn}	Inversion-eversion along X – axis
YT_{cn}	Inversion-eversion along Y – axis
ZT_{cn}	Inversion-eversion along Z – axis
X, Y, Z	Cartesian coordinates
T_1, $T2$	Force generated in plantar aponeurosis of foot
K_1, K_2, K_3	Spring constant.
C_1, C_2	Damping coefficient.
A	Talocalcaneal angle
B	Talonavicular angle
α	Angle between biomolar and foot axis
β_1, β_2	Flexion angle of foot
θ	Angle with respect to X – axis
$f_\theta(s)$	Projection data along θ direction
μ	Attenuation coefficient
$\mu(s, \theta)$	Attenuation coefficient as a function of position and angle called measurement space.
$g(x, y)$	Image space which determine density distribution with in object.
$N \times N$	Image reconstruction matrix
T_1, T2	spin – lattice and spin – spin, relaxation time constant in MRI imaging
L_1, L_2, L_3	Length of mechanical linkages of a mechanism
h_1, h_2, h_3	Movement in vertical direction.
i, j	Suffixes.
$n+1$	Number of defining polygon vertex of a parametric curve / along u parametric direction in case of a surface.

m+1	Number of defining polygon vertex along u parametric direction in case of surface.
N_i k (u)	Basis functions for a parametric curve / along u parametric direction in case of a surface.
$M_{j,l}$ (v)	Basis functions along v parametric direction in case of a surface.
x_i	Element of knot vector of a parametric curve / along u parametric direction in case of a surface.
y_j	Element of knot vector along v parametric direction in case of a surface.
K	Spring stiffness
Ψ	Constant multiplying factor
L_{max} , W_{max}	Maximum length and maximum width of foot.
S_{max}	Maximum perimeter of foot.

Chapter 1

INTRODUCTION

This chapter develops background for the present work and discusses the need to take up this research work. It presents modeling and analysis tools along with available relevant literature review. Objective and scope of the present work are also discussed.

1.1 Overview of clubfoot problem and corrective measures

Clubfoot is one of the oldest common birth defects known to man. There are Egyptian mummies with clubfoot. The defect causes one or both feet twisted inward. In most cases, the causes of clubfoot are not known and the exact causes of the condition have been debated for centuries and are still not clearly understood [40]. Some doctors feel that it may happen in the womb due to cramping or twisting position of foot, somewhere around 10^{th}-12^{th} weeks of pregnancy. However, there is no proven cause for the condition. It occurs twice as often in boys as girls and in 50% of the cases the deformity is bilateral (both feet) [47]. A true clubfoot affects all the joints, tendons and ligaments in the foot and is often technically referred to as "Congenital talipes equino varus CTEV". In most of the cases the cause is unknown and it is known as Idiopathic clubfoot. The two type of clubfoot are shown in Figure 1.1. Almost 5,000 babies are born with this deformity each year in the united state [78].

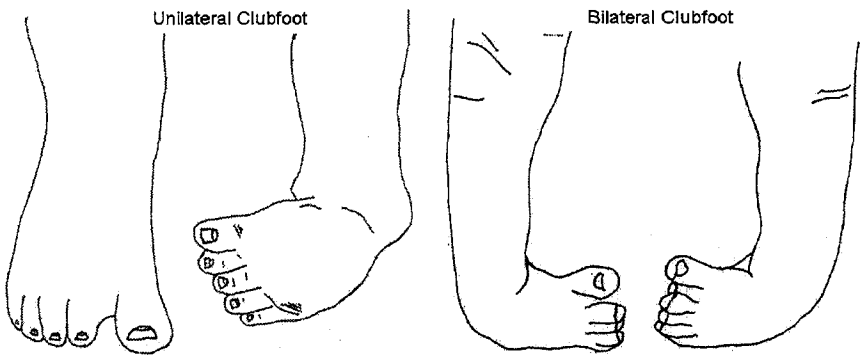

Figure 1.1: Unilateral and Bilateral clubfoot

1.1.1 Characteristics of clubfoot

Following are the characteristics of clubfoot [74]:

- The foot has a kidney-shaped appearance with a high arc (Cavus) at the midfoot, indicated by a transverse crease across the sole of the foot. The forefoot is turned towards other foot, known as adduction of forefoot.
- The heel is drawn up, because of tightened Achilles tendons, making it impossible to place the foot flat on the floor.
- The toes are pointed down, known as equines of forefoot.
- The bottom of the foot (heel) is twisted in, towards other foot, known as varus of heel.
- The foot and leg may be smaller in comparison to a comparatively normal child's foot and leg.
- The foot will lack motion and be noticeably stiff.
- The Calf muscle may also be smaller.

1.1.2. Diagnosis

Because of dramatic and obvious nature of deformity, most of the clubfoot is diagnosed at birth itself. The foot is in turned, stiff and cannot be brought to a normal position. The calf muscle may be shortened and underdeveloped. In unilateral (one foot) clubfoot the affected foot may be shorter than the normal foot [74]. The major components (equines, heel varus, forefoot adduction) of foot having different degree of rotation (0, 20, 45 and 90 degree) in clubfoot. By observing this degree of rotation in clubfoot, above components are graded clinically from grades IV to I (from most severe to most mild). Accordingly the deformity is classified into light, moderate, severe and very severe clubfoot [82].

1.1.3. *Methods of treatment*

Clubfoot is one of the most common, yet challenging pediatric foot deformities. How to best treat clubfoot continues to be a controversial subject among orthopaedic surgeons and many different opinions exist, concerning treatment regimes [74].

The goal in treating a clubfoot is to achieve and maintain as normal a foot as possible [40]. The extent of treatment varies, depending on the severity of each child's condition. Congenital clubfoot is usually mild to moderate while clubfoot that accompanies other condition is more severe.

Only experienced orthopedic surgeons should attempt to correct the condition, since cases that are treated poorly can compound the deformity and making further treatment difficult [74]. Below is the summary of some treatment procedure used [74]:

1.1.3.1 Physiotherapy

This is primarily a non-surgical treatment and mostly used for mild deformity. It involves frequent visits by a physical therapist who tapes and or manipulates the foot. This method has proved highly successful in mild deformity cases.

1.1.3.2. Serial casting

This may be beginning from the first day of life to several weeks after birth. The foot is pushed and twisted into an approximates corrected position by the orthopedist. The cast is then applied in order to hold the foot into this position, initially up to 2 to 3 week. The casts are changed frequently each time repositioning the foot a little closer to normal foot. Cast changes are then decreased to once every two weeks. This treatment, known as "Serial casting", continues until the child is 3 to 6 month old and involves between 5 and 10 application of plaster casts [2]. This method may be uncomfortable for the child. Doctors differ widely in their opinions regarding success rate of serial casting. Some say that procedure work only in few percents while some believe almost all cases when treated early can be corrected.

The Ponseti method of casting and manipulation can also be effective. This method was pioneered in the1940's by Dr. Ignocio Ponseti and is successful in most of the cases said Dr. I. V. Ponseti [74] [18] [96].

1.1.3.3 Surgery

This is a more aggressive treatment and is usually recommended for severe deformity to a child of at least 1 year age. There are many surgical procedures available for clubfoot. Most surgeries lengthen the posterior and medial structure. It also corrects the position of bone. Below is the list of commonly used surgical procedures [74] [40].

- Perctuneous tenotomy- The Achilles tendons is cut to allow the foot to drop.

- Posterior release.
- Medial release.
- Subtarsal release.
- Complete tendon transfer.

1.2 Need of Ankle Foot Orthosis (AFO)

According to Dorland's illustrated Medical Dictionary, 25th edition, defines an Orthosis as "an orthopedic appliances or apparatus used to support, align, prevent, or correct deformities or to improve the function of movable parts of the body [18]. When this Orthosis applied to foot and ankle, it can be more specifically said as Ankle Foot Orthosis (AFO).

From physical and literature survey no user friendly AFO is currently available which can give some corrective guarantee. The traditional available AFO [81] are inconveniences to the patients because their designs are bulky, unattractive and not particularly user friendly. Moreover, they do not have quantitative load applying mechanism. With the development of new materials and modern techniques such as Computer Aided Design (CAD) and Rapid Prototyping (RP), it is possible to fabricate new custom based, stronger, lighter, cooler and user friendly AFO for the new born babies patients. This AFO assists in controlling and keeping the clubfoot posture as close as to a normal foot.

A custom made AFO [62] is preferred to ensure a closer fit, proper pressure distribution and prevention of complication from skin breakdown. The aim of the AFO development is to correct the deformity as early as possible and that the patients should maximize their functional mobility and does not handicap their life-style. The design is finalized with close consultation of medical professionals to ensure practioner and patients satisfaction with the fit and function of our custom AFO.

1.3 Modeling tools

For the present research we used, the following tools

1.3.1 CAT Scan or CT Scan

A computerized axial tomography scan is a special test where X-rays are used to take pictures that look like slices through the bones of the foot and ankle. In other words it is an X-ray view of the body in sections.

Here X-ray machine takes X-ray images at many different angles around the body. These images are processed by a computer to produce cross-sectional pictures of the body. In each of these pictures the body is seen as an X-ray "slice" of the body, which is recorded on a film. This recorded image is called a tomogram. "Computer Axial Tomography" refers to the recorded tomogram "section" at different levels of the body.

1.3.2 MRI Scan

The Magnetic Resonance Imaging (MRI) scan is a radiology technique which uses magnetism, radio waves and a computer to produce images of body structures. The patient is placed on a moveable bed, which is inserted into the magnet. The magnet creates a strong magnetic field, which aligns the protons of hydrogen atoms, which are then exposed to a beam of radio waves. This spins the various protons of the body and they give NMR (Nuclear Magnetic Resonance) signal. These signals are received by an MRI scanner and the information is then processed by a computer and an image is then produced.

The MRI scan is useful because it shows not only the bones of the foot, but also the soft tissues like tendons, ligaments and cartilage.

1.3.3 INSIGHT

Before building the STL model in Rapid Prototyping system (FDM-1650) it is necessary to preprocess the STL file. INISGHT is the Stratasys software for preprocessing the STL model and generating tool path (SML) file. The preprocessing of STL file include following steps:

- Orienting the STL model.
- Slicing the STL model with a series of horizontal planes to create slice curves.
- Creating support curves that define where temporary supports will be built.
- Creating tool path fill for part and support curves.

- Creating tool path file (SML).
- Downloading tool path files to modeler for part building.

1.3.4 Rapid Prototyping

It is a new technique for fabrication of a 3D physical part of arbitrary shape directly from a CAD model; it is quick, highly automated and totally flexible process. Depending on raw material it is of three types solid, liquid and powder type. The FDM RP system, which we mainly use for our research work, uses Fused Deposition Modeling to turn computer aided design (CAD) geometry into physical models that can be used for design reviews, manufacturability studies, investment casting pattern and marketing with FDM RP system, we can take our project from design stage to concept model to final plastic prototype. The INSIGHT s/w, FDM Hardware and modeling material constituents 3 main part of FDM system. After slicing a STL file and creating a SML file, the SML file is downloaded to the FDM hardware for modeling. In FDM hardware, the FDM head moves in two horizontal axes across a foundation and deposits a layer of material for each slice. The material filament is pulled into the FDM head by the drive wheel. It is heated inside the liquefier in the FDM head and it comes out in a semi-liquid sate. The successive layers fuse together and solidify to build up an accurate, three-dimensional model of the design.

1.3.5 MIMICS

Materialise's Interactive Medical Image Control system is an interactive tool for interfacing from a medical scanner (mostly CAT or MRI) to Rapid Prototyping or to CAD system. Here visualization, segmentation and 3D rendering of human anatomy from its CT and MRI images is possible.

1.3.6 Imageware Surfacer

It is a powerful and intuitive surface creation tool for direct creation of freeform surface from 3D point cloud data. The flexible design environment, supports both Bezier and Nurbs surface patch layout. The functionality in surfacer can be divided into three main categories, point processing, curve and surface generation and entity analysis. It enables to design, accurately build and fully inspect high-quality, freeform shaped products in less time.

1.3.7 I-DEAS

The Integrated Design Engineering Analysis Software (I-DEAS) is a graphical modeling package to create models and analyze them or export them for analysis in another program. It facilitates a concurrent engineering approach to mechanical engineering product design and analysis. It is mostly used for creating solid model geometry. It has many different tools for part modeling, assembly modeling, mechanism analysis and tolerance analysis. These tools work together to support tasks from concept design and simulation to details design, drafting and manufacturing.

1.4 Analysis Techniques

1.4.1 FEM Simulation

The Finite Element Method (FEM) is a general procedure of numerical approximation to all physical problems capable of being modeled by differential equations. The general procedure of the method is that any body or structure is divided into smaller elements of finite dimension called as "Finite Element". The original body or structure is then considered as an assemblage of these elements. These elements are connected to each other at joints called as "Nodes" to form the entire structure. The properties of these individual elements are formulated and from these, the property for the entire body is obtained.

The equation of equilibrium for the entire structure or body is then obtained by combining the equilibrium equations of each element such that the continuity is ensured at each node. The necessary boundary conditions are then imposed and the equations of equilibrium are then solved to obtain the required variables such as stress, strain, temperature distribution, or velocity flow, depending on the application.

For our analysis purpose we are using MSC. PATRAN r2a version software, where we can create finite element models from their computer aided design (CAD) part, submit these models for simulation, and visualize the simulated model behavior. The results are then used to improve their product designs to better resist operating loads, reduce weight or material, or have higher performance.

1.4.2 Instrumentation

Stress analysis by electrical resistance strain gauge is one of the most widely used quantitative methods of evaluating stresses in material. The method consists of installing the resistance-based strain gauge in the location of interest and orientation and connecting them to the virtual instrument (VI), which consists of a computer workstation equipped with powerful application software. The virtual instruments represent a fundamental shift from traditional hardware centered instrumentation system to software centered system.

Lab VIEW is an integral part of virtual instrumentation because it provides an easy-to-use application development environment. LabVIEW offers powerful features that make it easy to connect to a wide variety of hardware and other software. By using LabVIEW the data were displayed, analyzed, graphed and stored to spreadsheet in Microsoft Excel. The strain gauge records the dynamic strain change during motion.

1.5 Human foot skeletal and its motion

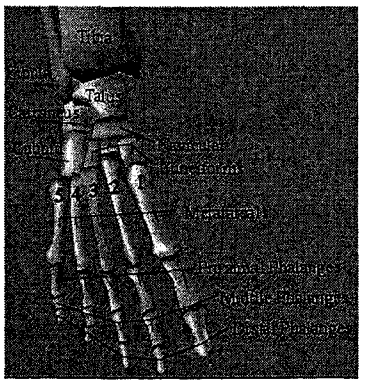

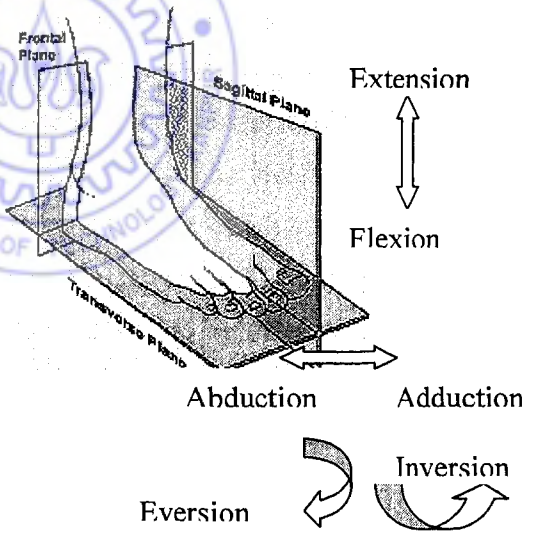

Figure 1.2: Basic skeletal of foot. Figure 1.3: Three views of plane and motion of foot

The skeleton of the foot and ankle [59] begins with the ankle joint itself. The two bones of the lower leg, the larger tibia and the smaller fibula come together at the ankle joint to form a very stable joint.

The two bones that make up the hindfoot are the talus and the calcaneus. The talus is connected to the calcaneus at the subtalar joint. The ankle joint allows the foot to bend up and down; the subtalar joint allows the foot to rock from side to side. The next group of bones, called tarsal bones, that work together as a group, these bones are very interesting in the way they fit together. When the foot is twisted in one direction by the muscles of the foot and leg, these bones lock together and form a very rigid structure, When they are twisted in the opposite direction, they become unlocked and allows the foot to conform to whatever surface the foot is contacting. The tarsal bones are connected to the 5 long bones of the foot called the metatarsals. There is a fairly rigid connection between the two groups without much movement at the joints. Finally, there are the bones of the toes and the phalanges. The joints between the metatarsals and the first phalanx is called metatarsal phalangal joint. These joints form the ball of the foot, and movements in these joints are very important for a normal walking pattern. The Figure 1.2 represents the dorsal (top) view of the basic skeletal system of the foot while Figure 1.3 represents three planes known as frontal, transversal and sagittal plane. The different movement of the foot is also shown in the Figure 1.3.

From functional point of view human foot [45] is a supporting structure, which has to carry considerable static loads in standing and even greater loads at the point of application of severe thrust forces, e.g. in kicking, pushing off, in running and landing on the feet when jumping from a height. Strength and resilience have to be the main features of the foot rather than the type of mobility, which is required in the hand for holding. The foot has massive tarsal and big toe bones bound together by powerful ligaments (soft tissue which connect bone to bone), and by binding the metatarsal of the big toe to those of the other toes so that it has none of mobility that the thumb has in its metatcarpal. Resilience is obtained by the presence of multiple joints each of which has very limited movement and by arrangement of the bones in an arc held tighter by massive ligaments on the plantar surface and by a strong toe-beam which binds the ends of the arch together and has its tension altered in different positions of the foot. When standing, the weight is supported on the heel and on the heads of the metatatrsals and lesser extent on the lateral border of the sole of the foot. When the foot is used in thrusting, the force is carried principally on the head of the first metatarsal and the big toe. The remaining metatarsals and toes are relatively weak and can be looked upon as a stabilizing flap. Without them the foot would have an unstable, two-point contact with the ground on the calcaneus and the ball of the great toe. The arched shape of the foot has the added advantage of giving protection to the structures in the sole, which would otherwise be subjected to pressure [45].

One special development to resist the pressures on the head of the first metatarsal (e.g. As in running) is the presence of two sesamoid bones on its plantar surface. To transmit the pull, a small tunnel exists between them through which the long flexor tendon (soft tissue which connect bone to muscles) can reach the toe.

1.6 Literature review

Rapid Prototyping (RP) technology has changed the way products are being designed and manufactured, although initially developed for engineering product development environment, has found its place in almost all areas of our lives. In recent years one of the most exciting applications of rapid prototyping is the "medical field". Application of RP in medical field cover a variety of area like pre-operative planning, surgical rehearsal, making of prosthetic and orthotic devices etc. Initial entry of RP in medical field begins with prototyping of surgical tools. **Jamieson et al** (1995) [46] compared the development of a surgical tool, manufactured by rapid prototyping with conventional cast and machining method and concluded that RP could certainly be used to reduce the amount of costly cast iterations by assisting in the development phase. They suggest that the final designed part could also proved to be cheaper, lighter and more ergonomic by utilizing RP techniques especially in the surgeon acceptance stages. In medical diagnosis, plain X-ray has been a traditional method for understanding tissue geometry. However, due to the limitation of a 2D-image, it is sometimes very difficult to three-dimensionally visualize complicated shapes. CT/MRI-scans, along with recently developed technology of image reconstruction and rapid prototyping models have made it possible to show the cross-section geometries of a tissue and to reconstruct a realistic model. **Swann S.** (1996) [90] linked the scanning technology from medicine field to rapid prototyping technology from engineering field to view the anatomical image data in a completely different manner from what was possible previously. The author interface Magnetic Resonance Imaging (MRI) with stereolithography rapid prototyping system and fabricated the soft tissue model of human brain with many difficulty encountered during early phase of integration. **Sanghera et al** (2001) [79] created a total of 16 orthopaedic, maxillofacial and dental's RP model by interfacing CT/MRI scans with RP system and shows that the physical models are very much helpful for patient treatment, planning and visualization instead of software generated 3D volumes on 2D screen, it also assists to plan complex procedures prior to surgery with potential to optimize patient treatment in operation theater. According to them the models helps in accurate observation of complex bone anatomy fragments, in the vicinity of fracture site and

the approach lead to better patient care regimes and the potential for reducing waiting lists. A very recent successful application of RP is in the separation of Conjoined twins was stated by **Amas Libermann** (2003) [5]. In this research the information from MRI and CT scans were used and an accurate life – size model of the heads of the conjoined twins was manufactured. This allowed surgeons to see and touch inside the area they were going to operate on – something that cannot be performed with a computer simulation. This highly accurate 3D model was used to plan the successful separation of conjoined twins in Los Angeles in August 2002.

Another medical application of RP is in the development of prosthetic devices. **Ng et al** (2002) [65] developed a customized Computer Aided Manufacturing (CAM) system known as Rapid Manufacturing Machine (RMM) for amputee prosthetic socket fabrication using Rapid Prototyping (RP) technology, whose working principal is same as that of the FDM and claimed that the system reduces socket making time from days to hour as in case of conventional manufacturing. They also conducted the clinical and biomechanical studies on the fabricated socket for evaluating its comfort and fit on patient during gait and shows that the functional characteristics of this socket are very similar to that of the traditional socket. One more approach known as Computer Aided Socket Design/Computer Aided Socket Manufacturing (CASD/CASM) for same prosthetic socket fabrication is developed by **Francis et al** (2002) [92], which is differ than the Ng et al system in the sense that it uses existing FDM-1600 RP system. They developed the CAD model of the socket from patient stump positive mould's digitized data, obtained from contact type scanner. After modifying the CAD model they created its STL, SLC, SML file and fabricated the socket in FDM-1600, RP system They did the clinical test for a trial period after wearing the fabricated socket on patient stump and found that the patient get acceptable degree of comforts and did not experienced any problem, which confirmed the viability of prosthetic socket fabrication using FDM technology.

Earlier an orthotic device of foot sole for keeping normal foot fit without using rapid prototype system but by using CAD/CAM was developed by **Timothy et al** (1989) [86]. This technique gave a push towards utilization of advance manufacturing of orthosis. In their technique the finished cast impression of foot is manually digitized by wand scanner and a CAD, 3D model of simple orthosis of normal foot is developed, after processing and modifying digital data. In their CAD technique limited modifications were possible, the 3D view is review and after doing necessary correction, the corrected digital data file of orthosis (sole portion of foot) was

sent to NC milling machine, which cuts out the completed orthosis die from a solid block of material. A wide variety of material such as Polyethylene, Polypropylene, Cork, Korex, Sponge rubber, Rubber crepes and foamed plastic were used for orthosis development. In this way they increases the accuracy of fabricated orthotic devices along with increase speed of production and avoiding the storing of finished cast foot impression, by storing its digital library. Using traditional plastic vacume forming process **Athearn et al** (1995) [10] utilized their own impression and model modification techniques and developed an Ankle Foot Orthosis (AFO) for idiopathic clubfoot by their own impression and model modification techniques. They cast the clubfoot and the caste model is corrected by their technique so that it appears like a normal foot. Finally the model is trimmed and smoothen which give die for plastic vacuum forming of AFO for clubfoot. Clubfoot is a historic foot deformity and many medico researchers did their research for finding it's exact cause corrective procedure but till today no one is succeeded in doing so, each one has their own theory and treatment. **Herzenberg et al** (1988) [37] studied the newborn's clubfoot and normal foot and said that the principal structural deformity in clubfoot is medial and planter deviation of the talus neck. The calcaneus is also found to in rotating position as compare to normal foot. They suggested that the correction could be best achieved in a young foot by soft tissue release. In their treatment the correction is maintained interaoperatively with pin fixation, appropriate tension of the tendon and postoperatively by castes and splints. **Downey et al** (1992) [25] did MRI study on normal and clubfoot by imaging in sagital, transversal and coronal plane for better understanding of clubfoot deformity. They observed that the talar neck having medial angulation while the anterior portion of calcaneus is shifted medially and its posterior portion shifted laterally. They also believed that the primary clubfoot problem is the talar head and neck deformity, with the anterior calcaneus following the deformed anterior talus and causing a pivot about the interosseous ligament so that the posterior calcaneus is forced laterally. **Song et al** (1999) [85] also studied the clubfoot model and define the inter positional relationship of the hindfoot bone in idiopathic clubfoot as compare to that of a normal foot. They determined the central principal axes of talus and calcaneus and showed that it is neutral rotated with reference to the bimalleolar axis in idiopathic clubfoot, whereas in the normal foot the talus is medially rotated and the calcaneus is laterally rotated.

As stated above there are several theories of clubfoot correction, but non of them is standardized **Brandish and Noor** (2000) [15] studied the Ilizarov method for clubfoot management which involved the gradual distraction and realignment of joint by using fixator

applied to the lower limb and foot whose toe was manipulated into straight position and stabilized by K. wire under general anesthesia and achieved the full correction. The drawback of the treatment is that it is in vitro and development of bone cysts were observed after the treatment. Some medico doctors developed their non-surgical correction technique for clubfoot deformity, one of them which is very popular today is developed by Ignovis Ponseti and it is known as ponseti technique. **Pirani et al** (2001) [72] did research to find the bone joint relationship of the clubfoot, treated with Ponseti technique. For this they performed MRI study on congenital clubfoot treated with non-operative Ponseti method that basically involves serial casting. They performed the scan at the beginning of, in the middle of and at the end of treatment. They claimed that the abnormal tarsal bone relationships along with abnormal shape of individual tarsal bones are corrected because of mechanical loading of fast growing tissues. They also mentioned the guideline for clubfoot treatment as stated by Ponseti.

The human ankle joint has already been extensively studied from anatomical and clinical point of views because of its strategic importance in human physical activities. In biomechanics it remain the last major joint system in the leg for which a three-dimensional analysis has yet to be performed. **Procter and Paul** (1982) [77] did 3D analysis of human ankle joint and formulated the models Mark-I and Mark-II, considering the ankle to be made up of two rigid free body segments namely the talus alone and the talus plus calcaneus. They suggest that the ankle is made up of two principal joint, namely the talocrural (Tc) or upper ankle joint and the talocalcaneo navicular (Tcn) or lower ankle joint. They considered Tc joint to be a simple hinge joint. Permitting flexion and extension of talus relative to tibia, the Tcn joint is also uniaxial one allowing inversion and eversion of calcaneus relative to talus i.e. they describe the rear foot motion by approximating it to be made up of tow simple hinge joint. They analyze these joint for data obtained from gait laboratory test. The formulated ankle models were based upon data gained from the literature together with dissection studied of embalmed cadaver material. They claimed that the Mark-II model is a suitable vehicle for the study of effects of ankle pathology upon gait and may be useful in the assessment of different types of ankle endoprostheses. This model was used to investigate the behaviors of the normal ankle joint while walking upon planes sloping sideways at ±10 degree. The mathematical modeling which is a key process for solving complex problem has provided a powerful tool for investigating the complicated behavior of human joint. **George et al** (1983) [101] developed the mathematical model of human ankle joint for defining contact areas and pressure distributions. They considered incongruent articulation of ankle joint, the uniform distribution of cartilage

thickness covering the joint component surfaces and the basic geometry of the ankle joint as the three major factors while designing the mathematical model. They depicted the contact area growth plots and generated pressure profile graphically. For varying applied load the graph represent complete picture of contact area growth of the talus. They show that as the load is increased, the two separate contact areas broaden and subsequently merge, forming one continuous contact area approximating a rectangular shape at full load. They proved this also in a quantitative study. The pressure profiles in the medial, lateral view are represented by a parabolic distribution and represent cross-sections from the pressure profile at different planes along the length of the model. The magnitude of stress depends directly on the amount and direction of the applied force. **Leardini et al** (1999) [55] developed an experimental set-up for kinematics study of ankle joint during passive flexion considering that the joint motion was constrained by the articular surfaces and the ligaments. They have studied the motion of calcaneus, talus and fibula relative to the stationary tibia in seven cadaver specimens. They showed that the calcaneus follows a unique path of unresisted coupled motion relative to tibia and most of the motion occurred at ankle, with little motion at the subtalar level. They found that the calcaneofibular and tibiocalcaneal ligaments together with the articular surfaces, guide ankle passive motion other ligaments limit but do not guide motion. Also during passive flexion, the articular surfaces and the ligaments alone prescribe a preferred path of joint motion at the intact human ankle complex. They concluded that their study emphasizes the complementary role of the ligaments and articular surfaces in guiding joint passive motion. Any change in their original geometry in the intact joint, such as bone fracture, erosion of the articular surfaces due to osteoarthritis, ligament injury and reconstruction or total joint arthroplasty, will alter the original number of DOF and lead to abnormal kinematics of the joint. For understanding the dorsi/planter flexion of ankle during unloaded condition a geometric model of ankle joint is also developed by **Leardini et al** (1999) [56] in the same year. He formulated a two-dimensional four-bar linkage geometric model of ankle joint complex and demonstrated that the human ankle joint complex behaves as a single-degree-of-freedom system during passive motion with a moving axis of rotation. The linkage model is formed by tibia/fibula, talus / calcaneal bone segments and calcaneofibular and tibiocalcaneal ligament segments. The developed geometrical model give an ideas about ankle joint stability in responses to the applied load and can be used to predict the effect of changes to the original geometry of the intact joint. He described that the ligaments and bones at the ankle form a mechanical linkage.

By his 4 BL geometric model he demonstrated the relationship between the geometry of the ankle ligaments and the shapes of the articular surfaces. He also explained that the human ankle joint can be modeled as a single DOF mechanism and the anatomical structures of joint allow and control movement (joint mobility) because the articular surfaces can slide and roll on each other and because the ligaments rotate about their origins and insertions on the bones. The effects of application of the external load and the consequents joint tissues deformation (joint stability) was also studied in the model. **Ning Ying and Wangdo Kim** (2002) [105] Described the Ankle joint motion in3D space using Dual Euler angle orthogonal approach. They used the concept of 3-screw motion along three predefined axes for describing displacements of ankle joint in full six degrees-of-freedom of model. Thy successfully explained the clinical motion of flexion-extension, adduction-abduction and internal, external rotation of ankle joint with this approach. They also show that when the foot moves from maximum planter flexion to maximum dorsiflexion it everts and externally rotates. **Ying et al** (2002) [104] proposed 3 D mathematical model of the ankle joint complex. Their model consists of two rigid bodies, namely tibia-fibula and talus-calcaneus bounded by six major ankle ligaments. For the study geometrical data was taken from foot cadaver specimen and they simulated the movement of dorsiflexion and planter flexion and concluded that the ligaments C. F. (calcaneofibular) and TiC (tibiocalcaneal) area always tight, during dorsiflexion- planter flexion. They also showed that the ligament PTT (posterior-tibiotalar), and PTaF (Posterior talofibular) vary from tension to relax while ligament ATaF (Anterior talofibular) and ATT (Anterior tibiotalar) vary from relax to tension during dorsi-planter flexion.

1.7 Objectives and Scope of the Present Work

The clubfoot is a historic congenital foot deformity in medical science, where the foot turns inward and points down causing walking on the toes and outer sole of the foot. Some of the bones in clubfoot are abnormal not only in their relationship to each other but also in shape and size. Shortened tendons on the inside of the lower leg together with abnormally shaped bones that restrict movements outward, causing the foot to turn inward. A tightened Achills tendon causes the heel to be drawn up and the foot to point downward.

The basic aim of the research is to develop a non-surgical engineering procedure that will give guarantee for the correction of clubfoot in newborn babies. The developing procedure will

eliminate casting and surgical correction (except in very severe case), which is not desirable for the babies at tender age group. Hence will be more comfortable for babies.

The research need an interdisciplinary "Bridge" between engineer, radiologist and surgeons for knowing joint anatomy and application of basic mechanics to the human body where it combines with multidisciplinary research, that include Solid modeling, RP-modeling and image analysis. By analyzing the simulation and mechanical testing of foot we can develop a highly accurate and sophisticated Ankle Foot Orthosis (AFO).

Hence the objective of the present research is "To develop a RP based AFO for non surgical correction of clubfoot deformity in new born babies".

So the present research is an attempt to use basic engineering mechanics and RP techniques with interdisciplinary work to reach the convergence of clubfoot solution by developing a user friendly AFO for new born babies.

The scope of the present work is the direct application of AFO to the society and hence a greater success rate achievement in clubfoot correction, which will be very much useful in the context of child development at national and international platform.

Chapter 2

BIOMECHANICS OF FOOT

The human foot is a very complex joint capable of executing many combinations of movements and motions. It is a load bearing structure for activities, such as standing, walking, running and jumping of body [36]. It consists of 26 bones (one quarter of the human body bones), 33 joints and more than 100 muscles and tendon that allow an active adaptation of this biomechanical structure to uneven surfaces during locomotion. It also guarantees a stable support to the body, attenuates harmful impact shocks and provides sensory information about the contact with ground.

In order to understand the biomechanics of foot it is necessary to know its anatomy and physiology from biomechanics point of view.

2.1 Foot anatomy

The anatomy of the foot presented here will not be exhaustive but rather highlight the structures that mostly relate to the construction and function of foot. The important structures of the foot can be divided into three major categories namely bone and joints, ligaments and tendons and muscles apart from the sensory and circulatory system like nerves and blood vessels.

In Figure 2.1, the two bones of the lower leg, the larger tibia and smaller fibula come together and meet to a third bone called talus thereby start beginning the skeleton of foot. The talus bone has a shiny joint surface, which allows ankle to glide effortlessly across the shiny undersurface of tibia. These three bones together form a very stable structure known as ankle joint [90], which allows the foot to bend up and down known as dorsiflexion and planter flexion motion of foot. On the inside of the ankle there exists a bump, which is a part of the tibia and is called malleoulus of the foot. The fibula prevents major ankle bone from shifting outward and its outer portion at talus is called lateral malleolus. The stability of ankle joint is

dependent upon the ability of these bones to keep the central bone in place while the ankle moves back and forth. The joint is more stable when foot is flat on the floor. The ankle is more rigidly held in place by the bony stabilizer of the fibula and malleoulus because they are closer to the talus.

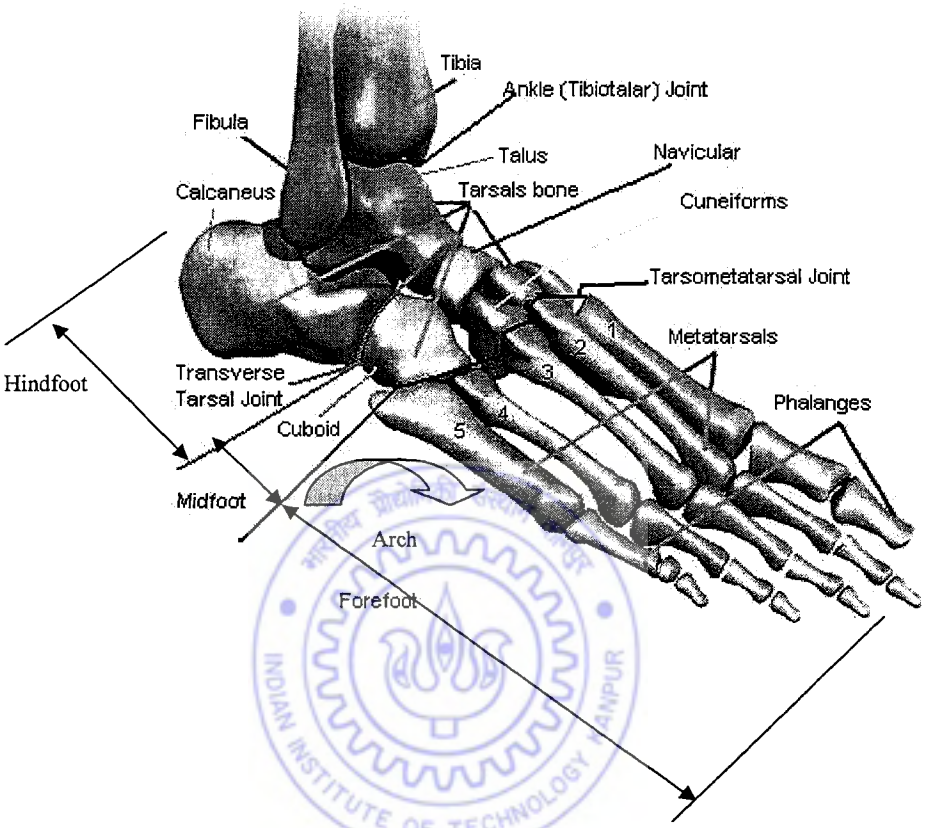

Figure 2.1: Skeletal of the foot and its division.

The back part of the foot consists of heelbone called calcaneus, which is the largest bone of the foot and is connected to the talus and forms subtalar joint, which allows the foot to rock from side to side. The set of five bones namely talus, calcaneus, cuboid, navicular and cuneiforms (just below the ankle joint), are called tarsalbones and work together as a group. These bones fit together in a unique way to form multiple joints [42]. During twisting of the foot in one direction by the muscles of foot and leg, these bones lock together and form a very rigid structure, while twisting in opposite direction, they become unlocked and allow the foot to conform to the surface, the foot is contacting. The tarsal bones are connected to the five long bones of the foot called metatarsals. These two groups of bones are fairly rigidly connected, without much movement at the joint. Finally, there are bones of the toes and phalanges. The

joint between the metatarsals and the first phalanx are called the metatarsophalangeal joint (MTP) and the movement of these joints is very important for a normal walking pattern. Not much motion occurs at the joints between the bones of the toes. The big toe (hallux) is the most important toe for walking [93].

In brief the skeleton of foot is divided into three segments namely hindfoot, midfoot and forefoot. The hindfoot comprises mainly of calcaneus and talus, midfoot contains navicular, cuboid and cuniform while forefoot having phalanges and metatarsal bones. The main joint in the hindfoot is the subtalar joint and in combination with the ankle joint, the subtalar joint allows pronation (coupled dorsiflexion, abduction, and eversion) and supination (coupled plantar flexion, adduction, and inversion) of the foot.

During pointing of toes the ankle becomes unstable because the distance between the bony stabilizers of ankle becomes larger hence it then relies more on the soft tissues including ligaments to continue to provide stability [97]. At birth the mechanical structure of the foot is predominantly soft tissue. The connection of the bones to a skeletal structure takes place with transformation of cartilage to bone.

Ligaments are soft tissue that attach bones to bones and are very similar to tendons, which attach muscles to bones and are made up of small fibers of collagen material. The collagen fibers are bundled together to form a rope-like appearance. Both ligaments and tendons occur in different sizes and are made up of many smaller fibers. It is also observed that thicker the ligament (or tendon), the stronger is the ligament (or tendon).

There are six major ligaments (Figure 2.2) that hold the ankle in place, four of these are located on the lateral part of ankle and attach to fibula. Most common of this ligament is called Anterior (front) Talo Fibular ligament (ATFL). The second one, which connects calcaneus to fibula is called Calcaneal – Fibular ligament, the third ligament, attaching fibula to the back of talus, called the Posterior (back) Talo – Fibular ligament and the fourth is called Syndesmotic ligament, which connects fibula to the tibia. Other ligament, which is infront of the ankle, is the capsule of ankle joint and helps in keeping the ankle from sliding forward along with other ligaments. The final stabilizing ligament which forms a triangle is on the inside of ankle and is known as Deltoid ligament and is the strongest ligament in the body attaching malleolus with

talus. Apart from this, many small ligaments hold the bones of the foot together and form part of the joint capsule, around joints of the foot.

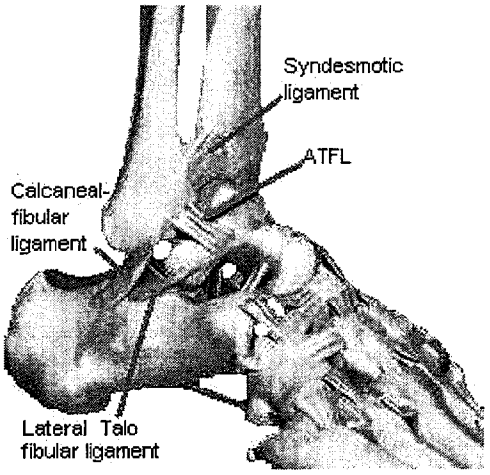

Figure 2.2: Major ligaments acting on the ankle joint.

The achilles tendon [73] is the most important tendon for walking, running, jumping and attaches calf muscles to the calcaneus for allowing toes to rise up. The foot which is a segmented structure can hold the load only if it is built with arch as such has three arches namely medial longitudinal, lateral longitudinal and transverse arch. The shapes of the bones and ligaments maintain the arches of the foot, muscles and tendons also help in supporting the arches [36]. On the sole of the foot a large broad tendon called plantar fascia connect calcaneus to one of the smaller muscle of calf, this tendon which is primarily a media structure, keeps the arch of the foot supported and provides support to foot with every step. The toes have tendons that bend the toes down and straighten the toes. The anterior tibial tendon allows raising the foot and other two tendons, which run from behind the lateral malleolus help in turning the foot outward.

Mechanically a muscle is an active system or a source of generator and its prime function is to generate force apart from maintaining posture, stabilizing joints and generate heat. However if it is deactivated, it still retains passive mechanical properties. Muscle tissue is endowed with some distinctive functional properties that enable it to perform its duties. These properties include excitability, contractibility, extensibility and elasticity [59]. An externally applied force will cause a deenergized muscle to stretch, so that a characteristic force – displacement curve is

generated. Such characteristics are common to many physiological tissues. Tendon and ligaments show this general behavior of stretch under load and it can be recognized that these characteristics define the storage properties of tissue [14]. In foot mostly skeletal muscles are present and are responsible for the movement of foot skeleton. [84]. The ends of these muscles are attached to bone, cartilage, or ligament by fibrous tissue called tendons. The muscles of the foot are classified as either intrinsic or extrinsic. The intrinsic muscles are located within the foot and the extrinsic muscles have their origin in the lower leg. The stronger muscles in the lower leg whose tendons connect in the foot cause most of the motions of the foot. Muscle has elastic properties and so the tendons and skeletal elements to which muscles are attached [4]. Contraction of the muscles in the leg is the main way that we move out feet to stand, walk, run, and jump. There are numerous small muscles in the foot and most of these are arranged in layers on the sole of the foot, called plantar surface where they connect toe, move toes and provide padding underneath the sole of the foot. The major muscles acting on the foot are shown in Figure 2.3.

The achilles tendon, which is an extension of two calf muscles, run down from the back of lower leg and attach with calcaneus thereby connecting strong leg muscle to the foot. It gives an ability to rise up foot and toes and facilitating the act of walking. The muscles peroneus tertius and peroneus brevis help in evertion of foot, the former also helps in dorsiflexion while later assists in plantar flexion of foot. The peroneus longus, planter flexes, everts and helps in keeping the foot flat on ground. Both extensor hallucis brevis (EHB) and extensor hallucis longus (EHL) help in extending the great toe, but the later also assists in foot dorsiflexion.

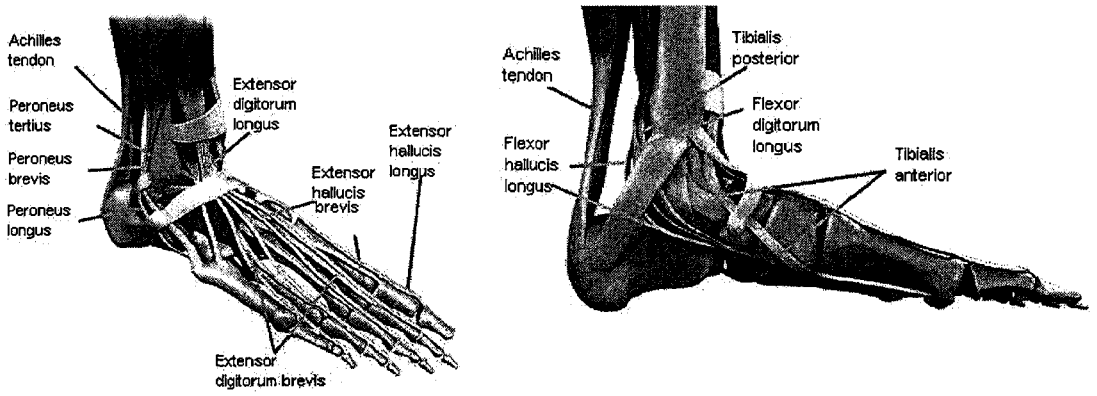

(a) (b)

Figure: 2.3 Major muscles acting on foot (a) top view (b) medial view

The muscle extenser digitorum longus (EDL) is the prime mover of toe extension and acts mainly at metatarsophalangeal joint and dorsiflexes the foot. The tibialis anterior (TA) and tibialis posterior (TP) which are acting on foot as shown in Figure 2.3 (b) support the medial longitudinal arch and inverts the foot, the former acts as a prime mover of ankle dorsiflexion, while later is a prime mover of ankle plantar flexion. The muscle flexor digitorum longus (FDL) and flexor hallucis longus (FHL) both plantar flexes and inverts the foot, the former help in foot griping at ground and the later flexes great toe at all joint and push off muscle during walking.

2.2 Biomechanics

The biomechanics can be defined in many ways; the most common definition [30] [52] is " the study of functional behavior of the living structure under the action of external and internal forces". Biomechanics plays a very important role for patient care and rehabilitation under the framework of pathophysiology [100]. Disease can be characterized by the control hierarchy of the individual who is unable to cope fully with deviations from normal healthy condition, resulting from internal and or external stresses, either because of deficiencies in the control system itself or because of the inability of the plant to respond adequately for changes in information flow. The patient's state, as seen by an observer, is formalized in a model, in which health status, diagnosis and treatment are related through target variables (symptoms) and policy instruments (treatment variables) to the well being of the patient in terms of his own value system (welfare function). The model permits an objective evaluation of the patient's status and the relative effectiveness of alternative therapeutic procedures through optimization of the welfare function [30]. With in this framework, biomechanics play four major role [30] as follows:

1. To quantitatively analyze the relationships between structure and function of living tissues in health and disease.

2. To derive from these analyses reliable and sensitive indicators for mechanical performance of biological systems and thus a more realistic basis for the construction of patient models and the patient care.

3. To define adequately tissue-transducer interfaces for the purpose of measuring these indicators more reliably by noninvasive, or at least, nontraumatic techniques.

4. To define the physical properties of living systems in such a way that reliable, long term internal and external prostheses/orthosis can be designed and produced economically.

Under above aspects of biomechanics, substantial effort for the design and development of appropriate transducer is emphasized with particular consideration to the clubfoot problem.

The main function of the soft connective tissues is to perform mechanical activities like, to transmit or resist forces [3]. The skeleton of the bone provides a major part for the stability of a body structure. However for structures which does not have bone, their stability is provided by soft connective tissue In clubfoot the alignment of different bone segments is not proper and hence it result in lack of stability. The poor alignment of these bones is associated with symptoms like arch pain, heel pain, ankle pain and variety of other postural related symptoms. Foot, leg and back discomfort are common among those with poor foot alignment especially if they are active or stay on their feet all day on hard surfaces. An orthosis, designed properly, decreases the risk of poor tissue alignment and improve the malalignment of bone in foot and help in remedy of associated unwanted symptoms.

There are considerable differences between mechanical properties of different types of tissues. These differences are caused by variations in the proportions and types as well as in the geometrical configurations of the components that constitute the various tissues. And hence when analyzing the mechanical properties of a particular tissue, the measured properties is highly dependent on its morphological characteristics at all levels of its shape and size.

The complexity of the analysis is further increase, when a functional unit consisting of different types of tissues is studied. The purpose of this study is to observe the biomechanical functions of soft connective tissues, such as muscle, tendons and joint ligaments, in relation to forces arising either from internal or external sources. One of these functions is to transmit forces from muscles to bone or from bone to bone. Another one of this is to protect other components in joint and consists of stabilization of joints. These tissues never function alone and always work in conjunction with other tissue and hence are in interaction with other tissues.

Stress values of the magnitude of the breaking strength for collagen material, which is the basic constituents unit of different tissues are never reached in such tissues under normal physiological condition (tissue activities). Hence it is necessary to study the parameter under which failure of mechanical strength of this tissue occurs, one such parameter is the tensile strength and the corresponding strain value of different major tissue which are of our interest are tabulated below [103].

S. No.	Tissue	Ultimate tensile strength Newton/mm^2	Strain
1	Skeletal muscle	0.3	1.4
2	Spongious bone	1.2	0.006
3	Compact bone	150	0.015
4	Tendon	60	0.10

Table 2.1: Mechanical properties of different tissues

Biological materials under load demonstrate viscoelastic behavior [29] and this viscoelastic property allows biological tissue to absorb different amounts of energy when loaded at differing rates. Whether the energy capacity before failure is increased or decreased with an increasing loading rate, can be determined only when the failure criteria are identified. The absorption of energy into a material usually results in a temperature rise within that material.

Biomechanics has found its greatest application in orthopaedic, rehabilitation, and muscular skeletal system. One branch of biomechanics is the gait analysis or human motion analysis [99]. The most common terminology of human motion analysis is the gait cycle, which is defined as the period from heel contact of one foot to the next heel contact of the same foot. This cycle is divided into stance and swing phases, with further subdivisions of each phase. Stance phase is subdivided into initial contact, loading response, mid stance, terminal stance, and pre-swing, while swing phase is subdivided into initial, mid, and terminal swing [75]. Each sub phase is accompanied by a change in position, ground reaction force, and / or internal muscular force. A walking gait cycle of a normal healthy subject is shown in Figure 2.4. On an average, the gait cycle is about one second in duration with 60% in stance and 40% in swing. The stance phase is further divided into an initial double stance, followed by a period of single stance and then a final period of double stance. Double stance indicates that both feet are in contact with the ground; single stance is the period when only one foot is in contact with the

ground. During walking, there is a period of double stance and in running, this period is called, flight phase, during which neither foot is in contact with the ground. During early part of stance phase, the heel is in contact with the ground, progressing to foot – flat during single stance and then to the forefoot contact during final double stance phase ending with toe – off.

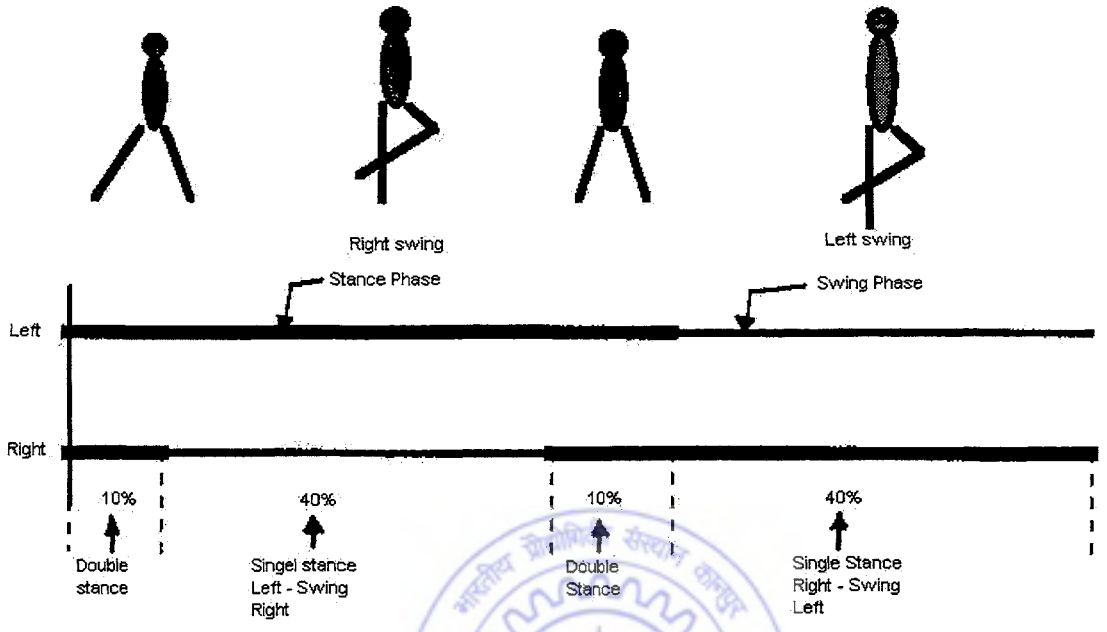

Figure 2.4: Gait cycle of a walking subject

During double stance, the weight is transferred from one foot to other. During single stance, the body center of gravity (c.g.) passes over the foot in preparation for shifting to the other limb. Walking is defined as a series of falls from one limb to the other and it is obvious that the greatest danger of an actual fall is during this period of transferring weight. The above is valid for normal healthy person only, however the gait cycle is greatly varied for different pathological conditions of foot. For example in clubfoot, the equines gait is characterized by the forefoot, striking the ground first and then the lateral contact area, progressing to the posterior in some cases, while in other the heel never contacts the ground.

The goal of an efficient gait is a smooth progression of the body c.g. with minimal oscillation during the gait cycle.

2.3 Ankle biomechanics

In biomechanical study of human ankle joint [77], ankle is considered to be made up of two rigid free body segments (Figure 2.5), namely talus alone and the talus plus hindfoot having two joint, talocrural or upper ankle joint (Tc) and talocalcaneonavicular or lower ankle joint (Tcn). Both Tc and Tcn joints are considered to be simple hinge joint, one allowing flexion and extension of talus relative to shank while other permit inversion and eversion motion of hindfoot relative to talus [1]. The three-dimensional biomechanical models of this ankle joint whose dimensions were based upon cadeveric anthropometrics data were analyzed for gait cycle during stance phase of normal locomotion of subjects. The axis of rotation in embalmed cadaver material was determined by optical method, which involve fixing of one segment while rotating the adjoining segment and the point of least motion indicate the location of axis, in this case fixing of tibia and rotating talus in flexion–extension give stationary points medially and laterally on the talar body through which Tc axis was assumed to pass. In addition joint profile information was also collected by profile gauge indicator. The Tc axis system was defined as fixed relative to the shank segment and the Tcn axis system as fixed relative to the hindfoot segment. The Tc flexion–extension axis which is positive from medial to lateral direction was used as the ZTc axis with an origin situated midway between the medial and lateral malleoli. The ZTc axis together with vector passing through the origin, and perpendicular to the sole of the foot, define the YZTc plane. The XTc axis which is positively directed from posterior to anterior is then defined by a vector normal to the YZTc plane and passing through the origin. A similar procedure was established for Tcn inversion–eversion axis whose positive direction was considered from anterior to posterior and the origin was defined as the point on the Tcn axis midway between the anterior and posterior talocalcaneal articulation. The free body diagram of Tc and Tcn joint system and joint forces together with relative orientation of Tc and Tcn axes are shown in Figure 2.5 (a) and (b).

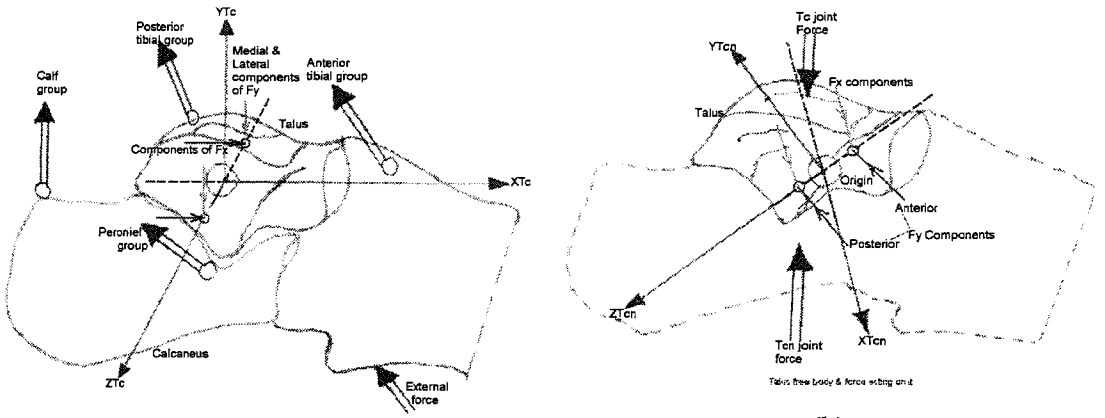

Figure 2.5: Forces acting on free body of (a) talus and calcaneus of foot (b) talus of foot (**See color section**)

This mechanical measurement for anatomical studies were necessary with a view to reduce unknown loads in the ankle to a level, at which an equilibrium solution during gait analysis could be obtained. The Tc joint facets are slightly bicondylar and the X and YTc forces were divided into medial and lateral components acting through points on ZTc axis ±1.0 cm on either side of the origin. The Tc force was assumed to act as a single force along ZTc axis as shown in above figure. Similarly the Tcn facets were also made up of two compartments, posterior talocalcaneal and anterior talocalcaneal plus talonavicular. The X and YTc joint force components were assumed to pass through points on ZTcn axis ±2.0cm on either side of origin. This gives two components, having X and YTcn joint forces. The choice of points on each Z-axis through which the joint force components were assumed to pass was not arbitrary. The origin for each system approximately divided the respective joint facets into two compartments, the points on either side of origin were chosen to be centrally situated in the compartments and the actual dimensions were based upon cadaver data.

Of the twelve major muscles acting on foot across Tc and Tcn joints, as illustrated in anatomic study of foot (Figure 2.3, a, b.), the plantaris and peroneus tertius were neglected, being small or absent. The remaining muscles were combined into four groups namely peroneal, anterior tibial, posterior tibial and calf group, which are acting on Tc and Tcn joint as shown in Figure 2.5(a). Hence five components of joint force acting on each joint system provide sufficient necessary components for force action, transmitted by the two joints. These joint forces together with four muscle group comprises a total of fourteen unknowns. Two mathematical models were formulated known as, model I and model II to predict the same. In model I, only

two muscles groups out of four muscles groups, namely calf group and anterior tibial group were considered while in model II, all the four groups were considered. These two models were solved for equilibrium condition of stance phase, considering free body for Tc and Tcn system, which gives Tc joint forces, as plotted in Figure 2.6.

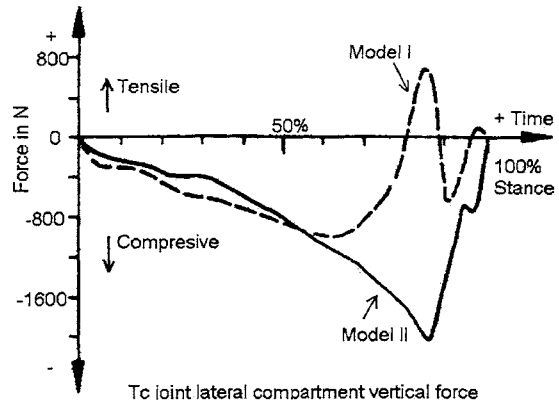

Figure 2.6: Tc joint's vertical force on lateral part of foot

As during stance phase of normal locomotion, the ankle joint forces are always of compressive nature and from the plot of model I, the vertical components of Tc joint force changes abruptly from compressive to tensile and back again to compressive at 85% of stance phase, but in model II the plot is of compressive nature through the gait cycle and the joint compressive force are maximum at about 90% of stance phase. This concludes that model I is incomplete and unacceptable while model II represents realistic musculoskeletal ankle joint system under some acceptable assumptions.

Hence for level walking, model II is suitable for the study of effects of ankle pathology, upon gait and is useful for investigating the behaviors of ankle joint under some limitations.

2.4 Foot biomechanics

The principles of biomechanics in the lower extremity must be understood before attempting to proceed for the design of orthosis devices.

The segmented foot structure [51] can be considered as a set of linkages, joined at rigid or flexible joints. Deformation of the foot is restricted by the plantar aponeurosis (mid and fore foot's bottom portion) and by the ligaments at each joint. This structure is a strong supporter of the longitudinal arch of the foot, a function that it shares with the ligaments and the intrinsic and extrinsic muscles of the foot. The functions of the plantar aponeurosis are to assists in absorbing midtarsal joints force and to maintain longitudinal arch of the foot.

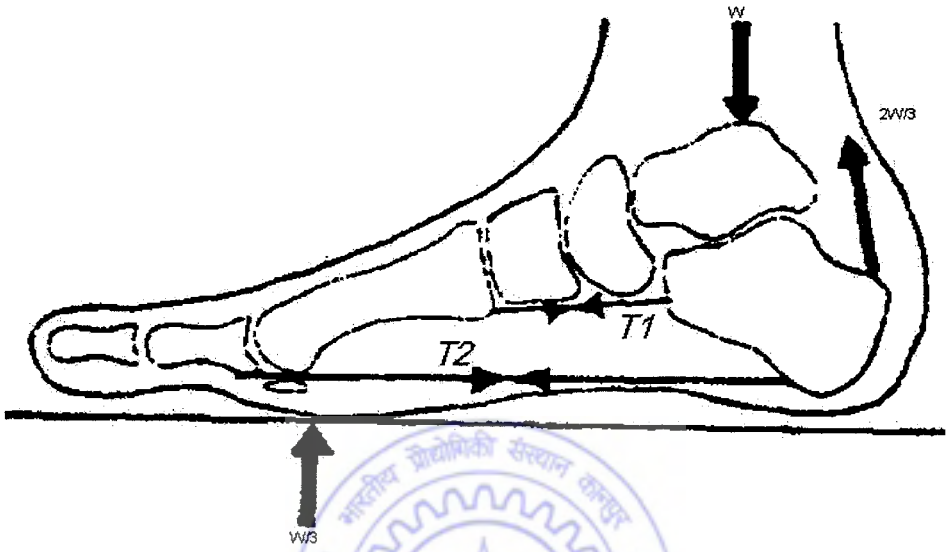

Figure 2.7: Segmented foot structure and acting force during normal standing position

As shown in Figure 2.7, a downward principal force on the talus is counteracted by an upward force on the toes and metatarsal head along with an upward force on the calcaneum. The two upward directed forces produces moments, which tend to deform and flatten the longitudinal arch. These moments can be countered either by the bending stiffness of the bones of the arch and their joints or by the horizontal forces tending to tie the forefoot and heel together. These forces *T1* and *T2* are generated in passive structure (plantar aponeurosis) and by the active contraction of intrinsic and extrinsic muscles.

Figure 2.8 shows a two dimensional medial foot's biomechanical model, having first metatarsal, cuneiform, navicular, talus and calcaneus bony segments which are considered to be rigid and mass less.

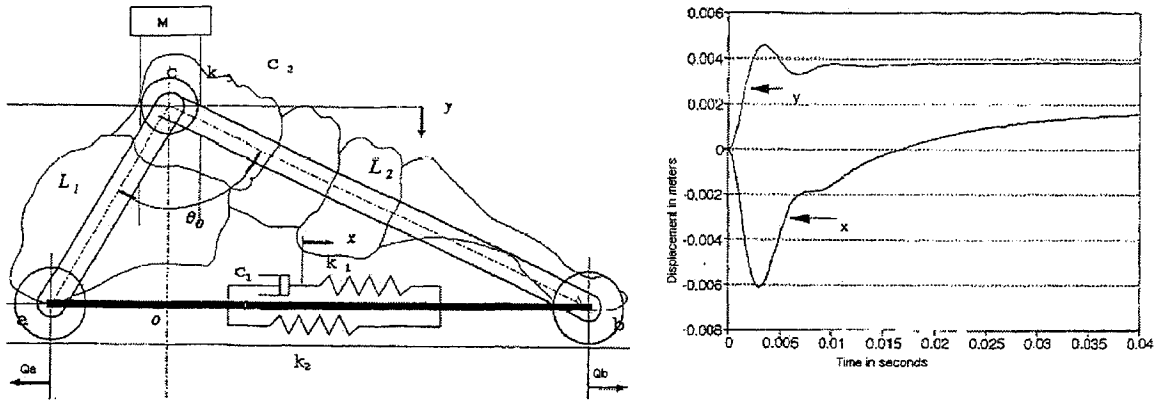

(a) (b)

Figure 2.8: Two dimensional medial foot (a) biomechanical model (b) displacement vs. time plots of plantar fascia

Because of large articulation surface of talus and calcaneus we assume it to be a rigid joint. The medial longitudinal arch is represented by plantar aponeurosis and is modeled as a viscoelastic Kelvin model having *k1* and *k2* as the spring constant and *c1* as the damping coefficient. As most of the biological tissue behave like viscoelastic material [30] and hence in biomechanics, generally viscoelastic model are presented. The major advantage of the above model is that the plantar aponeurosis can be separated from rest of the foot function – the arch of the foot and the intrinsic and extrinsic ligaments between the arch and hence the relevant parameters can be easily determined from the experiment. The tibia, which is attached to, the talus is assumed to be a freely rotating joint and can move only in vertical direction depending upon the loading condition. During loading, at internal joint of the bony segment the deformation is restricted by plantar aponeurosis ligaments at each joint. The spring effects of the arch shape of the foot, the intrinsic muscles of the foot, the tendons of those extrinsic muscles all are modeled as one torsional spring (*k3*) and one torsional viscous damper (*c2*). These are connected in parallel between two rigid linkages (l1 and l2) of the bony structure of foot. Because of small inertial forces, the inertial effects of the linkage system were neglected. A downward vertical force produced vertical displacement (y) of ankle joint and a corresponding displacement (x) between *c1* and *k1*, which is the viscoelastic properties of the plantar fascia. The other parameter can be determined from the constraint equations and are therefore functions of x and y.

Kim and voloshin [51] mathematically formulated the above two dimensional biomechanical model based on total energy principal, having five unknown parameters *k1, k2, k3* and *c1, c2*. For obtaining value of these parameters they performed the experiment on above model with many set of external load and finally they averaged each value of these parameters. By using this calculated value they plotted the displacements of ankle joint and plantar fascia under load Vs time and shown in Figure 2.8 (b). From this figure it is observed that initially the displacements behave in a transient way and subsequently become steady state. This model was effective for investigating the foot geometry (lowering of the arch), they concluded that by lowering of the ankle joint degenerated the load bearing capacity of the foot proportional to the amount of the distance lowered. But the described model is suitable only for stance phase of the gait cycle

2.5 Pathological anatomy of clubfoot

The clubfoot is associated with poor bone alignment [74], the navicular, cuboid and calcaneus bone segments are medially displaced and found to be in inversion (turned around their axis) in relation to talus. The finding of the clubfoot study shows that the main anamali resides in the medial and plantar deflexion of the neck and head of the talus. It is also stated that the anamalies of the muscles, tendons and ligaments of the foot and leg were secondary to the skeletal deformity.

In all clubfoot, the talus is in severe flexion [74], its body is small and altered in shape, as compared to normal talus. The calcaneus is adducted and inverted underneath the talus and most of its anterior tuberosity is under head of the talus and not lateral to it, as in normal feet. Its body is consistently in severe flexion and slightly medially bowed. The cuboid is medially displaced and inverted in front of the calcaneus. The navicular is uniformly flattened or laterally wedge shaped and severely displaced medially and inverted. The cuneiform and metatarsals are very abnormal and its anterior joint are very narrow or absent, whereas the middle joints are varied in size [24].

The fibers in the muscles of the clubfoot are smaller in size and the muscles triceps surae, tibialise posterior, flexor digitorum longus (FDL), and flexor hallucis longus (FHL) are found to be in contracted position. In the ankle, the tendons of the tibialise anterior, extensor digitorum longus, and extensor hallucis longus are severely displaced medially while the

tibialise posterior tendon is large and further enlarged down to its insertion. The medial talocalcaneal ligament is markedly thickened while the anterior part of the deltoid ligament and plantar calcaneonavicular ligament are short and thick in all clubfoot. The posterior tibiotalar, fibulotalar and the fibulocalcaneal ligaments are also thick and short and often matted together with abundant fibrous tissue.

Hence it is concluded that for varus deformity of heel in clubfoot, the inversion and adduction of calcaneus is accounted and this heel varus along with adduction and inversion of navicular and cuboid are responsible for clubfoot supination. The forefoot skeletal components are adducted in front of the medially displaced navicular and cuboid while the cavus is resulted because of more flexion of first metatarsal than the lateral metatarsals.

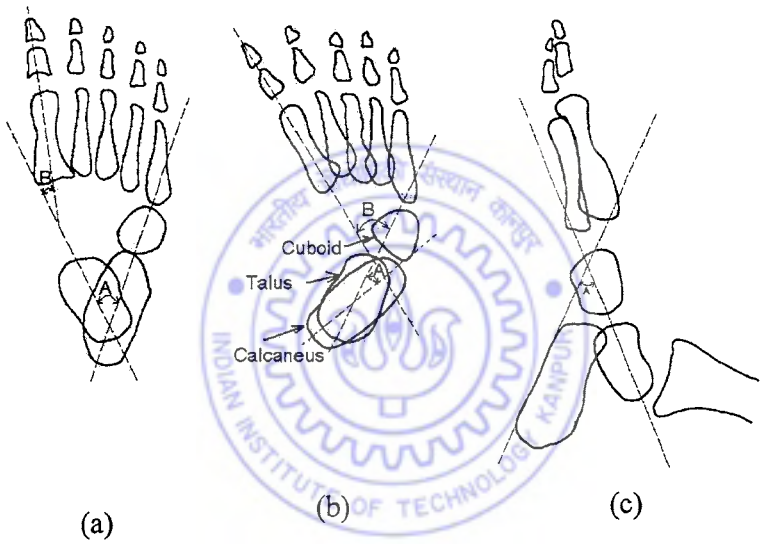

Figure 2.9: Foot skeletal (a) top view of normal foot (b) top view of clubfoot (c) lateral view of clubfoot (*Courtesy of Dr. I. V. Ponseti*)

Figure 2.9. (a) and (b) Represent the top view of normal and clubfoot's skeleton while Figure 2.9 (c) Shows the side view of clubfoot skeleton. In this Figure *A* represent the talocalcaneal angle and *B* represent talonavicular angle in top view of foot skeleton.

Figure 2.9 (c) Represent talocalcaneal angle (*A*) in its side view. The normal range of the talocalcaneal angle (*A*) in top view is about 20-40 degree, while it is abnormal if $A<20$ degree.

Similarly the normal range of this in lateral view is about 25 – 50 degree while it is abnormal if A<25 degree [74] [49] [64].

2.6 Functional anatomy

The tarsal joint kinematics in the normal foot has been studied long before [93], but even today much controversy exists among expert about how they actually move [74], according to Dr. Ponseti, Farabeuf shows that the calcaneus moves under the talus by rotating around the inner fibers of the interosseous talocalcaneal ligament in normal foot. He showed that as the calcaneus rotates under talus, it adductes, flexes, and inverts, because of the inclined contours of the talocalcaneal joint surface. As the foot goes into varus, the calcaneus adductes and inverts under the talus, while the cuboid and the navicular adduct and invert in front of the calcaneus and the talar head [39]. The displacement of the tarsal bones in a child's clubfoot in most extreme positions is caused by excessive pull of the tibialis posterior abetted by the gastrosoleus, tibialise anterior, long tow flexors, and plantar muscles. Farabeuf states that the deformity of talar neck is not " a morphological caprice of nature", but results from the "moulding" caused by posteriorly displaced and inverted navicular. Also the skeletal deformities in infants are usually reversible, if not treated timely, the subluxations of the navicular and the cuboid, worsen with the progressive displacement of these bones. Although these deformities may be corrected and if proper care is not taken for maintaining the correction, the "deforming power" of soft tissues causing recurrences [94].

According to ponseti, Huson shows that the tarsal joints belong to a "constraint mechanism", this is because the motion of the tarsal occurs simultaneously and if one of them is blocked, the others are functionally blocked too.

During plantar flexion (Inman, 1976) [74], the head of the talus swings towards the medial side and the calcaneus inverts. The axis is not fixed but changes continuously throughout the range of movement. It may alter considerably during the arc of motion and differs significantly among individuals.

Lundberg (1988,1989) [74] stated that, external rotation of the leg is followed by external rotation of talus, causing the calcaneus to invert and abduct slightly owing to slope of the posterior talocalcaneal joint. Inversion and slight abduction of the calcaneus cause inversion

and adduction of the cuboid and the navicular, thereby raising the arch of the foot and thus inducing the first metatarsal to flex so that it reaches the ground.

In clubfoot, the kinematics are greatly altered [53] by the severe shortening of the medial and posterior tarsal ligaments and by the tightness of the tibialis posterior and gastrosoleus muscles. The fibrotic and contracted deltoid ligament holds the calcaneus in inversion. The navicular is held severely medially displaced and inverted by the fibrosis of the tibionavicular, the plantar calcaneonavicular ligaments, and the pull of the tight tibialis posterior tendon.

The mobility of the posterior part of the foot is very restricted. In severely supinated tarsus of clubfoot, the range of passive motion varies greatly. Only a few degrees of passive abduction can be obtained in the tarsus of rigid feet, while 20 to 30 degrees are reached in less severe cases. Even with forced abduction, the tarsus of an untreated clubfoot cannot be moved to a neutral, normal position.

In clubfoot the tarsal bones are displaced and the tarsal joints are misshaped, but they are congruent in its position and both the talonavicular and talocalcaneal joints are in close-packed position. The deformed surfaces of the calcaneocuboid joint are in restricted contact only. The joints become incongruent when correction of the deformity is attempted unless the correction is made gradually for several months allowing for the gradual remodeling of the joint surfaces. The joints of the anterior part of the foot are nearly normal even though the first cuneiformetatarsal joint may be medially slanted in some clubfeet [74] [82].

In clubfoot, active and passive mobility of the anterior part of the foot and toes is only slightly restricted. In most cases at birth, the forefoot adduction can be corrected to a near normal position and the metatarsals can be flexed and extended throught a normal range of motion. Even in cases where the first cuneiformetatarsal joint is medially slanted, the first metatarsal can be moved into the proper alignment with the other metatarsals, thereby eliminating the cavus [69].

The supination and pronation movement in normal child foot is very free but attempts to pronated a clubfoot will only pronate the forefoot but not the hindfooot. Also the hindfoot ligaments are very stiff and the axes of motion of the tarsal joints are severely medially displaced resulting from the extreme medial rotation and displacement of the tarsal bones.

Hence the medial ligaments can be stretched. The inversion of the calcaneus, navicular and cuboid will gradually decrease, as the foot is further abducted. Forceful pronation of clubfoot will cause a breach in the midfoot and increase the cavus.

In severe clubfoot with very stiff medial tarsal ligaments, a full reduction of the medial rotation of the nevicular is not possible. The calcaneus cannot be fully abducted to its normal position under the talus. A partial correction of the tarsal displacements, however, is sufficient for a good function of the foot.

2.7 Proposed approach for clubfoot correction

An approach based on non-surgical method that utilizes basic biomechanics with the utilization of modern available technology is presented in this dissertation. The dissertation forms an interdisciplinary "bridge" among engineer, surgeon, radiologist and patients as shown in Figure 2.10. Theories of multidisciplinary subject like foot anatomy, image analysis, rapid prototyping, solid modeling, instrumentation and finite element analysis is applied in this research.

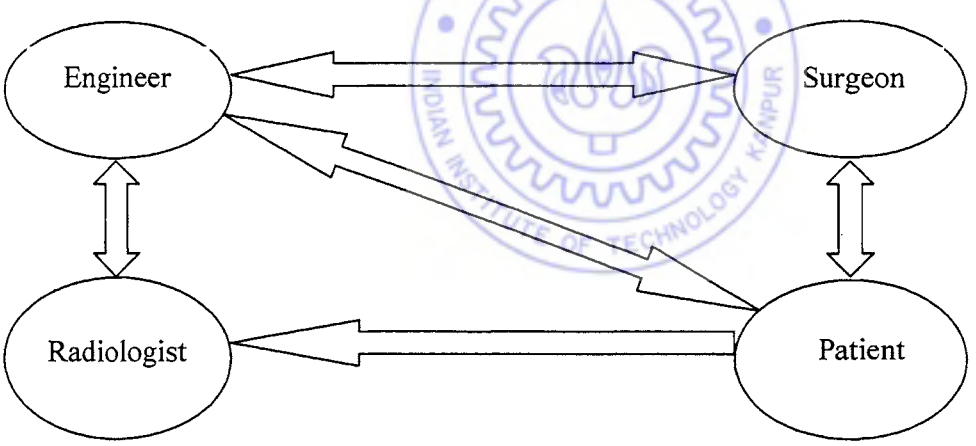

Figure 2.10: Relationship among related professionals

Medical research on clubfoot from anatomy and surgical correction point of view is already reported in many medical journals. A brief introduction of clubfoot correction using external fixator (UMEX-frame) is given in *Appendix A*. In literature survey, study on non-surgical correction particularly that utilizes AFO, designed using CAD / CAM techniques, is not at all reported in any medical and engineering journal. To facilitate the challenge and to determine

the possibilities of success on newborn babies, a research study involving non-surgical correction of clubfoot deformity in newborn babies was initiated in conjunction with noted orthopaedic surgeons of Kanpur city (India).

By studying the related literatures, development of an ankle foot orthosis (AFO), capable of quantitative corrective force with suitable low weighted polymeric material is planned in this research. The research goal is broken down into following specific task.

2.7.1. Biomechanics of clubfoot correction

From the knowledge of foot anatomy and its biomechanics, consultation with orthopaedic surgeons was done and correction is planned in following steps:

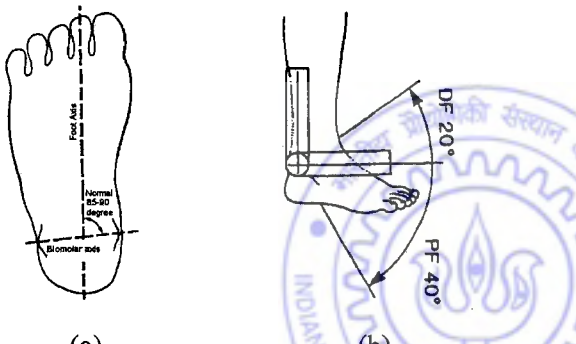

(a) (b)

Figure 2.11: Normal foot angles (a) tope view (b) dorsiflexion (DF) and plantar flexion (PF)

From Figure (2.11a) and (2.11b), we know that for normal foot, the angle α between biomolar axis and foot axis is in between 85°-90°, also the range of dorsiflexion (DF) and plantar flexion (PF) β_1, β_2 is 20° and 40°. Hence we should develop a technique by which gradually we can achieve β_1, β_2 to be nearly 0° and α to be nearly 90°.

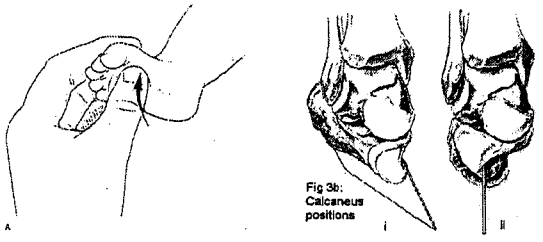

(a) (b)

Figure 2.12: Clubfoot's (a) dorsiflexion (DF) (b) calcaneus position (*Courtesy of Dr. I. V. Ponseti*)

Figure (2.12a) shows that dorsiflexion correction technique that will help in removing the equines of foot, the force should be applied in such a way, so that the varus of the heel (figure 2.12b) is removed and the calcaneus should come to the normal position.

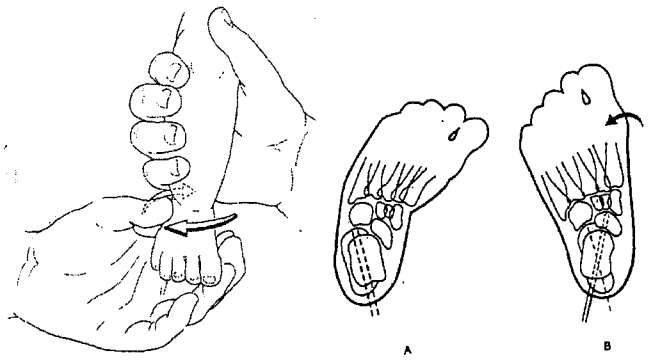

(a) (b)

Figure 2.13: Clubfoot abduction (a) outer view (b) skeletal view

After performing this treatment the next correction procedure of forefoot abduction is started as shown in Figure (2.13a). The effect of the applied force should correctly align the misaligned bone as shown in Figure (2.13b). In this corrected position the navicular and talus are aligned properly and the cuboid will come in line with calcaneous as in case of normal foot

Hence according to biomechanics the present dissertation tries to develop the above techniques for proper clubfoot correction.

2.7.2. Clubfoot modeling

The CT/MRI scan data of the patient is taken from the hospital with the help of orthopaedic surgeon and radiologist, and image processing of these data is done in MIMICS software. The clubfoot STL file is exported for its prototype fabrication in fused deposition modeling (FDM-1650), rapid prototyping system. The fabricated clubfoot prototype is further used for producing silicon rubber foot model and experimental study on this rubber foot model for strain measurement due to corrective load is performed. These study give an idea about the clubfoot behaviors due to application of corrective load.

The next step is the solid modeling of clubfoot, for which initial strategy is prepared, according to which the point cloud data of clubfoot is sampled, over which curve are fitted and a smooth surface model is generated in imageware surfacer software. This model is then imported in I-DEAS software, where all unstitch surface patches are stitched together and its watertight geometry (solid model) is created. This solid model is imported in FEM software, for simulation study, which further provides information regarding the clubfoot behavior due to corrective load application.

2.7.3 Fabrication of AFO

The third step after model study is the design of AFO and its prototyping. As our research at this stage is limited to customization and hence after proper AFO design strategy, its surface model using deformed foot point cloud data is created. The surface model is then converted into solid model and is fabricated in FDM-1650, whose testing is done on silicone foot model and after its success, actual testing is extended to patient.

Chapter 3

CLUBFOOT MODELING

This chapter deals with the adopted methodology for the current research work. The chapter mainly describes the acquisition of medical imaging data of patients, Computer Aided Design (CAD), Rapid Prototyping (RP) and Silicon Modeling of clubfoot. The flow diagram in Figure 3.1 Represents the main sequence of operations to be performed for conducting the present research. Initially, we scan the adult foot with CT and after successful integration of CT with RP we extend the techniques to MRI for baby's clubfoot.

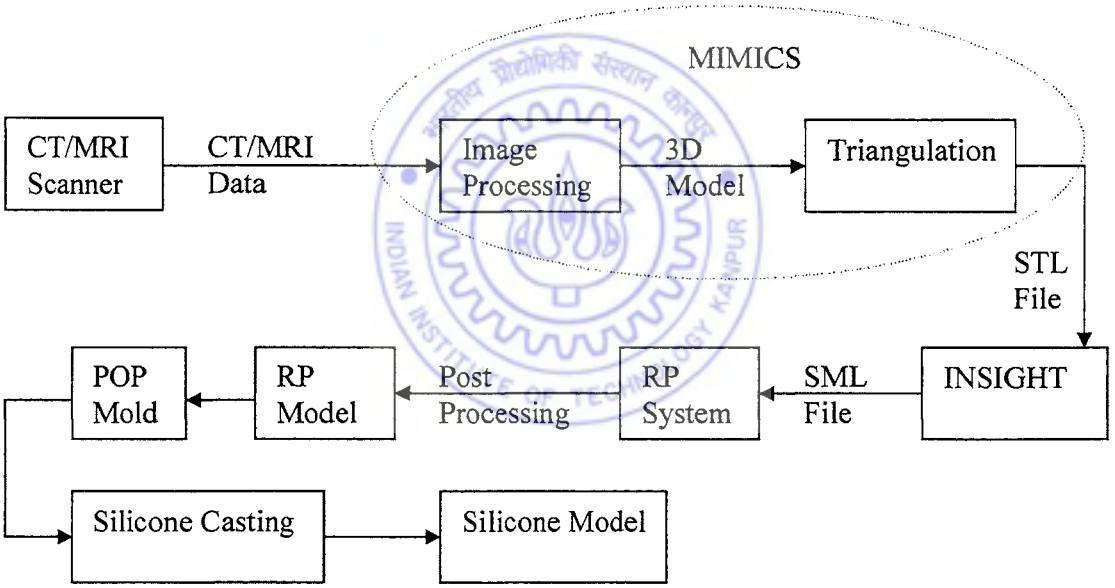

Figure 3.1: Integrated approach to produce Silicone 3D foot model.

3.1 Computed Tomography (CT) data acquisition

Computed Tomography (CT) is an important reverse engineering strategy that can provide the necessary digital data for computer-aided design and rapid prototyping system [27]. In present

work the sequence of the CT scan data of human foot is acquired from SIEMEN spiral CT machine, in Digital Imaging and Communication (DICOM) format in the following steps:

(a) CT Image acquisition

X-ray computed tomography (CT) is an imaging modality that produces cross-sectional images representing the X-ray attenuation properties of the body. Image formation of a cross-section is shown in figure 3.2 and is based on the following procedure:

A set of lines is scanned covering the entire field of view [91] using a thin X-ray beam with fan beam geometry as shown in figure 3.2 (b). This process is repeated to obtain line attenuation measurements for all possible angles and for all possible distances from the center. Based on all these measurements, the actual attenuation at each point of the scanned slice can be reconstructed. Fig. 3.2 (c) shows the cross section of an imaged object, and projected in θ direction. The $f_\theta(s)$ shows the projection data.

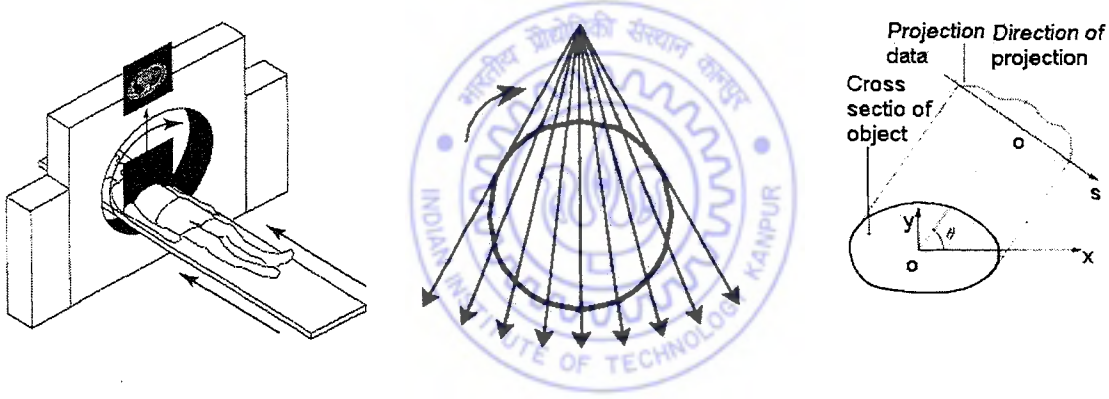

(a) (b) (c)

Figure 3.2: Schematic representation of (a) CT scanner (b) fan-beam geometry (c) cross-section of an imaged object and its projection

In spiral CT or helical CT, the X-ray tube rotates continuously around the patient and at the same time the patient is slowly translated through the gantry. Hence, the tube describes a helical movement with respect to the patient. This allows continuous rapid volumetric data acquisition over large areas of the body. Data interpolation schemes developed for spiral CT, permit the reconstruction of images with arbitrary position and spacing for three-dimensional

display. The attenuation of monochromatic X-ray in non-homogeneous objects like human body is governed by [89]:

$$I = I_0 e^{\int \mu(x)dx} \tag{1}$$

where

I_0 = Initial X-ray beam intensity before entering the tissue.

I = Final X-ray beam intensity after coming out the tissue.

μ = Attenuation coefficient of an X-ray passing through the tissue whose value is considered to be different at each position in the tissue.

dx = Length of small tissue element.

A quantity proportional to the total attenuation coefficients along the X-ray path can be obtained when I_0 and I are measured. Further more, when various points of the projections are measured from various directions the distribution of the attenuation coefficients μ of the cross-section can be obtained. The CT image at this stage is only the distribution of CT numbers, which are proportional to the attenuation coefficient and are stored on a magnetic disc as an array whose elements are called " pixels". The spiral CT images consist of 512 * 512 pixels representing the CT number, which is expressed in *Hounsfield Units* (HU) [89].

$$\text{CT number (in HU)} = 1000 \times \frac{(\mu - \mu_{water})}{\mu_{water}} \tag{2}$$

where μ is the linear attenuation coefficient. With this definition it could be drawn that air, water and bone have CT numbers of –1000 HU, 0 HU, and 1000 HU respectively. Objects with higher density than water will have positive CT numbers and objects with lower density than water will have negative CT numbers.

(b) Patient preparation

Normal male adult subject who as per his wish, was ready to scan his feet for delivering CT-scan data for the research purpose was prepared for the scan. All metallic material and clothing around the patient's foot are removed because they can produce artifact and interfere with the

clarity of the images. Since the scan technique is painless the patient was not given any medication. The radiation dose given to subject is kept minimal during scan.

The patient is laid on the movable examination table of Somatom Esprit Siemens spiral CT machine of local diagnostic center in India, such that he is lying in supine position "feet first" and the sole of the foot must be perpendicular to the table. During the scan the patient was advised to minimize any body movement by remaining as still and quiet as is possible. This significantly increases the clarity of the CT-images.

(c) Scanning

After patient preparation, his registration information is entered at the Diagnostic Main Console (DMC) and scanned projection radiographs, which are used for localization, are acquired and the appropriate ranges for set of table locations for the study are defined. Image acquisition parameters are then chosen from a present protocol menu. A typical protocol for foot spiral CT is: "Extremities foot" mode, 130 kV, 60 mA and 14 seconds [33].

Scanning is then started and 134 slices, each of 4 mm thickness, are acquired. These 2-dimensional foot slice images can be read into a 512 by 512 by 88 voxel 3-dimensional arrays. The reduction from 134 to 88 slices is due to the overlap information of foot angular region.

Once the CT images are archived to optical disk, they are transferred over an Ethernet network to a remote Diagnostic Satellite Console (DSC, from Siemens medical system, Inc.) for further processing and reconstruction. On the host system these image data sets, are reviewed for quality assurance, using Metal Artifact Reduction (MAR) and Volumetric Analysis Reconstruction (VAR) software and further reprocessed for CT image reconstruction by selecting an algorithm.

(d) Image reconstruction

The measurements obtained by a CT scanner will result in a series of attenuation coefficients which are functions of position and angle, $\mu(s,\theta)$. These are called the measurement space. Computer manipulation is required to convert this into the image space, $g(x,y)$, to determine the distribution of attenuation coefficients and hence the density distribution within the object.

There have been many different algorithms developed over the years to accomplish this task, few of them are Matrix Inversion, Iterative Approximation, Back Projection and Filtered Back Projection (FBP).

Filtered Back Projection (FBP):

This is one of the most popular algorithms in use today [89]. It involves two parts, back projecting along the projection lines used, and filtering the image, thus removing the blurring, caused by back projection.

i) Back projection

Here attenuation along a line through the object is known by simply assigning the mean attenuation coefficient, given by equation (1), to each point along that line. This back projection is repeated for all angles. The attenuation coefficient for a particular point will be built up from all the projections passing through that point. In reality, the image under reconstruction is not continuous, but is composed of discrete pixels. The projection lines will not pass perfectly through the center of each pixel in their path and it is necessary to establish a method for describing the projection line in terms of individual pixels within a matrix [89].

The nearest neighbor interpolation is a simple method for doing this. One begins by establishing a $N \times N$ reconstruction matrix- $g(x, y)$, where N is the number of translation pixels in the s axis. For a given angle θ in measurement space a value of s can be calculated for each pixel in the $N \times N$ matrix as follows:

$$s = x\cos\theta + y\sin\theta \tag{3}$$

The values of s are rounded to the nearest measurement point and out of range values are discarded. These pixels in the matrix can then be assigned attenuation coefficient values from the measurements:

$$g_\theta(x, y) = \bar{\mu}(s, \theta) \tag{4}$$

This process is repeated for each angle and final back projected image is obtained from its average values.

$$g(x,y) = \frac{1}{N_\theta} \sum_{\theta} g_\theta(x,y) \tag{5}$$

ii) Filtering

The above back projection, gives blurred reconstructed image, hence mathematical filtering must be applied to obtain an accurate image. Many mathematical filters are available in choices, the most commonly used is the *Shepp-Logan* filter, which combines a sinc function with the ramp filter. Filtering and back projection both are linear operations, so the order in which they are performed does not matter. However, filtering in one dimension is much simpler tasks than in two dimensions. For this reason, the filtering is applied prior to back projection. Filtering is performed by multiplying the Fourier transform of a waveform by the filter function, the result is then inverse Fourier transformed to produce the filtered waveform.

Once both the filtered and back projections have been performed, the result is a two dimensional array of attenuation coefficients. With the help of (2), these attenuation coefficients are converted into CT numbers in units of Hounsfield.

The obtained 88 CT image slices of different cross section of an adult foot from CT scan is shown in Figure 3.2 for reference.

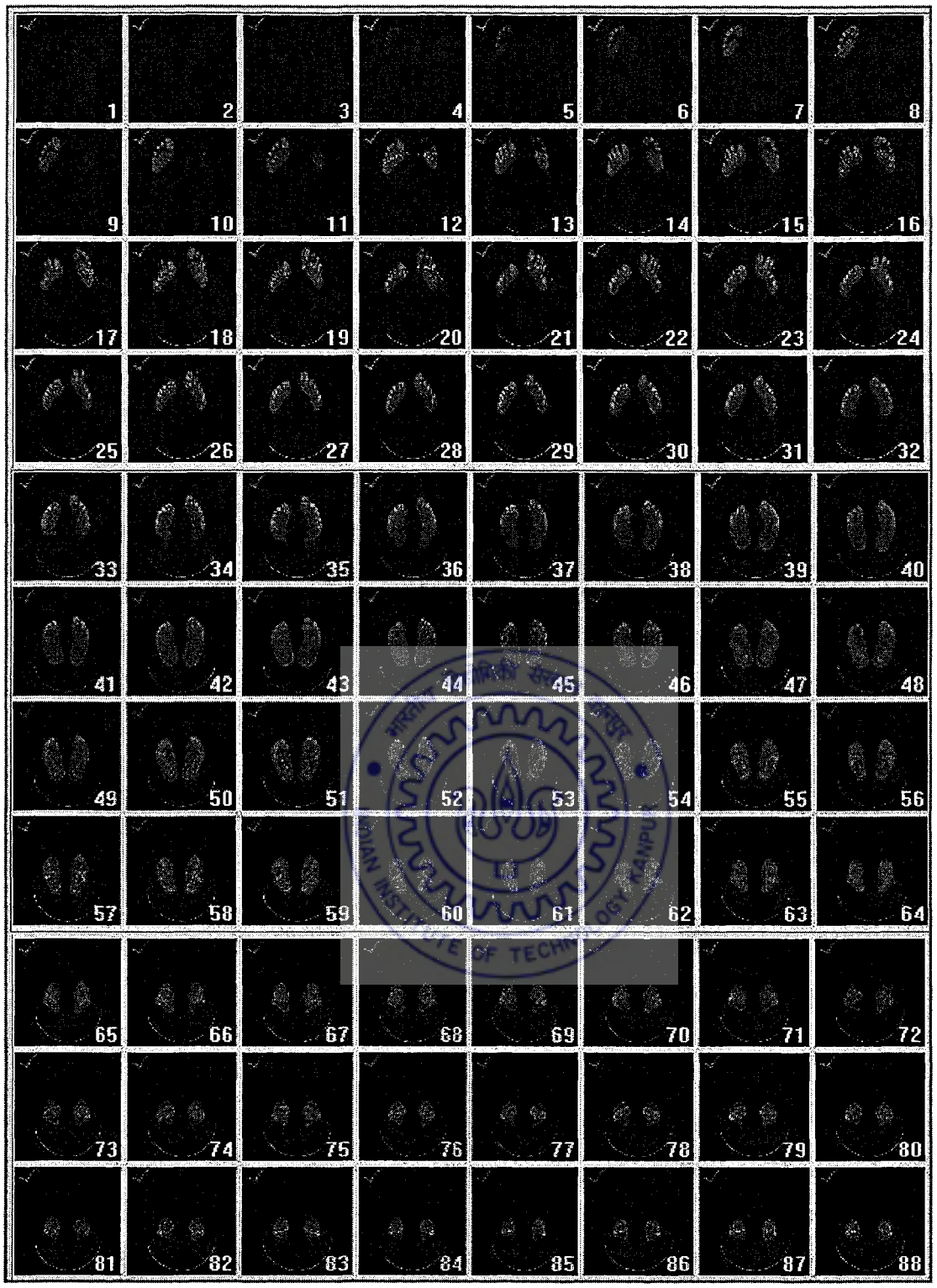

Figure 3.3: CT data of an adult foot in Mimics own proprietary format (mpj format)

3.2 Magnetic Resonance Imaging (MRI) data acquisition

Magnetic Resonance Imaging (MRI) is an imaging technique used primarily in medical to produce high quality images of the inside of the human body [89]. MRI is based on the principles of Nuclear Magnetic Resonance (NMR), a spectroscopic technique used by scientists to obtain microscopic chemical and physical information about molecules. The technique is called magnetic resonance imaging (MRI) rather than nuclear magnetic resonance imaging (NMR) because of the negative connotations associated with the word nuclear in the late 1970's. MRI started out as a tomographic imaging technique that produced an image of the NMR signal in a thin slice through the human body.

3.2.1 Basic principle of MRI

In MRI the nucleus of the atom is resonating under certain conditions in presence of a magnetic field. The two stages that take place during NMR process are [83]:

1. Here the patient is placed in a strong magnetic field and exposed to an oscillating magnetic field in the radio-frequency (RF) region of the electromagnetic spectrum, which causes nuclei in the patient to resonate about their equilibrium position.

2. The RF radiation is then switched off but the nuclei continue to resonate, resulting, the emission of RF radiation from the resonating nuclei within the patient, which can be detected as an NMR signal. Afterward the nuclei return to their original equilibrium position.

Here the RF radiation transmitted through the patient is not attenuated; but, it stimulates the tissue itself to produce a signal. The frequency at which nuclei resonates is directly proportional to the magnetic field strength and is referred to as the resonant frequency or Larmor frequency. The resonance of the nuclei is a complex phenomenon with two principal components, characterized by T1 and T2, relaxation times. These are time constants relating to the exponential decay of two components of resonance and are measured in milliseconds (ms). Alternative names for T1 and T2 are spin-lattice and spin-spin, respectively. There are number of nuclei whose properties enable them to be measured by NMR, but it is the combined sensitivity and abundance of hydrogen, which make MRI possible. Although some tissues may

have a high T1 and T2 or a low T1 and T2, there is no direct relationship between the two relaxation times but the following is always true

T1>T2

The majority of the NMR signals will come from water within the tissues, hence it is the behavior of the water, which determines the values of T1 and T2. It is generally accepted that the concept of free and bound water gives the best understanding of variations in T1 and T2. A proportion of the water in tissue is bound to the surface of proteins and, in consequence, its motion is slowed by proximity to the large molecules, this results in the lowering of T1 value. Other water in the tissue will not be bound to protein and is considered to be free, resulting in a higher T1. The T1 of pure water, equivalent to free water in the tissue, is of the order of 3s. T1 in tissue is much lower than this and will depend on the relative proportions of free and bound water within the tissue, larger the proportion of bound water, lower the T1. It is generally assumed that the increase in T1 in tumor tissue compared with normal tissue is due to a release of bound water, resulting in an increase in free water.

The effect of magnetic field strength on the two relaxation parameters is different. Grey matter, for example, will have a T1 of around 400ms in low-strength magnetic field increasing to over 800 ms in a high-strength magnetic field. Compared with the large variation in T1 with field strength, there is a little variation in T2 and most biological tissues have a T2 values in the range of about 50 - 150 ms, T2 in free water is also longer than that in bound water, resulting in an increase of T2 in lesions, which have more free water than normal tissue.

3.2.2 Preparation of Patients scanning and imaging

All metallic objects on the body are removed prior to obtain an MRI scan and the patient is placed in a magnetic field (Fig3.4) [38]. The scanning requires the patient to lie still for best accuracy; hence, occasionally he will be given a sedative medication to decrease anxiety and relax him during scan. Patient lies within a closed environment inside the magnetic machine. Relaxation is important during the procedure and patient is asked to breathe normally. Interaction with the technologist is maintained throughout the test. The scanning time depends on the exact area of the body studied and patient's cooperation and in our case it ranges from half an hour to an hour. The magnetic field aligns the atoms with a magnetic moment, such as

hydrogen atoms. The hydrogen atoms are then perturbed by an RF signal. As the atoms return to their equilibrium position, they emit their own RF signal with a frequency that depends on the local magnetic field strength. By introducing variable gradients in the applied fields, and taking phase shifts in the signal into account, the hydrogen density within a particular volume can be reconstructed from the RF signal. The information obtained in this way is a measure of the amount of magnetization of the hydrogen in each volume element. This value differs for different types of tissues due to differences in the hydrogen density and its chemical bonds.

During the scan, the RF pulses are applied and the gradients switched on and off so that a number of different NMR signals are produced, which are usually 64, 128 or 256 and recorded in a computer. Generally, spatial information is stored in the phase and frequency of each signal and a two-dimensional Fourier transform (2DFT) of all the signals will produce an image. The image is stored in a matrix of 128×128, 256×256 or 512×512 pixels [83].

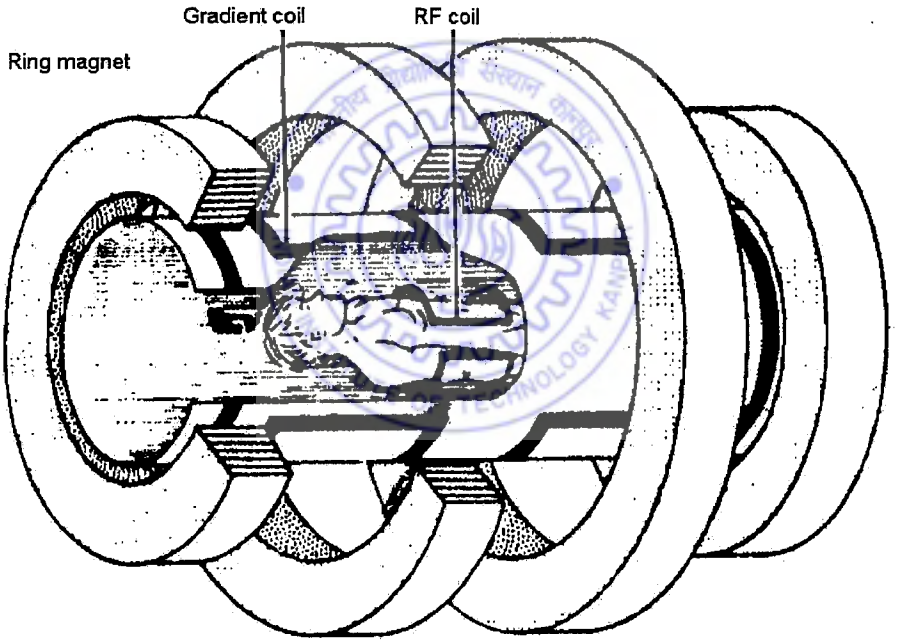

Figure 3.4: MRI equipment with patient

3.2.3 Advantages of MRI over CT scans

MRI is considered to be much more non invasive in comparison to CT scan. Following are some of its major advantages [68]:

- The electromagnetic radiation used to charge the hydrogen atoms is much, lower in energy and much less damaging than the X-ray
- The produced magnetic field does not have any adverse effect on human body.
- There is no limit of the number of MRI scan, a person can have
- MRI can see right through bone to other hard tissue
- It gives images of brain tumors, swelling, bleeding, nerve damage and other disorders that increase the fluid contents of tissue.

After successful accessing of the CT scan data and considering the above advantages of MRI over CT, we used MRI imaging modality for clubfoot data acquisition of newborn baby patients. A total of 7 clubfoot babies of different age and sex were considered for this research study. These Patients having age of 6 days, 1 month, 40 days, 3 months, 4 months, 5 months and 4 years. For the sake of convenience, these Patients shall be here after referred to as Patient I, Patient II, Patients III, Patient IV, Patient V, Patient VI and Patient VII, according to their increasing age. Following are medical scans data of above different patients.

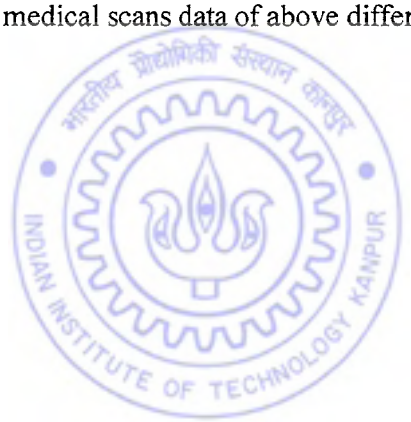

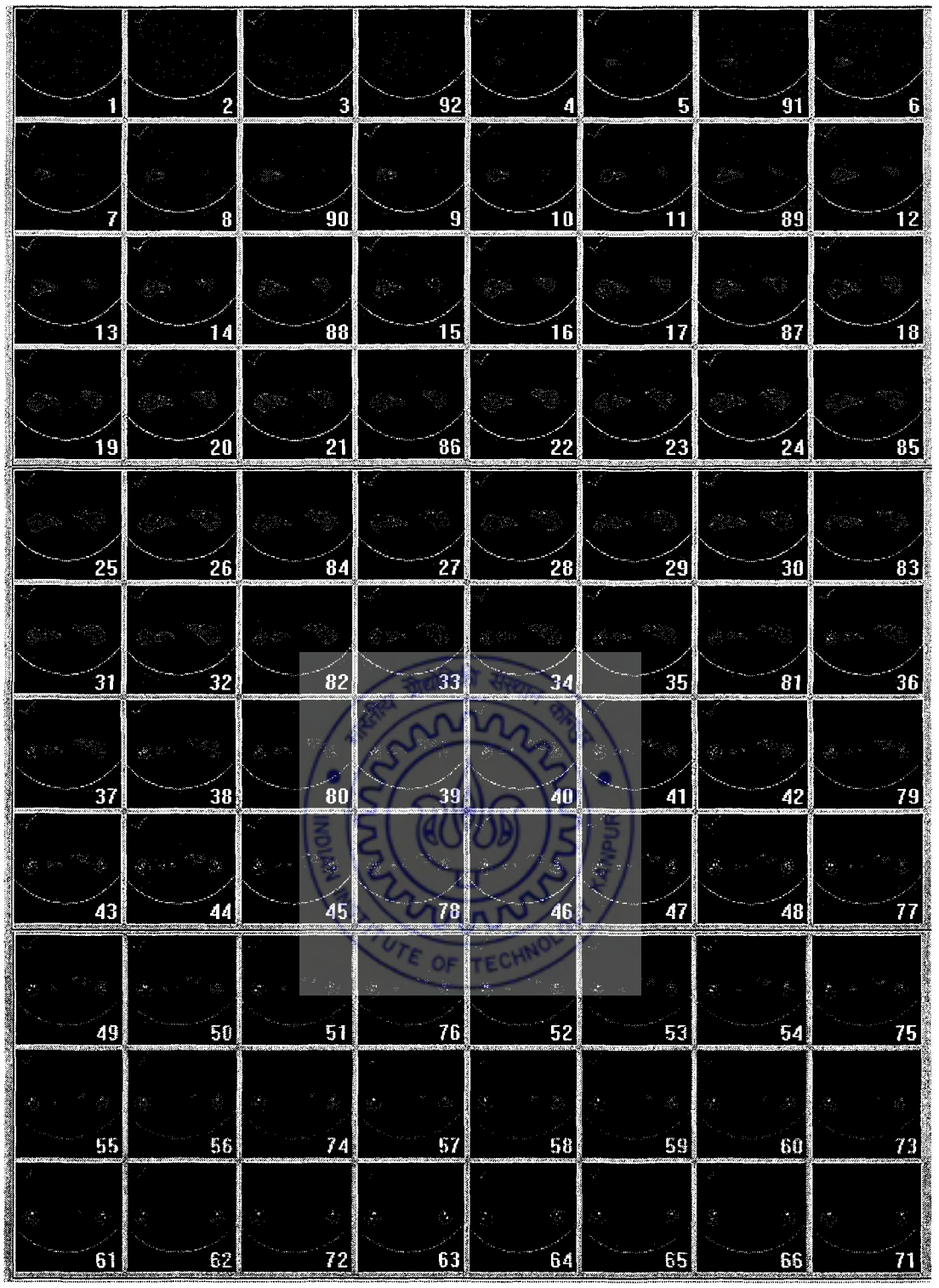

Figure 3.5: MRI scan data of clubfoot of Patient I

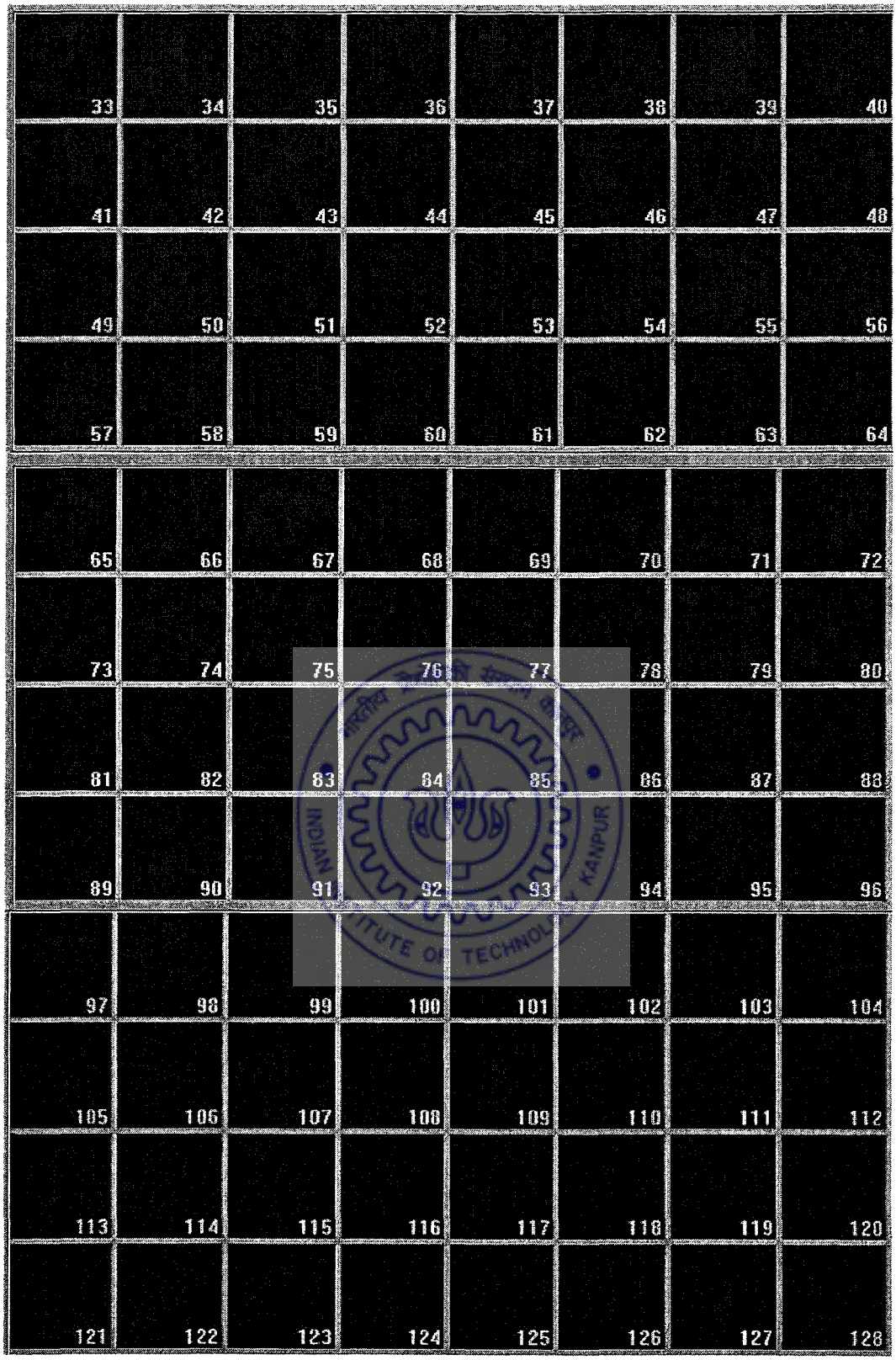

Figure 3.6: MRI scan data of clubfoot of Patient II

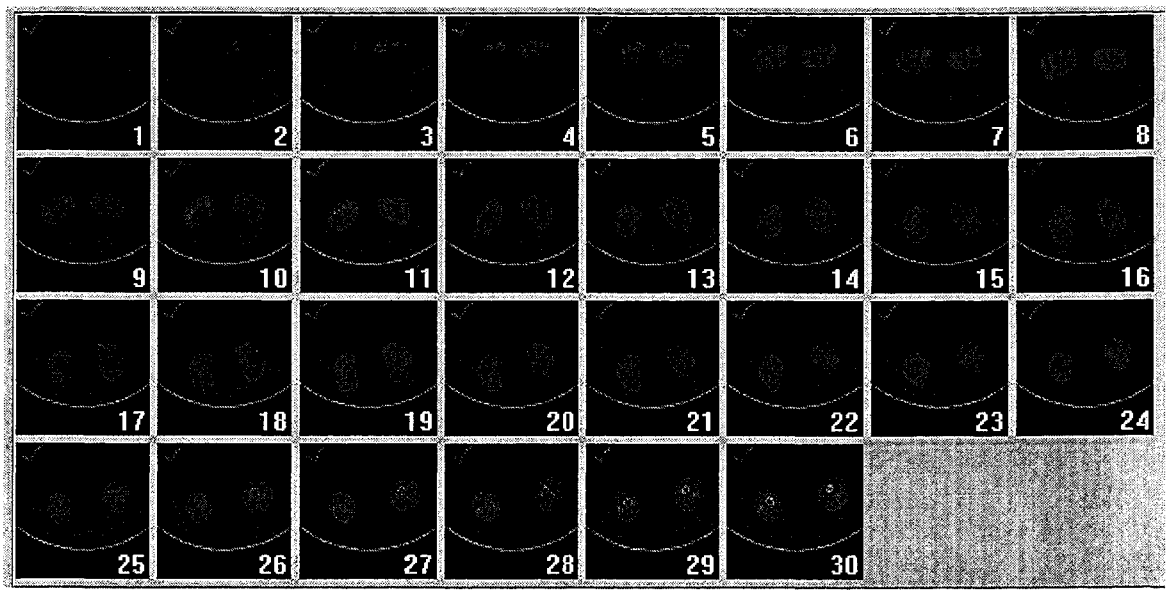

Figure 3.7: MRI scan data of clubfoot of Patient III

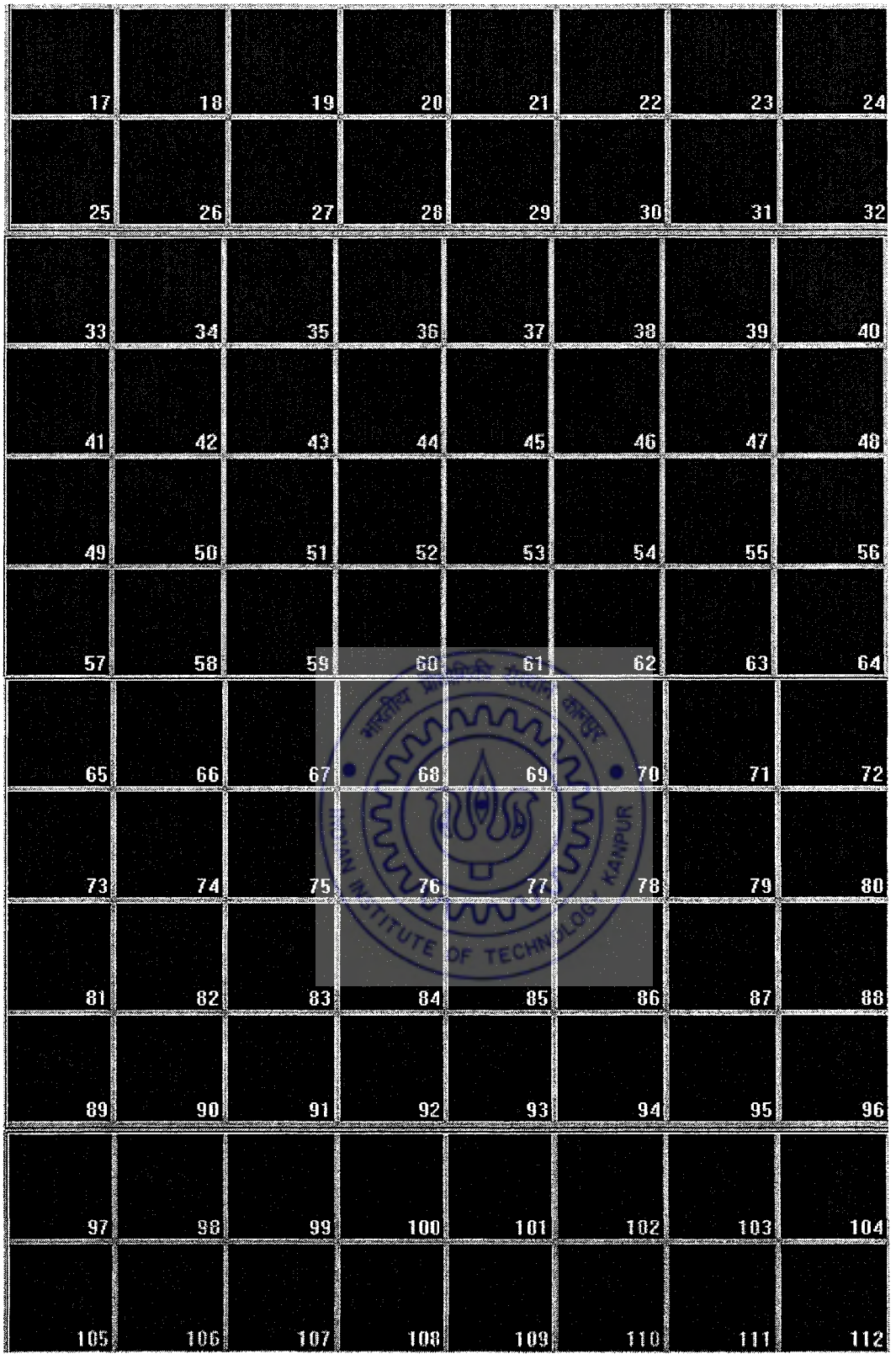

Figure 3.8: MRI scan data of clubfoot of Patient IV

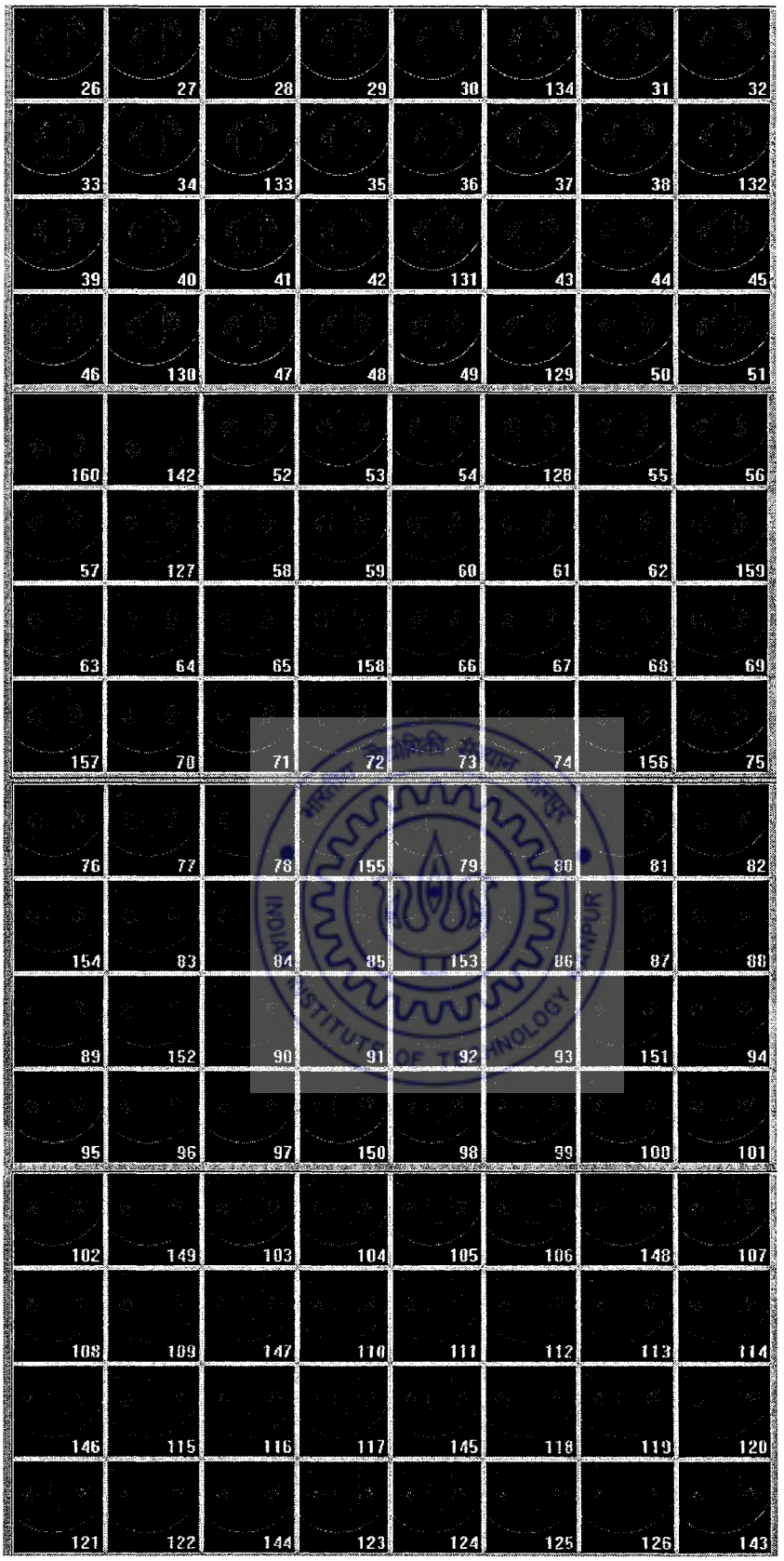

Figure 3.9: MRI scan data of clubfoot of Patient V

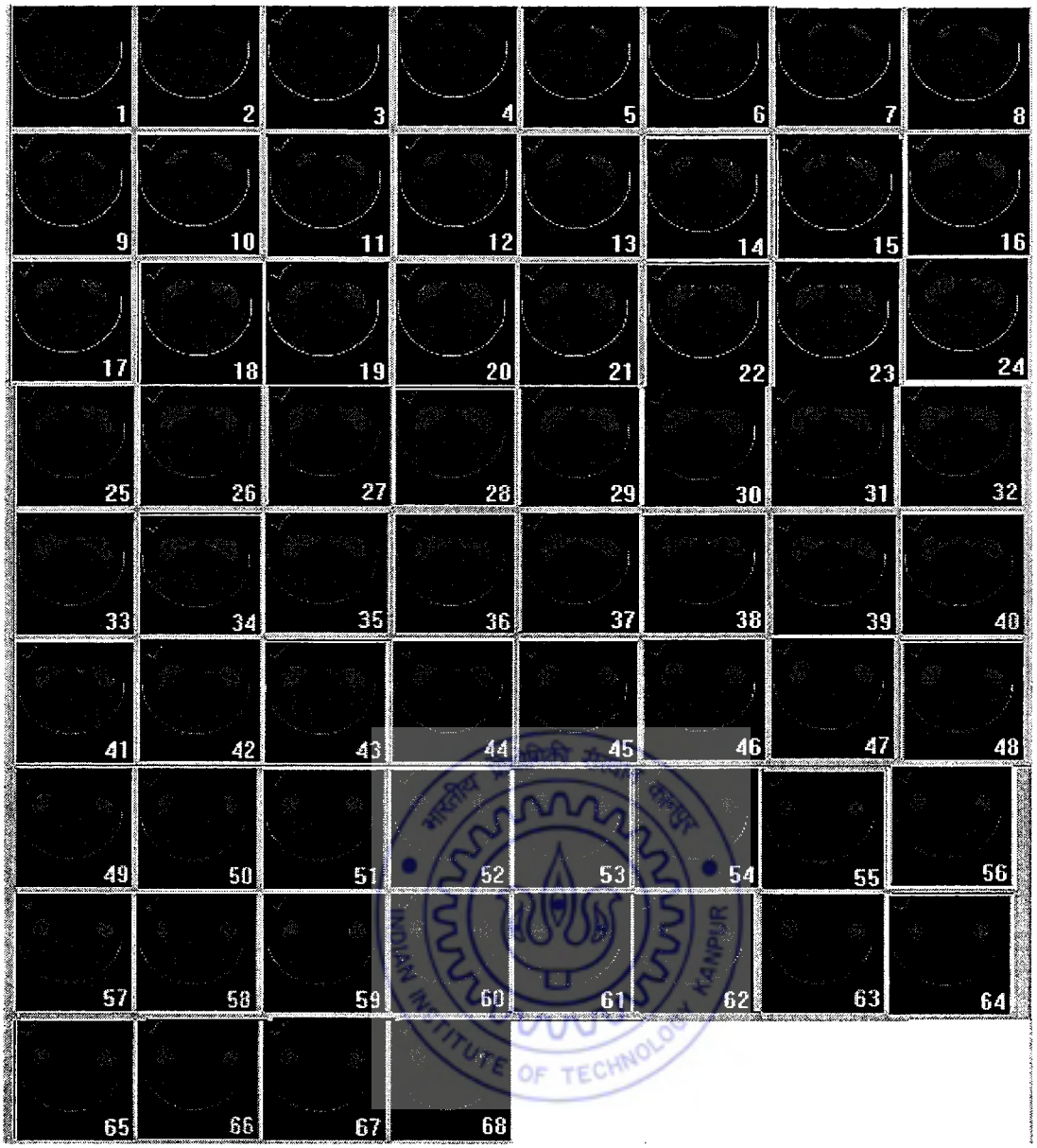

Figure 3.10: MRI scan data of clubfoot of Patient VI

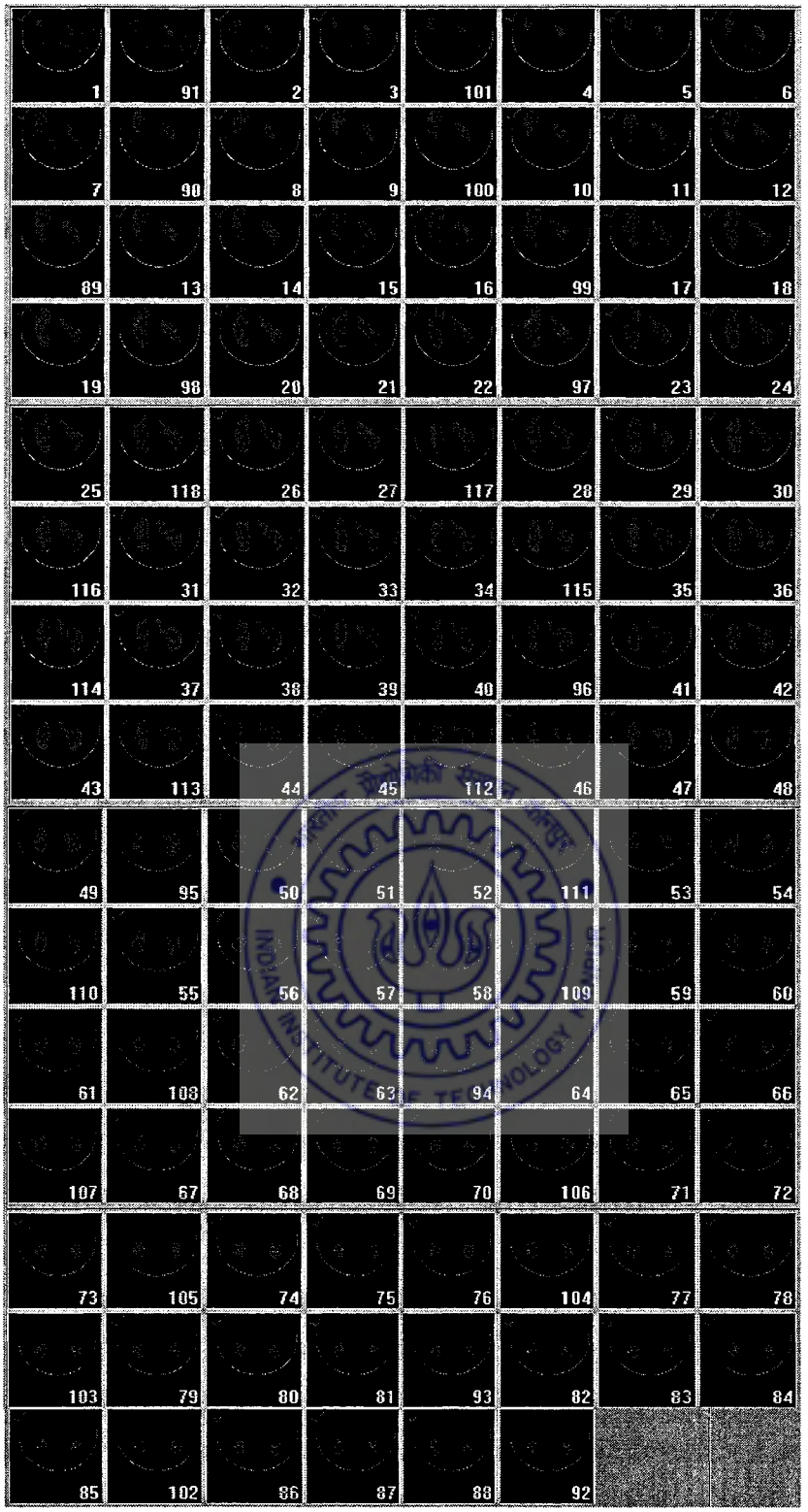

Figure 3.11: CT scan data of clubfoot of Patient VII

3.3 CT/MRI image processing

3D model of real object can be generated, using many different algorithms [54]. In this case the above acquired data are processed with the help of commercial MIMICS (Materialize Inc.) software and the processed data are used to compute 3D foot model. Segmentation is an image enhancement method by which a particular object, organ, or image characteristic is extracted from the image data for the purpose of visualization and measurement. This is a central problem of image analysis because it is a prerequisite for the majority of analysis methods, including image registration, shape analysis, motion detection, and volume and area estimation [66].

The Materialise's Interactive Medical Image Control System (MIMICS) software is used for visualization and segmentation of above CT/MRI images data where user can modify the image by definition [60]. In our case the procedure of image segmentation can be separated into following different classes:

i) Data visualization ii) Thresholding
iii) Image editing iv) Region growing
v) Boolean operations vi) 3D image calculation/generation.

Initially, all the slices of DICOM format CT/MRI images, are brought into MIMICS software and converted into MIMICS project file. Various orientation parameters are selected and all the images are fixed with respect to proper orientation parameter and with "gray value interpolation algorithm" the contrast of the entire 2D slice image data is adjusted.

Threshold is the first action to be performed for creating a segmentation mask. Due to the wide separation of gray scale levels between the high signal intensity of bone and other soft tissues, we define the bone based on a lower and a higher threshold value, so that it can be easily segmented from CT/MRI images [67]. Hence, the bone tissue of interest is defined as having 1350 lower and 2300 upper threshold values in CT image of normal adult foot. The pixel value must be in between threshold values which are, to be part of the segmentation object. Accentuating or deleting all pixels above or below the mentioned threshold value is sufficient to provide the classification required.

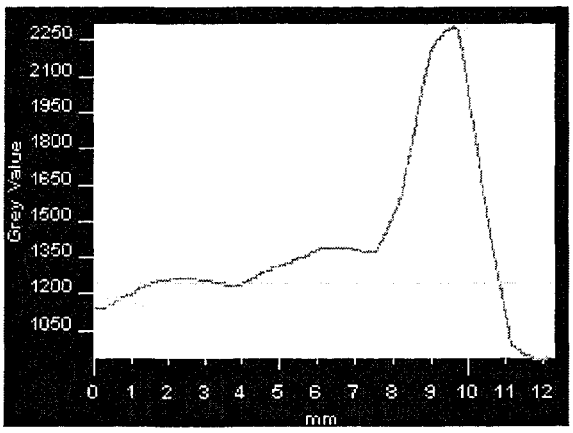

The Figure 3.12 Represents the profile of the gray value having minimum of 900 and maximum of 2300 gray value units. The profile is started from internal zone of tibia bone having gray value of 1140 units, which will reach to a maximum value of 2300 at bone region and then start falling to 900 for soft tissue zone.

Figure 3.12: Threshold profile of bone tissue.

Once a good value of threshold, which brings most of the bone into mask as shown in above profile, is fixed, some image editing operations like erasing and drawing are done and then the region of interest is isolated from the whole image by 'region growing' followed by 'dynamic region growing'.

The region growing limits the region of interest and can help in separating parts. Dynamic region growing allows us to segment cracks in targeted small objects, where following segmentation rule is obeyed [60].

$\left|\hat{i} - i\right| < \delta$ where

$\hat{i}$ = the average gray value

i = the new gray value

δ = the deviation.

In this case according to maximum and minimum threshold values of masks, a threshold value of the created mask will be set automatically. When we select a pixel, creation of the new mask will begin and the MIMICS will start comparing the gray values of the neighboring pixel. The pixels with gray values that obey the above rules will be added to the new mask. In the above rule instead of adjusting the threshold, we specify the deviation from the selected pixel, according to upper and lower threshold values. The deviation means that the region will grow to density values slightly above and below the selected pixel's values. If the deviation is too big we will get all the soft tissues and in case if it is too small we do not get all the regions of

interest. Hence, care must be taken while choosing the deviation value. As our region of interest is the bone, we choose a pixel that lies in the bone, in this way all the bone region of interest is segmented and new masks are created.

After getting different masks, morphological operations like, closing, eroding, dilating etc. [50], are to be performed on different masks. All these functions take or add pixels from source masks and help in getting the real shape. The Boolean operations allow us to make all different kinds of combinations based on two masks, created during region growing and found to be very useful to reduce the work that needs to be done when separating two joints. After performing appropriate Boolean operation (subtraction, union, intersection) on selected source masks, the threshold of the resulting mask is automatically updated according to the values of the selected masks. Figure 3.13 shows two segmented slices of right foot of subject from 88 such segmented slices.

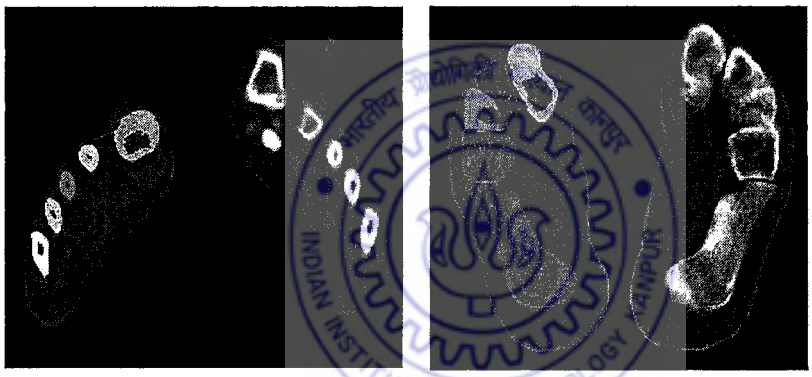

(a) (b)

Figure 3.13: Region grew segmented image of two slices (a) section at metatarsal region (b) section at tarsal region (**See color section**)

After using all above segmentation tools, masks for all regions of interest are finalized and 3D model for high quality is computed.

We have taken a total of 8 patients, imaging data during the research study, two of them was exposed to CT and 6 of them was exposed to MRI, all of them are of different age groups and sex. The image processing of these data is done as explained above and their 15 foot, 3D models were developed and are shown below from Figure 3.14 to Figure 3.22.

Figure 3.14: Skeletal of an adult normal foot (**See color section**)

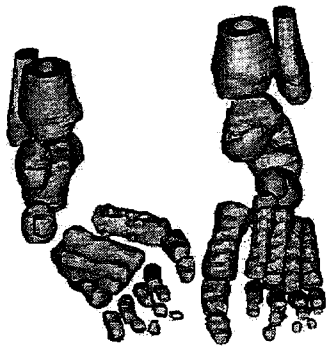

Figure 3.15: Skeletal of unilateral clubfoot of Patient VII (**See color section**)

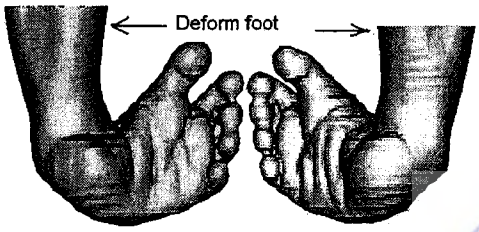

Figure 3.16: Bilateral clubfoot model of Patient I (**See color section**)

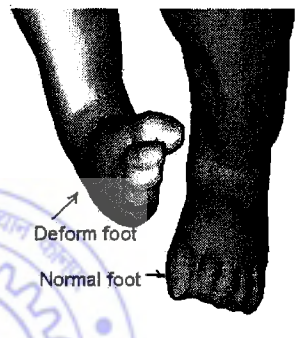

Figure 3.17: Unilateral clubfoot model of Patient II (**See color section**)

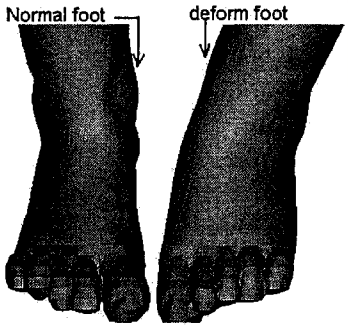

Figure 3.18: Unilateral clubfoot model of Patient III (**See color section**)

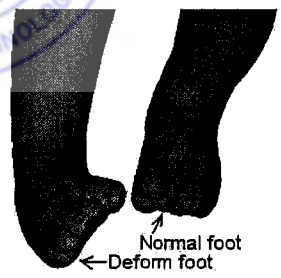

Figure 3.19: Unilateral clubfoot model of Patient IV (**See color section**)

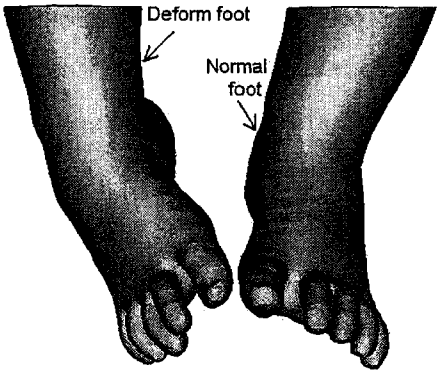

Figure 3.20: Unilateral clubfoot model of Patient V (**See color section**)

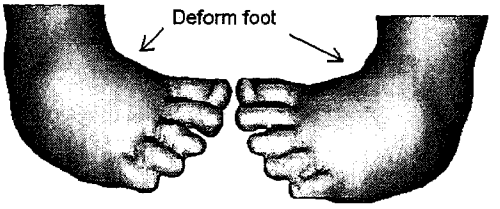

Figure 3.21: Bilateral clubfoot model of Patient VI (**See color section**)

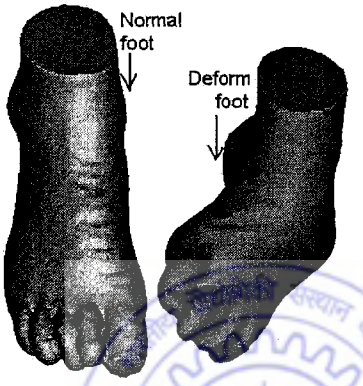

Figure 3.22: Unilateral clubfoot model of Patient VII (**See color section**)

3.4 Geometric modeling

A geometric model provides the complete geometric and topological information of an object [23]. In Geometric Modeling the geometrical construction of an object is done by specialized software such as imageware surfacer and I-DEAS, which we used mostly for solid modeling [19] and rendering appropriate view of clubfoot and Ankle Foot Orthosis (AFO). Modeling and rendering are the basic steps in geometric modeling [54]. It comprises parametric modeling and solid modeling. Parametric modeling includes wire frame modeling and surface modeling. Surface modeling techniques facilitate description of shape of the objects in terms of their surfaces [26] [106]. Solid modeling though leads to "informationally complete" representations of three-dimensional (3D) solid objects but surface models give detailed information on free form surfaces [58].

Geometric modeling methodologies have been found to be successful in specifying the geometry of complex surfaces such as scalling in sport shoes [38]. The biparametric surface definitions such as Bezier surface, Coon's patch etc provide extensive freedom to the designer for designing complex surfaces [26]. In many practical situations a component is broken up into different surface patches and each patch is defined over a limited region. While doing so it is necessary to ensure the continuity condition among adjacent surface patches [22]. The overall specification of a surface model is usually governed by a set of finite parameters. These parameters in turn, control the shape and size of each surface patch in model [107]. Hence It is convenient and economical to substitute a model for the real object or process which is easier to analyze rather than a real object.

Computer aided design (CAD) normally refers to the activity of geometric modeling, engineering analysis and optimization methodology used for developing engineering components and assemblies [63].

For making solid model several commercial software are available, we are using I-DEAS for developing solid model after preprocessing data through MIMICS and Imageware Surfacer software.

3.4.1 Solid modeling

A valid solid model is one, which is bound, closed, regular and semi-analytic subset of a three-dimensional Euclidean space. A solid model should provide the following mathematical properties [106]:

- Rigidity
- Homogeneous three-dimensionality
- Finiteness and finite describability.
- Closure under rigid motion.
- Closure under regularized Boolean operation.
- Boundary determination.

For representing solid models of a real object, various schemes are available. The most popular schemes for solid model representation are constructive solid geometry (CSG) and Boundary representation (B-rep)

3.4.1.1 CSG and B-rep

A solid is represented as an algebraic expression that uses rigid body motion and regularized set operations. The traditional operations are regularized union, intersection and difference. Regularized set operation requires taking the closure of the interior of the set-theoretic result. In classical CSG a solid is represented as a set-theoretic, Boolean expression of primitive solid objects, of a simple structure. Thereby both the surface and the interior of the final solid are implicitly defined. The CSG representation is valid if the primitives are valid. The surface of a solid is closed and orientable and encloses a volume.

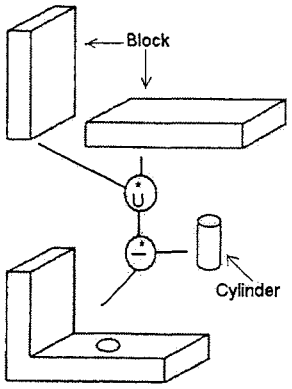

Figure 3.23: Constructive Solid Geometry (CSG)

The traditional CSG primitives are block, sphere, cylinder, cone, and torus. Each solid has a default coordinate system. Using a rigid-body transformation, the solid is positioned relative to a global coordinate system. A Boolean operation then combines the solid with respect to the common coordinate system as shown in Figure 3.23.

Boundary is the primary interface between the solid and surrounding environment

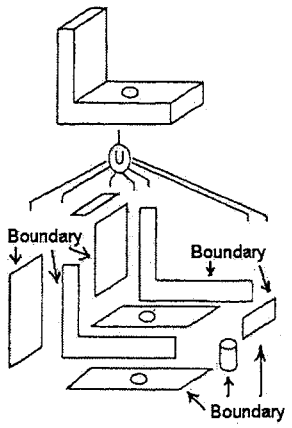

Figure 3.24: Boundary Representation (B-rep)

A B-rep model is based on the topological notion, that a physical object is bounded by a set of faces. These faces are subsets of closed and orientable surfaces. Each face is bounded by edges and each edge is bounded by vertices. Thus topologically, a boundary model of an object is comprised of faces, edges, and vertices of the object, linked so as to ensure the topological consistency of the model as shown in Figure 3.24 [106].

The database of a boundary model contains both topology and geometry.

Topology is created by performing Euler operation [63] and geometry is created by Euclidean calculations. Euler operators are used to create, manipulate, and edit the faces, edges, and vertices of a boundary model. Since topology and geometry are interrelated and can not be separated entirely, any change in topology should reflect in corresponding changes in geometry and vice versa. B-reps may be combined using the regularized Boolean operators, to create new B-reps

If the curved objects are represented by using the exact definitions for the surfaces and curves required for the faces and edges, the resulting boundary scheme is known as exact B-rep scheme. If the curved faces are approximated to a number of planer facets, the B-rep scheme is termed as faceted B-rep or tessellated geometry.

We develop the solid model from computed tomography (CT) and magnetic resonance imaging (MRI) data of patient foot. Based on the availability of surface definitions, as well as the geometric nature of clubfoot, it has been found that the geometric modeling of clubfoot would help the design and manufacturing process of AFO.

We have exported the point cloud data of the clubfoot from MIMICS software and did the surface modeling and solid modeling as described above. Figure 3.25 and Figure 3.26, Shows the various models during solid modeling of patient II clubfoot.

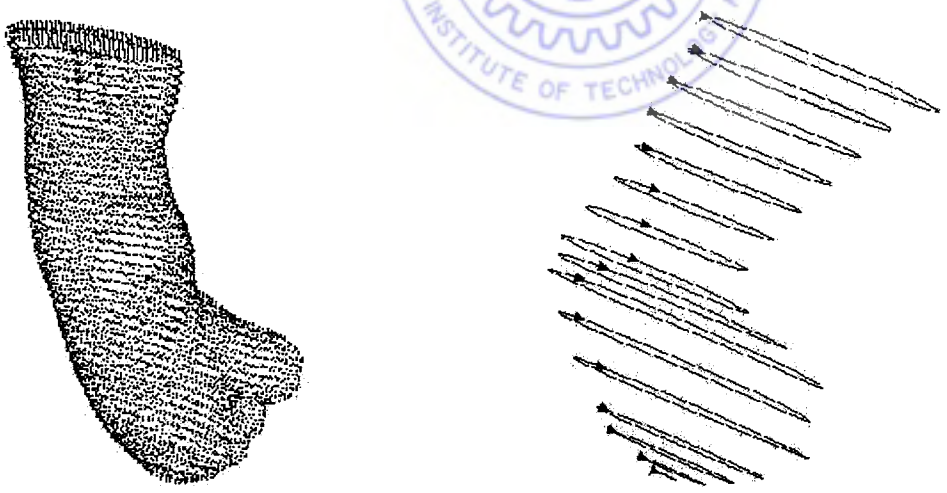

(a) (b)

Figure 3.25: Curve modeling (a) point cloud data of clubfoot (b) curve model of clubfoot (**See color section**)

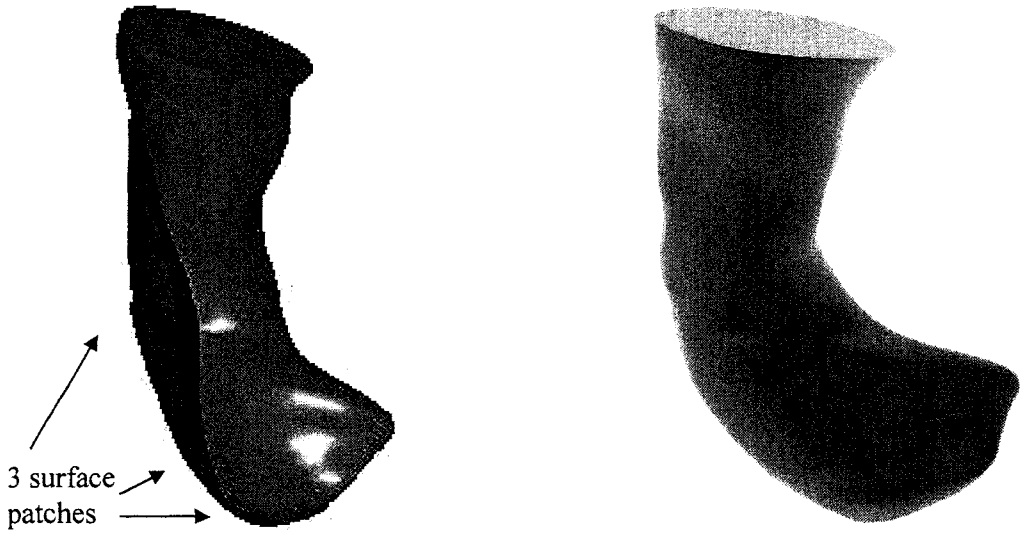

Figure 3.26: Solid modeling (a) surface model of clubfoot (b) solid model of clubfoot (**See color section**)

The general prerequisite of RP process is the requirement of steoreolighography (STL) file of solid model of parts. The STL file format is a boundary representation of 3D-volume geometry using a list of triangular facets. Each triangular facet contains the coordinate of its three vertices and a surface normal, pointing away from the material. Triangles are the lowest common denominator in 3D geometric modeling systems. Topology can be used to reduce the redundancy present in the STL file format.

The quality of STL file depends on the deviation of the tessellated surface from actual surface. We normally controlled this by specifying the Chord Height parameters, which specifies the maximum distance between a chord and a surface. The smaller the chord height less is the deviation from actual part surface, which can be clear from figure 3.27. The chord height must lies within lower and upper bound of a part. The lower bound for the chord height is the function of part accuracy, and the upper bound corresponds to the part size. The part size is defined as the diagonal of an imaginary box drawn around the part.

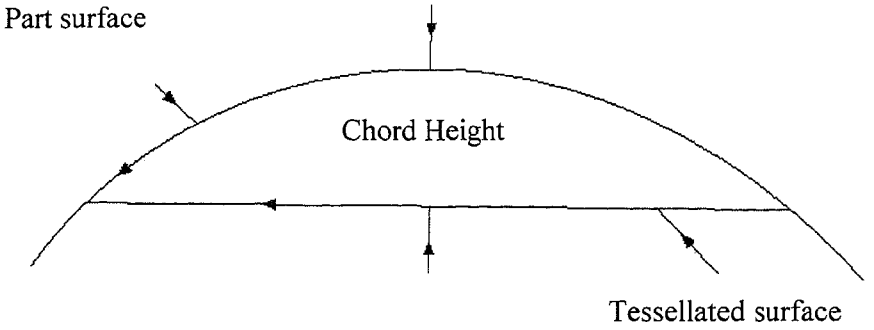

Figure 3.27: Chord height for controlling quality of STL file

The STL file is of two formats, one is the ASCII format and the other is the binary format. The size of an ASCII, STL file is larger than that of the binary format, but is human readable [48].

3.5 Rapid Prototyping (RP)

Prototyping is an essential part of the product development cycle required for assessing the form, fit and functionality of design before a significant investment in tooling is made. Until recently, prototypes were largely hand-made by skilled craftsmen, adding weeks or months to product development time.

Rapid Prototyping is defined as the fabrication of a physical 3D part of arbitrary shape directly from a CAD model by a quick, highly automated and totally flexible process [32].

This means that designers have the choice of making physical models of the conceptual design more frequently, allowing them to check the form and assembly of the design. This also allows them to discuss manufacturing issues with an ease to interpret prototype, which can be held, viewed, studied, tested and compared. Consequently, a product is improved and product development cycles and costs are substantially reduced, It has been claimed that RP can cut new product costs by upto 70% and product development time by upto 90% [71]

Medical model built with RP technologies represent a new approach for surgical planning and simulation [70] [17]. Building the medical model with RP, also known as biomodel, is a new

technology that allows three-dimensional CT / MRI data to be used to generate solid plastic replicas of anatomical structures [95] [13] [109].

We explain briefly the process sequences of rapid prototyping system and an overview of some RP processes which are also utilized for medical application.

3.5.1 Process sequence of Rapid Prototyping system

For building physical prototype of part, the process sequence of RP consists of four tasks:

a. Geometric Modeling
b. Tool path file creation
c. Part building
d. Post processing

This can be shown with the help of following block diagram of Figure 3.28.

Figure 3.28: Process sequences of RP process

a. Geometric Modeling:

Creating an accurate and complete solid model is a general prerequisite of RP processes. The solid model must be of water-tight geometry. The selection of the available solid modelers depends upon particular application and need. We generate solid model from CT and MRI scan data.

b. Toolpath file creation:

Geometric data of CAD model to a RP system is primarily transferred through the Stereo Lithography (STL) file format. This format has become a *de facto* standard for interfacing with RP systems. The solid model is converted to STL format. The STL is a faceted format and consists of connected three-dimensional triangles representing the part shape. The vertices of the triangle are ordered to indicate which side of the triangle contains the part mass [48]. From

a mesh generation point of view, triangular meshes are easy to generate than a quadrilateral meshes. This is because a triangle is a simplex while a quadrilateral is not [108].

Some time during STL file conversion it results in some errors and the typical errors are flipped normal, mid-line node, closure errors (holes) and truncation errors [48]. Hence the validity of the STL file is verified and the file is repaired.

c. Part Building:

Preprocessing the STL model and its orientation [102] is the primary requirement before part building is started. We process the STL model in Stratasys Inc. software known as INSIGHT following is the major operation that takes place during preprocessing of STL model [41].

- Orienting the STL model for optimum part orientation.
- Slicing the STL model with a series of horizontal planes to create slice curve.
- Check the slice curve and repaired them if some found to be erroneous.
- Creating support curves that define when temporary supports will be built.
- Creating toolpath fill for part and support curves.
- Creating toolpath file (Stratatsys Machine Language, SML file).
- Downloading toolpath file to modular for part building.

The machine then builds the part described by the file, and the process requires no or minimal human intervention. The machine thus builds the part.

d. Post processing:

When building is finished, supporting structures are removed and the model is cleaned, further cured if require, or polished to complete the process. After this, the part is ready for final look and use. Depending on the use of the model, it can be sterilized for assistance in an operating theatre.

3.5.2 Overview of RP processes

Some of the RP systems that are also used for medical application are briefly summarized here.

3.5.2.1 Fused Depositional Modeling (FDM)

It is a solid based process and it builds up objects by the extrusion and speedy solidification of melted filaments. This is more suited for placement in a hospital environment than a stereolithography machine, since an FDM machine is a compact machine with "dry" materials that are easy to handle in a hospital environment, MedModeller based on this technology has FDA clearance for placing the machine in a hospital environment. There are choice of materials including different colors, and medical grade ABS that can be gamma sterilized.

In the FDM process of Stratasys Inc. [88], a spool of 1.27 mm in diameter filament feeds into the unit's extruding head. The extruder head moves in the XY-plane (Figure 3.29). The filament is melted to liquid inside the extruder head at 2.70.°C by a resistance heater. Initially, the model is converted into STL format in the CAD system and sent to the FDM slicing software, called INSIGHT. There the STL file is sliced into thin cross sections of desired thickness, creating a SLC file. Support are created for overhanging parts and sliced as well. The sliced model and support are converted into a SML file (Stratasys Machine language file) that contains actual instructions for the FDM machine. A toolpath is generated which is followed by the numerically controlled extruder head.

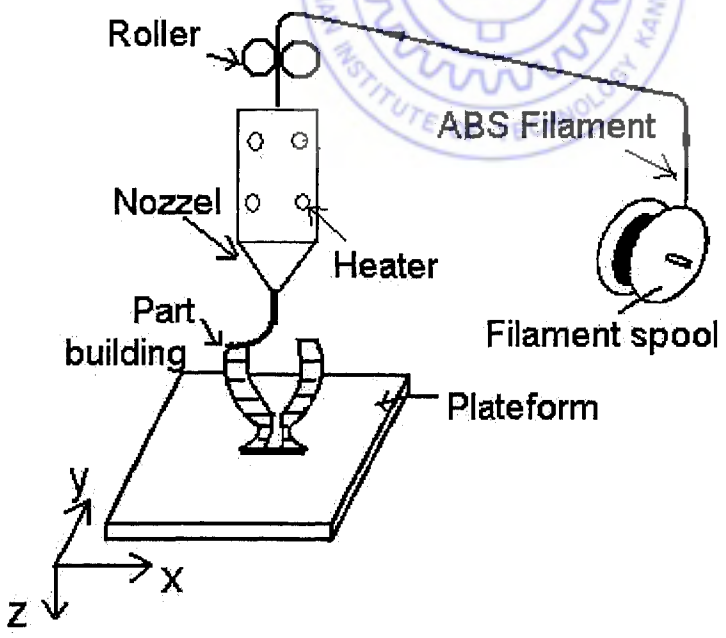

Figure 3.29: Schematic sketch of FDM RP system

As the head moves in X and Y directions following the tool path, the thermoplastic material is extruded out of a nozzle and then deposited in think layers, one layer at a time. Since the envelope surrounding the head is maintained at a temperature below the melting point of material, the extruded material quickly solidifies [87]. The extruder head has two nozzles, one for the part material and the other for the support material. The support can be easily removed by breaking away. The part is built on a foam foundation attached on a Z-stage platen. The Z-stage platen moves downwards as the part is built progressively. The system uses ABS (Acrylo Butadyne Stryne) a tough nylon like thermoplastic as a modeling materials.

The work volume of FDM-1650 machine is 254×254×254 mm. The operator may select a layer thickness between .05 and 0.0762 mm. Models can be produced within an accuracy of +-0.127mm.

Parts made by this machine have a high stability since they are not hygroscopic. The system doesn't waste material during or after producing the model. No post curing of model is required [87].

3.5.2.2 Stereolithography

It is the best known and used RP techniques for all RP applications, including medical model building [43].

Stereolithography builds models layer – by – layer using laser – scanning of a light sensitive resin in the area defined by the object's cross section, e. g. a patient's bone structure as defined by CT data. Further curing in a UV oven ensures the model is completely solidified. Overall, the distinguishing factor between this technology and other technologies described below for medical models includes [48]:

(1) Ideal compromise between model sizes needed and overall accuracy for medical models.
(2) Very reliable technique
(3) Using acrylate materials, the technique allows high transparency, fast building (trauma cases, less cost) and possible medical grade models, with selective coloration of regions of interest.

Currently, a low toxicity and FDA approved resin is commercially available from Zeneca Specialties. Selectively colored parts produced in this material can, after sterilization, be in contact with the patient during surgery.

Currently Stereolithography technology is not ideally suited to a hospital or office environment due to the size and structure of machine, and the liquid photo polymer material used within this process.

3.5.2.3 Solid Ground Curing (SGC):

This technology also builds models from light sensitive resin, but instead of laser scanning the surface, the areas to be solidified in the layer are exposed instantaneously to a UV-lamp through a mask. After each layer, the old mask is erased and a new one made. The unsolidified resin is removed and the gaps are filled with wax. The whole layer is milled to the correct height.

3.5.2.4. Selective laser Sintering (SLS):

It forms an object by laser sintering of selected areas of thin layers of meltable powder. The technique also has the advantage of inherent supports and will be comparable in speed with SLA (depending on the model features it can be faster).

Surface quality and model details will be somewhat less than with SLA models but the range of different materials (polystyrene, nylon, wax, etc), which can be used on the machine, is a big advantage. Also FDA approved medical grade Nylon that can be sterilized is available for use in making medical models with this technology. The technique is believed to be more applications rather than transparent models of skull, etc.

3.5.2.5. Laminated Object Manufacturing (LOM):

This technique creates objects by bonding and cutting of sheet materials (such as paper, plastic, etc) and is very interesting for foundry applications and for large volumes (e.g. Orthopaedic) since the complete volume does not have to be scanned.

3.5.2.6. 3D Printing:

It is a technique where a printhead deposits the blinding material on to a thin layer of powder and on completion of all the layers the object is placed in an oven. This is essentially an inkjet based technology, which is compact, accurate and is suitable for small parts that can be built at low cost. Machines on the market are Model Maker from Sandrs, Actua 2100 from 3D systems and Z402 from Z Corporation.

3.5.3 Developed RP model of foot:

We used FDM-1650 for all of our clubfoot research. Figure 3.15 (a) and (b) Show the preprocessing of one of the foot STL model in Stratasys Inc. INSIGHT software which interfaced with FDM-1650 [102] [41].

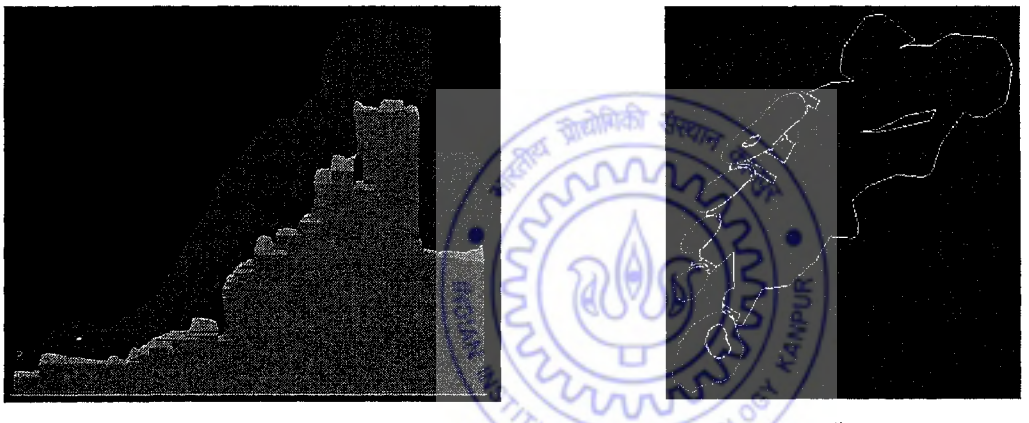

(a) (b)

Figure 3.30: Support generation for foot RP modeling (a) generated support (b) one slice at typical foot-support section (**See color section**)

Following Figures Shows the RP model developed of an adult foot skeletal along with various clubfoot whose STL file was developed as described above.

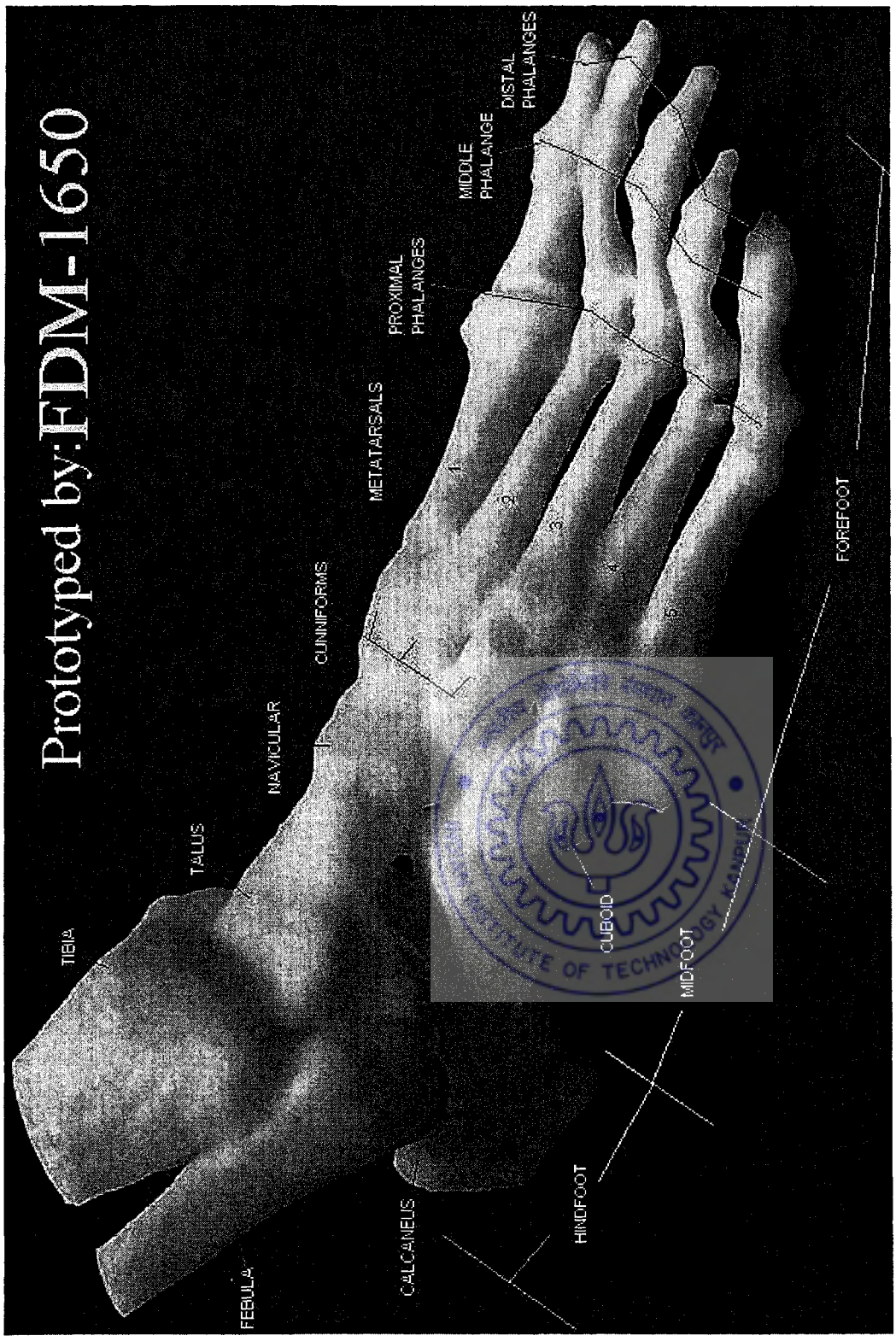

Figure 3.31: RP model of skeletal of foot (**See color section**)

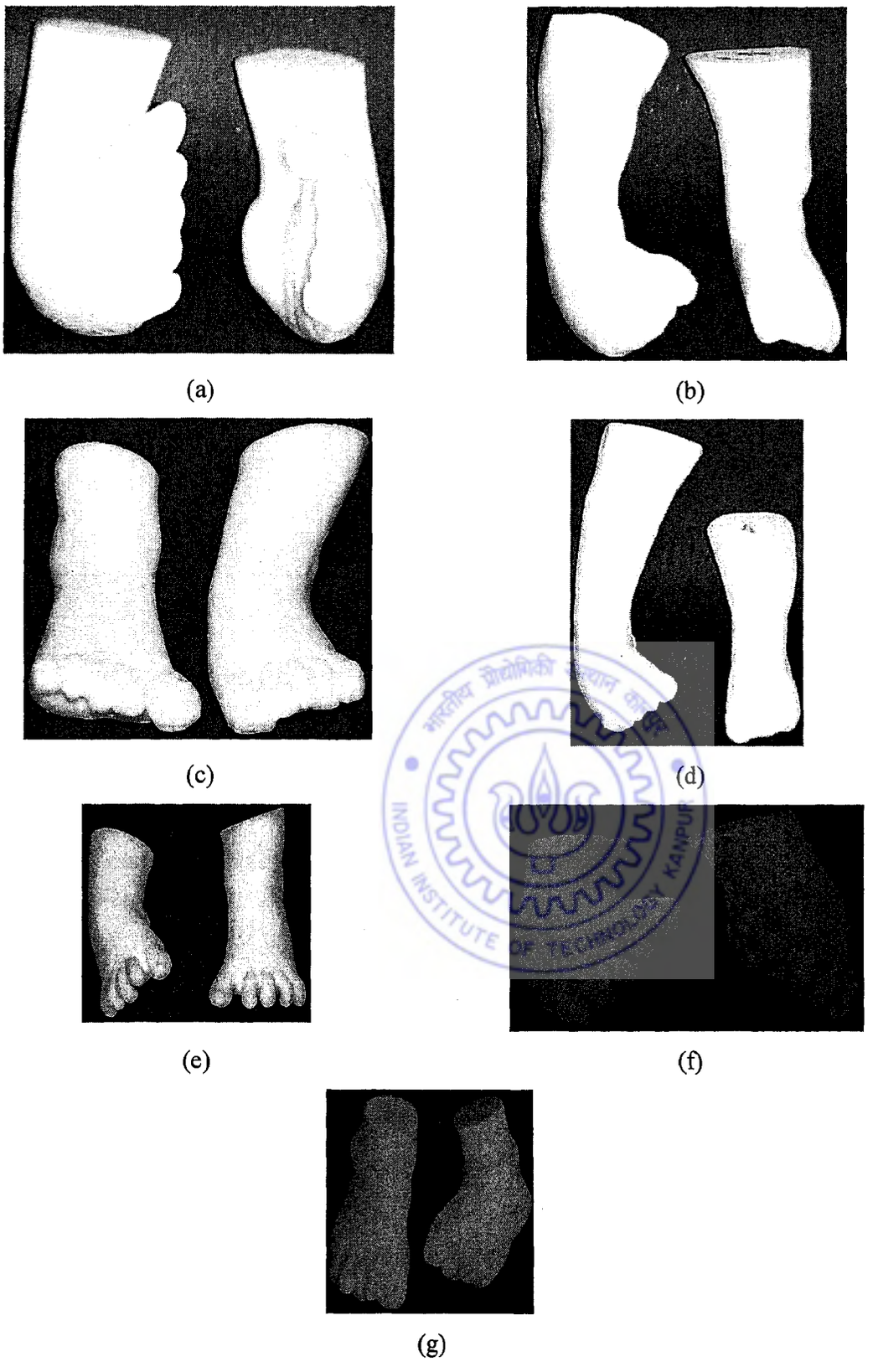

Figure 3.32: RP model of clubfoot of (a) patients I (b) Patient II (c) Patient III (d) Patient IV (e) Patient V (f) Patient VI (g) Patient VII (**See color section**)

3.6. Clubfoot Model making with Silicone material

The ABS clubfoot model is rigid in nature and is not deform because of applied corrective load so we cannot perform the experimental study on it and hence the need of silicone foot model is arise. The Silicone clubfoot model plays an important role for understanding the behavior of the foot model due to physiotherapy. This model also found to be very useful for doing the experiment on it due to applied corrective load. The entire process begins with a pattern (usually one created from a RP system) and the mold making and duplication process proceeds as per following block diagram of Figure 3.33.

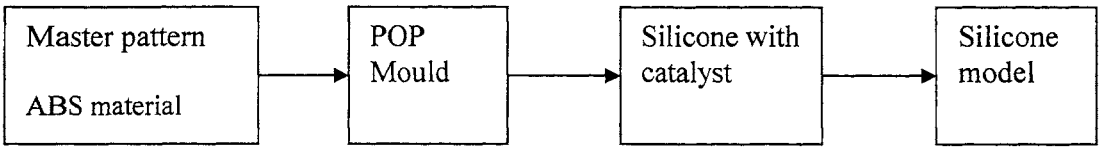

Figure 3.33: Flow chart of silicone foot integrated process

3.6.1 Vacuum casting of RP clubfoot model

MCP Vacuum casting machine [35] is used for silicone clubfoot model making.

Here we develop the mold by using the technique of plaster cast, which is applied to the patient extremities during fracture etc., in hospital. For making the silicone rubber foot model, the RP foot model, which we built in FDM-1650, is used as a master pattern for making the mold. To eliminate any difficulties when trying to remove the ABS master pattern from mould, a single lap of white petroleum jelly is applied over the whole surface of RP- foot model. The plaster of Paris bandage (P-400) of 4"size is used as a mold material [65] [92]. This bandage is cut into patches of suitable length. Each patches after immersing into water, is carefully wrapped over Vaseline RP-foot model and the process is repeated till whole surface of foot model is covered in a thickness of about 4mm. This wrapped model is left as it is for about 10 minutes. Once the P-400 bandage is set, a suitable parting line with a marker pen is drawn & it is cut by surgeon's blade and the RP-foot model is carefully removed. The parting edges of this mold are matched again, joined and lapped with a new POP bandage strip, which give us, the foot mold.

This mold is dried in an oven at 35° Celsius for about 24 hours, which removes all of its moisture & it become hard. The surface finishing on the interior of this mold is very important, as the surface finish and tolerance will be faithfully reproduced in the finished cast. For better surface finish the inside cloth textures of the POP mold is covered completely by solid lubrication and painting. For solid lubrication, one-fourth volume of the mould is filled with fine boric powder, shacked thoroughly and the powder lubricant is taken out completely. The inside surface of the mold is then evenly spray-painted with Royal Luxury Acrylic Emulsion paint, which gives very smooth wall finish. The painted mold is backed in MCP oven at 40° C for about 25 hrs. This gives us mirror like mold surface finish, it is sprayed evenly with Silicon release agent spray S3 (for MCP vacuum casting) [34]. The mold is now ready for use (Figure 3.35 a and b).

After completion of the mold, silicone rubber and a catalyst were mixed in proper proportion for creating the cast. The amount of silicone to be used was determined by multiplying the volume of the mold by a constant factor of 1.1, the specific gravity of the silicone. The required amount of catalyst is 10% by weight of the silicone. The two materials were poured into a glass jar and mixed thoroughly. After mixing, the container was placed inside the vacuum chamber of the MCP System equipment (Figure 3.34) and the vacuum was started. This is the de-gassing stage and was completed in approximately 10 minutes. The resulting de-gassed silicone mixture was then removed from the chamber and poured under the mold very slowly and steadily. During this stage, it is important to maintain the steadiness and to avoid sudden rushes of rubber in the mold to prevent bubbles and damage to the mold set-up [34]. Figure 3.36 Illustrates the poured of the silicone into the POP clubfoot mold.

Next the mold was cured in an oven set at 40°C. Molds may be cured at room temperature, however curing in an oven accelerates the process, which is completed in 4-8 hours depending on the size of the mold. When curing process was completed, the mold was removed from the oven and the mold bandages were taken out by immersing the whole unit in water. These give us finished silicone clubfoot model ready for experimental use.

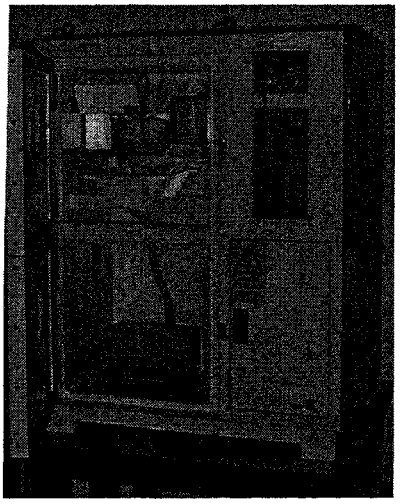

Figure 3.34: MCP vacuum casting machine **(See color section)**

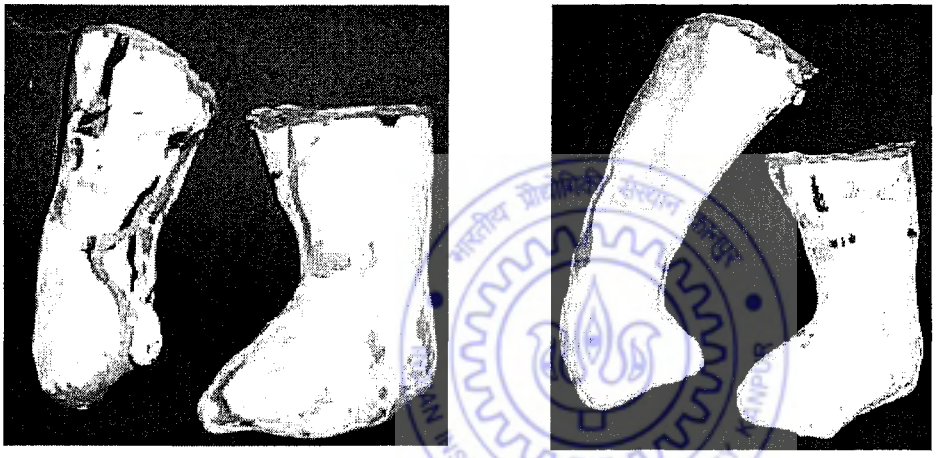

(a) (b)

Figure 3.35: POP mold of feet (a) patient II feet (b) patient IV feet **(See color section)**

Figure 3.36: Process of Silicone casting (**See color section**)

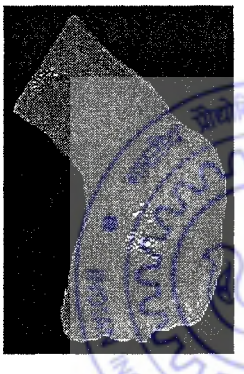

Figure 3.37: Silicone clubfoot model of patient VII (**See color section**)

3.6.2. Making silicone model with strain gauge instrumentation:

We are interested to perform the experimental study on clubfoot model by strain gauge instrumentation at region of interest. Hence, casting of integrated strain gauge clubfoot model is done. Hence, on developed POP mold of clubfoot, marking with marker pen is done at three point of interest and the mold is punctured with hospital spinal needle of Comet make (L. P. needle) No. 20. The strain gauge (make: Tokyo Sokki Kenkyujo Co. Ltd., Made in Japan with Gauge Factor 2.11) leads are soldered with different color fine insulated wire. The two free ends of this wire is inserted into LP needle from inside of mold, while its other rend having strain gauge is lying in the mold itself. The free ends of wire are pulled from outside of LP needle such that the strain gauge just touches the tip of needle. The same procedure is adopted

for other 2 LP needle. After this the LP needle is adjusted inside the mold and at a particular region of interest the needle is fixed by creating a joint between needle and mold by applying different color magic clay on different mold places along with needle (Figure 3.38 a). This prevents the relative motion between needle and mold and the strain gauge position and location remain fixed during gradual casting process. With this position and location of strain gauges in mold, the silicone with catalyst as described in previous section is pored in mold. After curing the casting, the POP mold is taken out carefully, which gives silicone clubfoot mold with localized strain gauges, ready for experimental use (Figure 3.38 b).

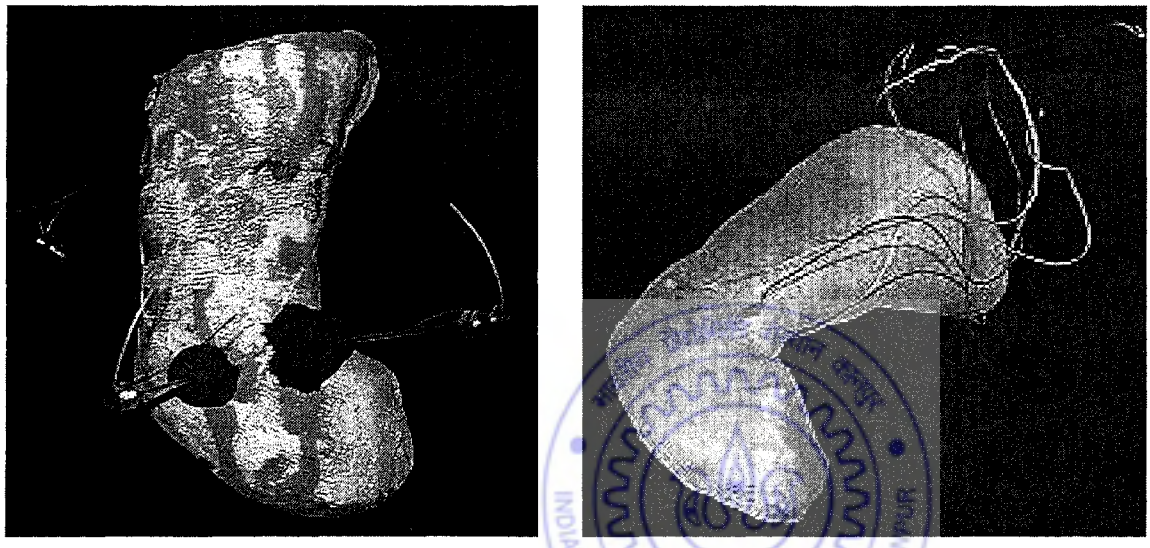

(a) (b)

Figure 3.38: Instrumented silicone foot manufacturing (a) mold with strain gauge fixing arrangement (b) silicone foot with strain gauge (**See color section**)

Chapter 4

DESIGN OF ANKLE FOOT ORTHOSIS

Using Computer Aided Design (CAD), a designer is able to conceive and render the geometry of a shoe or a car or an aeroplane in an effective and efficient manner. Designing of show lasts, nesting of cut-pieced, development of curved surfaces are some of the activities which are now carried out using CAD systems like Imageware surfacer, I-DEAS, etc. [21].

Using a RP system in computer aided manufacturing (CAM), a designer is not only able to render a shoe last on a computer screen but is also able to realize or make a physical full-scale model in a polymer material. These RP models are very useful for form, fit and function evaluation of a design [21].

Traditionally Ankle Foot Orthosis (AFO) designing and manufacturing have been a matter of skill and experience and even till now there has not been proper scientific methodology for designing and manufacturing of the same. The recent developments in CAD/CAM technology has been successfully demonstrated to foot orthotics, particularly for the comfort of athletes and adult person foot. It is a commercially viable method for replacing most of the normal manufacturing stages [86].

This chapter deals, mechanical design consideration of AFO, proposed mechanism for corrective procedure, our approach of AFO design and manufacturing with traditional method, with indigenously developed unique technique based on geometrical modeling and prototyping of AFO solid model.

4.1 Mechanical design consideration

A growing child will always need new AFO of variable size frequently, while making an AFO following things are to be considered [28] [20].

- How does AFO Works?

- How does AFO fit?
- How is the AFO made?
- Is the type of AFO appropriate for infants?

An AFO, like any other product has four aspects to it

1. Function,
2. Strength,
3. Ergonomics and,
4. Aesthetic

All these aspects are equally important. Functionally an AFO provides protection as well as grip to the clubfoot. It should rotate the clubfoot as per required degree of rotation so as to achieve the normal foot geometry, in a given time period. It should be plane at forefoot and sufficiently hard so as to prevent wrong deformation of clubfoot during its timely growth. The design should be such that the patient's feel comfortable and happy while wearing it. It should not act as an obstacle while patients perform his/her, daily normal activities. The AFO should have adequate ergonomics design with proper ventilation, required padding, etc., that allows plenty of room for growth, because babies foot continue to take shape during initial periods of his/her growth. Aesthetics of AFO is also a major factor as the people like AFO that add beauty and style to their baby.

The primary purpose of AFO is to correct clubfoot and in order to do so, it must have a corrective load applying mechanism and must fit well to foot. Poorly designed and fitted AFO can cause discomfort, other foot problem and will not correct the deformity. The design of AFO should conform to the shape of normal foot, on wearing it the clubfoot should be forced to conform to the shape of AFO.

Apart from the above four major design considerations, following recommendations for the design of AFO should also be kept in mind. This recommendation helps in evaluating the performance of AFO during its fit on foot.

4.1.1 Recommendations for AFO design

The following recommendation should be considered during design of AFO [7] [9].

1. Measure the baby foot before AFO design
2. AFO should be made in different parts, so as to incorporate required joint for it, and hence the foot effective movement.
3. The toe area of AFO should be rounded/curved with proper clearance from the end of toe boundary to the end of AFO, for better attention towards toes.
4. For fixing AFO to foot, Velcro fixing arrangement should be provided at minimum 3 different places of AFO.
5. The material from which AFO is made can affect fit and comfort, softer material decrease the amount of pressure the AFO places on foot, stiff material can cause blister. A counter may be used by placing skin protection padding of suitable thickness.
6. AFO should fit properly to heal as well as toes of babies.
7. After AFO fitting on foot, the baby should be able to freely wiggle all of his/her toes.

4.2. Proposed mechanism for corrective procedure

The mechanism designed in the present work, to remove abduction, varus of heel and equines of forefoot in clubfoot for making correction is illustrated here. The designed six link mechanism is shown in Figure 4.1 (a) [80].

The analysis of the mechanism is as follows

In Figure 4.1(b), the length *L2* and *L3* is of constant length (decided on the basis of nature of deformity) and when length *L1* is decreased by applying quantitative torque with the help of fly nut at A, the point *h1* is shifted to point *h2*, decreasing the length of *L1* by *h1h2*, which reduces angle θ1 to angle θ2. Similarly when *h2* shift to *h3*, the angle θ2 reduces to angle θ3 and the point *h3* makes the link *L3* horizontal, which is correct position of forefoot. Hence it removes equines of forefoot. Keeping point A as fixed, periodically varying θ1, θ2, etc., helps in reducing equines of forefoot in clubfoot

The spring whose one end is hooked with screw and other end is hinged with AFO, provide smooth motion to the clubfoot (Figure 4.1 a) during load transmission. The stiffness of spring depends on the tissue properties of foot more the stiffness of tissue, stiffer will be the spring. The one end of screw link to which the fly nut is screwed, having sliding joint and can slide in a cantilever hole located at point A, at its other end as said above the spring is hooked. As the axis of screw is located in fixed direction and when the torque to the fly nut is applied, the spring axis (which is not align initially with screw axis) tends to align with the screw axis, this give abduction to the fore foot. Hence the mechanism helps in correcting adduction of forefoot.

The link *L3* and cantilever link of this mechanism is interconnected by an equivalent ankle joint namely ball and socket joint at point P. For smooth function of mechanism, the link *L2* and *L3*, have hinge joints at its both ends. During torque application on fly nut, the points *h1*, *h2*, *h3* etc. will move on the arc of a circle having diameter equal to length of link *L3*. This rotation gives lateral rotation (eversion) to the heel of the clubfoot at point P and hence will correct the varus of heel in clubfoot.

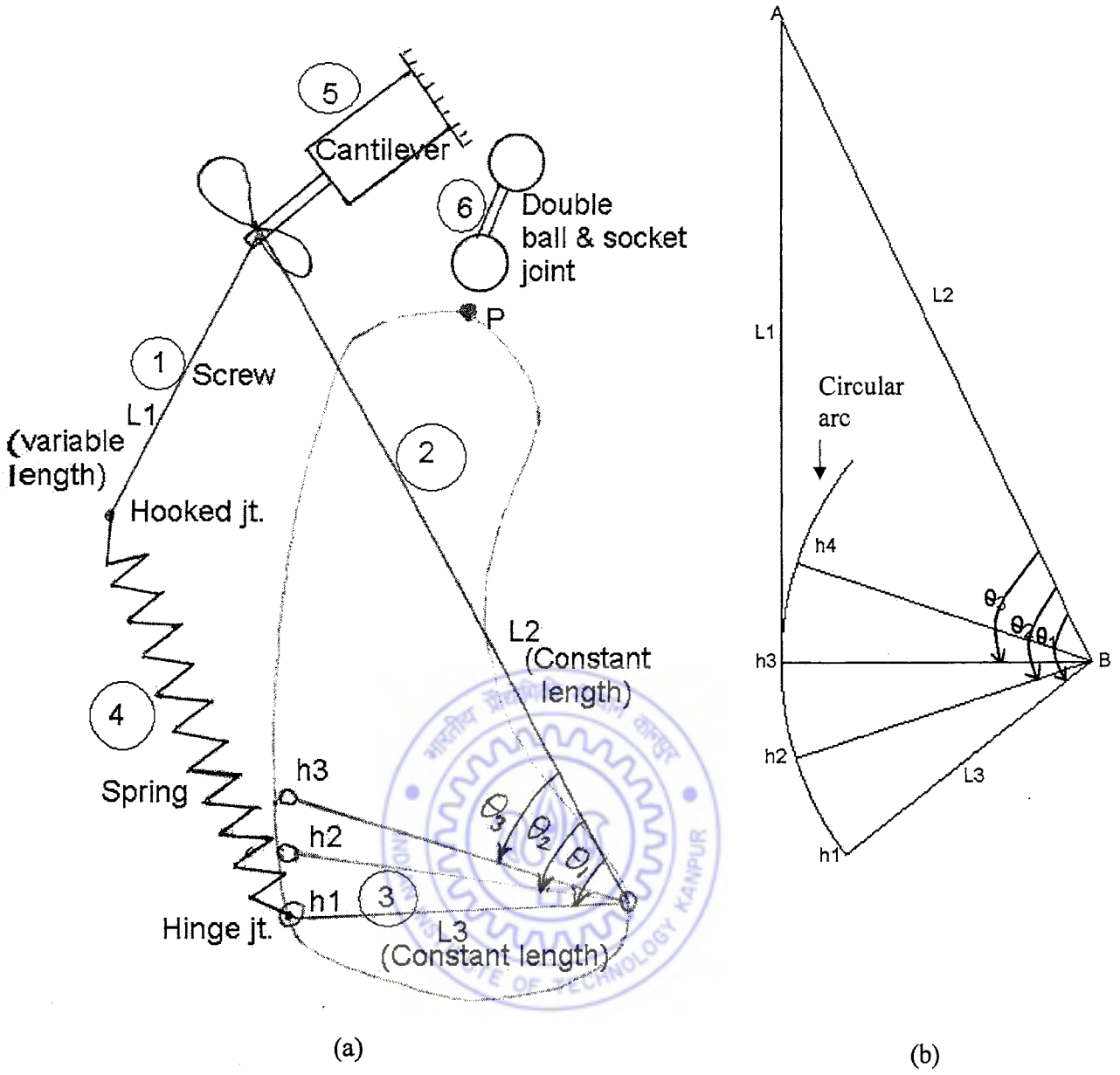

Figure 4.1: Proposed mechanism of AFO (a) mechanical elements (b) line diagram (**See color section**)

Inventory of mechanical elements

In order to meet the functional requirements of mechanism as per above analysis, it is very important to select the mechanical elements. The various selected mechanical elements along with their specifications are tabulated in table 4.1.

S. No.	Particulars	Specifications (mm)	Material	Quantity	Remarks
1.	Cantilever (link, 5)	W= 12, T= 6, L= 140	Acrylic	1 No.	
2.	Nylon bar (Link, 2)	L= 100, Dia= 6	Nylon	1 No.	
3.	Stud (link, 6) Ball	L= 25, D= 5 OD= 14	SS Polymeric	1 No. 2 Nos.	
4.	O-ring	OD= 16, ID= 12 Cross – section= 2φ	Rubber	2 Nos.	
5.	Pin (a) Straight (b) U-shape	 $L1$= 9, $L2$= 6, D= 1.5 D= 1.8, W= 12	 SS SS	 2 Nos. 1 No	
6.	Fasteners (a) Rivet (b) Screw	 L= 8, Dia.= 8 L= 12, Dia= 3.14	 Brass Brass	 2 Nos. 3 Nos.	
7.	Screw (link, 1)	L= 75, D= 4.6	Brass	1 No.	
8.	Fly nut	D= 20	Brass	1 No.	
9.	Velcro Cosmetic padding	W= 20, L= 200	Velcro	3 Strips	
10.	Spring (Link, 4)	Wire Dia. = 0.8, Free Length= 55	Spring steel	1 No.	
11.	Adhesive		Adhesive	10.0 gms	

Table. 4.1 Mechanical elements used in mechanism

4.3 Conventional/traditional manufacturing process

The traditional manufacturing process of AFO takes place according to the design flow chart as shown in Figure 4.2.

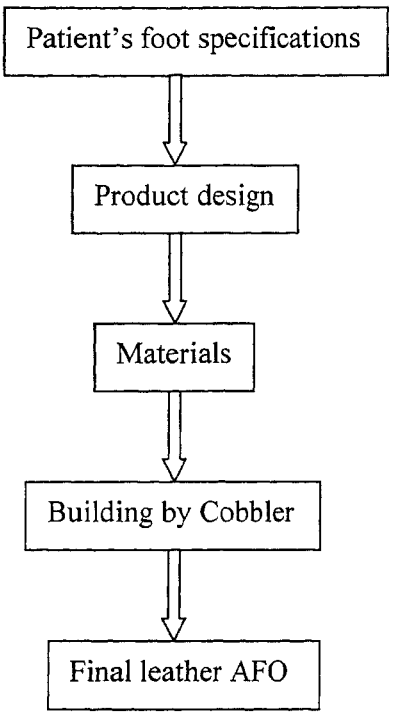

Figure 4.2: Conventional manufacturing of AFO

Initially the foot of the baby is placed on a cardboard paper and then with the help of a marker pen, the foot boundary is plotted on this paper. Based on this plot, the minimum and maximum size of foot is determined. According to the obtained foot profile (Figure 4.3), a flat stiff wood material of about 2mm thick is taken and finished, so as to match the foot profile, but about 10-15% size is kept more, in order to give clearance [38].

On the outer top surface (lateral side) of this wood strip, a wedge shape (30-35 degree) leather piece depending on the nature of deformity, is glued with adhesive to the above finished wood piece. This wedge should be fixed in such a way so that it helps in reducing the equines of fore foot and heel varus of clubfoot. After this a soft padding of about 1mm thick is glued to the top surface of both this wood strip and wedge.

Because of strength and stretchability properties we used leather as the material for fixing to the upper side surface of the wood profile, which will help in fixing the foot. So leather patches after marking on it of different shape and size as per foot shape and size are cut and stitched together by cobbler, which give an approximate leather envelope. This upper leather envelope

is fixed and glued to the previously developed wooden profile. This will give traditional leather AFO shown in Figure 4.4, which will be fitted to the baby foot.

The method has limitation, because it is time consuming, involve experienced skill and a designer is not able to visualize clearly how the AFO will come up when it is actually placed and fitted over the foot.

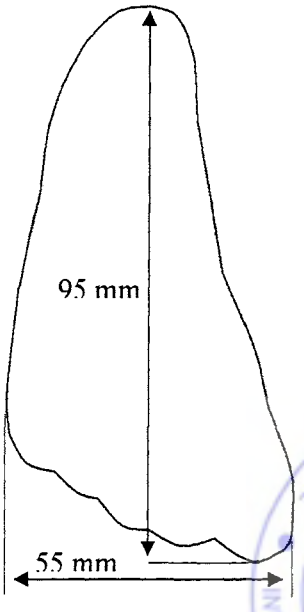

Figure 4.3: Foot profile of one month old baby

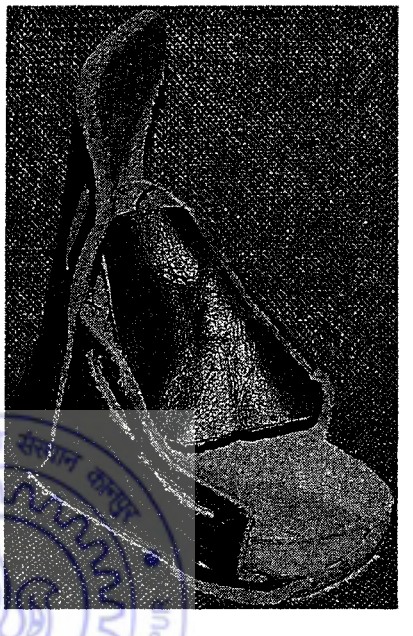

Figure 4.4: Traditional leather AFO

4.4 CAD manufacturing process

If traditional techniques are employed, each new design takes considerable amount of time, as the method is based on skill as well as on trial and error and the product may not be competitive any longer, thus a need exists to adopt modern technologies to reduce this lead-time and decrease development cost. We utilized CAD/CAM modern tools for effective designing and manufacturing of AFO [61] [57] [6].

4.4.1 Curve and surface modeling

A curve can be modeled by selecting few controlled points on the curve and then applying a mathematical function. The B-spline curve has been widely adapted in various applications

because it affords much better control over the resulting curve, hence making it easier to modify the shape to the desired degree, also the use of B-spline is computationally more efficient than other schemes and thus has been implemented in the present research [38] [61].

Most curve-defining techniques do not provide for local control of shape, consequently local changes (a small change in the position of a point on a spline curve or a vertex of a characteristic polygon of a Bezier curve) tend to be strongly propagated throughout the entire curve. This is some time described as a global propagation of change. The B-spline curve avoids this problem by using a special set of blending functions that has only local influence and depends on only a few neighboring control points [63] [21].

B-spline (basis splines) curve were investigated by a number of researchers, but the most useful tool to derive B-splines for the computer implementation is the recurrence formula of de Bore 1978 and Cox 1981. Given $n+1$ control vertices (or de Boor points) $B_i (i = 1, 2,...., n+1)$, a B-spline curve shown in Figure 4.5 of order k (or degree k–1) is defined as:

$$P(u) = \sum_{i=1}^{n+1} B_i N_{i,k}(u), \quad u \in \left[u_{\min}, u_{\max}\right], \quad 2 \le k \le n+1$$

where $N_{i,k}(u)$ are polynomials of degree k–1 known as B-splines of order k. In most practical applications, B-spline basis functions are derived from the following knot vector:

$$x_1 = x_2 = ...= x_k,\ x_{k+1} \le .... \le x_{n+1},\ x_{n+2} = ...= x_{n+k+1}$$

where, x_i forms the knots. The reason to select the first and last k knots to be equal, is that the control vertices B_1 and B_{n+1} are points on the curve. Furthermore, the tangent direction of the curve at B_1, is from B_1 to B_2 and the tangent direction at B_{n+1} is from B_n to B_{n+1}. Due to these properties, the shape of a B-spline curve resembles the shape of its control polygon formed by the control vertices B_i, although such resemblance is not as intuitive as that of Bezier curve. The n–k knots x_{k+1} , x_{k+1} , x_{k+2} , ...x_{n+1} are called the interior knots. If the interior knots are all distinct, then the B-spline curve has n – k + 1 non –vanishing spans (the arc length of each span is not zero). There are several methods to derive the B-spline basis function $N_{i,k}(u)$ in terms of the knot vector. The recursive formula derived by de Boor and Cox is as follows:

$$N_{i,k}(u) = \frac{u - x_i}{x_{i+k-1} - x_i} N_{i,k-1}(u) + \frac{x_{i+k} - u}{x_{i+k} - x_{i+1}} N_{i+1,k-1}(u),$$

with

$$N_{i,1}(u) = \begin{cases} 1, u \in [x_i, x_{i+1}] \\ 0, elsewhere \end{cases}$$

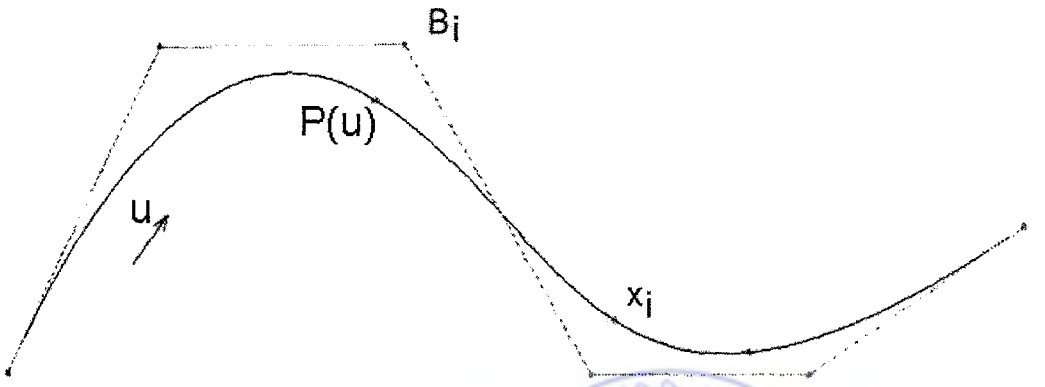

Figure 4.5: B-spline curve with nomenclature.

Similarly a Cartesian product B-spline surface shown in Figure 4.6, is defined as

$$Q(u,v) = \sum_{i=1}^{n+1} \sum_{j=1}^{m+1} B_{i,j} N_{i,k}(u) M_{j,l}(v),$$

where

$u \in [u_{min}, u_{max}]$, $2 \le k \le n+1$, $v \in [v_{min}, v_{max}]$, $2 \le l \le m+1$

where $N_{i,k}(u)$, $M_{j,l}(v)$ are the B-spline basis function in biparametric u and v direction. The definitions of the basis functions are

$$N_{i,k}(u) = \frac{u - x_i}{x_{i+k-1} - x_i} N_{i,k-1}(u) + \frac{x_{i+k} - u}{x_{i+k} - x_{i+1}} N_{i+1,k-1}(u),$$

with

$$N_{i,1}(u) = \begin{cases} 1, u \in [x_i, x_{i+1}] \\ 0, elsewhere \end{cases}$$

and

$$M_{j,l}(v)=\frac{v-y_j}{y_{j+l-1}-y_j}M_{j,l-1}(v)+\frac{y_{j+l}-v}{y_{j+l}-y_{j+1}}M_{j+1,l-1}(v),$$

with

$$M_{j,1}(v)=\begin{cases}1, v\in[y_j, y_{j+1}]\\ 0, elsewhere\end{cases}$$

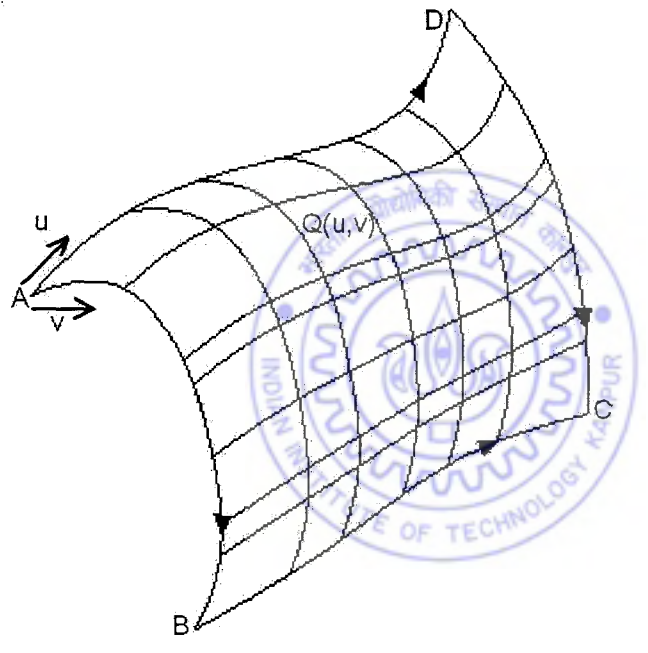

Figure 4.6: B-spline surface with nomenclature

4.4.2. *Approach for AFO design*

This section introduces a new technique for the customized design of AFO, which fit properly to the baby clubfoot and give nice and more comfortable feel. Some suitable joints, which resemble the anatomic foot joints, are kept in its design [11]. Hence the AFO become flexible and helps in moving the clubfoot for correction with the help of a mechanism fitted to it. The

point cloud data of a patient clubfoot, which is exported from MIMICS, is the basic input for design.

The technique is based on clubfoot point cloud analysis, curve design, composite surface design, solid model creation and prototyping of AFO. The techniques utilized one given in the flow chart shown in Figure 4.7.

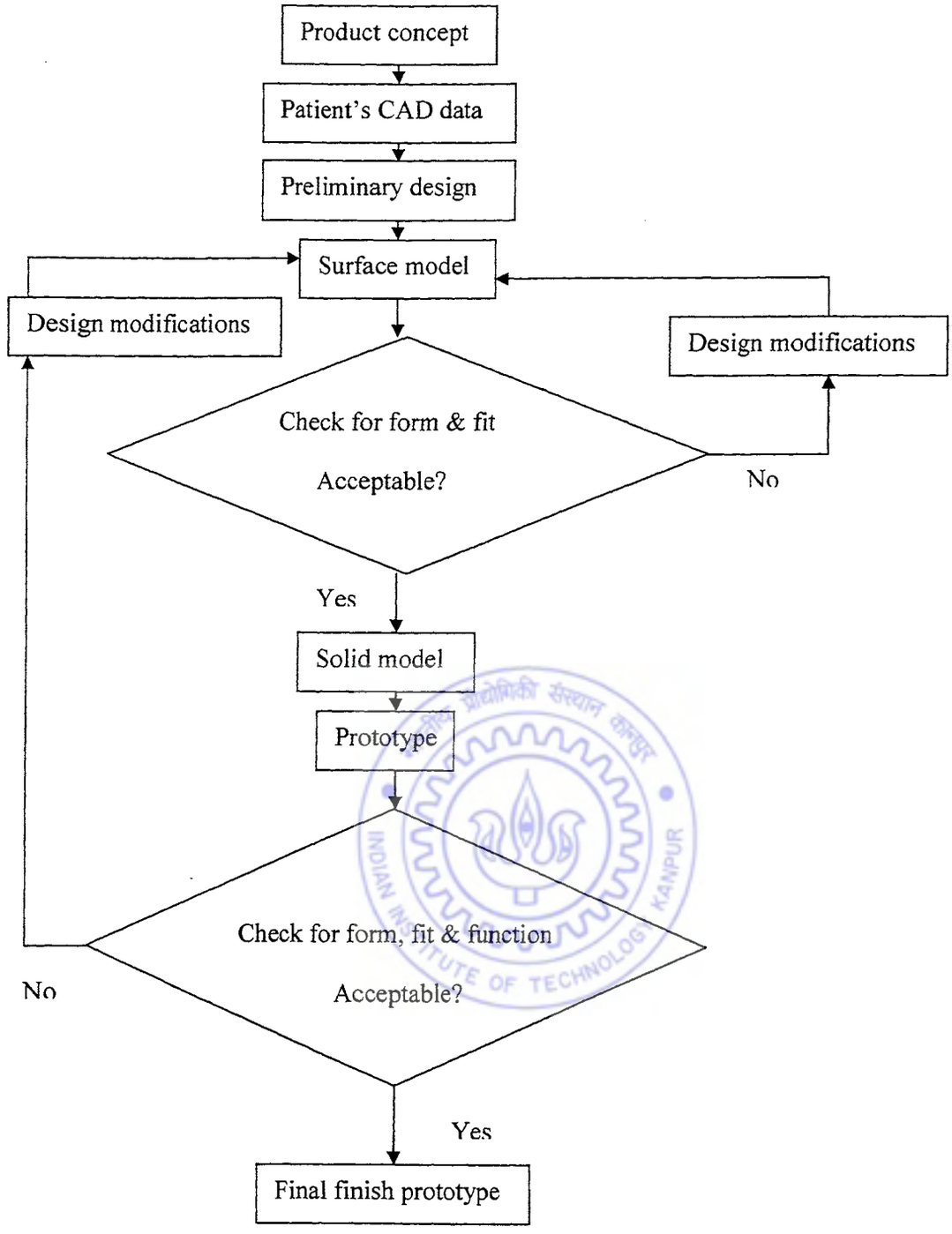

Figure 4.7: CAD manufacturing of AFO

4.4.2.1 Point cloud analysis

In point cloud analysis certain key points, which are important for critical design of AFO, are identified. Before segmenting the cloud and creating the surface model it is important to decide the strategy for surface fitting. Hence outlined strategy is as follows.

- Sampled the point cloud and remove noise if any,
- Segmenting the point cloud,
- Create cross sections,
- Create curves from the cross section and modify it,
- Create surfaces from the curves,
- Check the quality of final surface.

Keeping above strategy in the mind we proceeds for point clouds as follows.

1. Data reduction

Mostly the original dense point cloud is not needed to extract the clubfoot surface geometrical information. Hence sampling of clouds is done which modifies the cloud by reducing the number of point. Figure 4.8 (a) and Figure 4.8 (b) shows the dense point cloud and its sampled cloud, having 129749 points and 43251 points respectively of clubfoot. Also the points data, which are not important for design, are deleted.

Figure 4.8: Point cloud data of clubfoot (a) Dense cloud (b) Sampled cloud

2. Extracting features and segmenting point cloud

The data is broken into meaningful portions by identifying points along feature lines, based on angular, curvature and edge in the original object as observed in its RP model (chapter 3). All point clouds must be readjusted to create the digital image of the complete clubfoot in one

coordinate system. This is called registration. Figure 4.9 (a) and Figure 4.9 (b) show extracted clouds and its segmentation into three interested regions of shank, heel and foot.

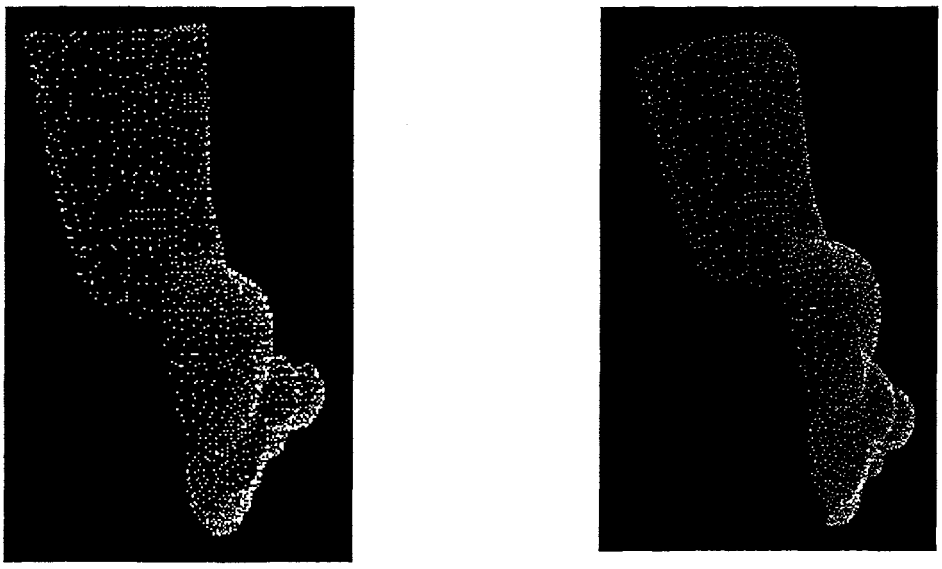

(a) (b)

Figure 4.9: Segmentation of point cloud (a) single segment (b) three segments **(See color section)**

3. View alignment and cross section creation

Align the cloud view so that suitable meaningful cross section can be created. With this aligned position create point cloud network (cross section), which are necessary for creating correct curves. Figure 4.10 shows the network of point at different sections of clubfoot.

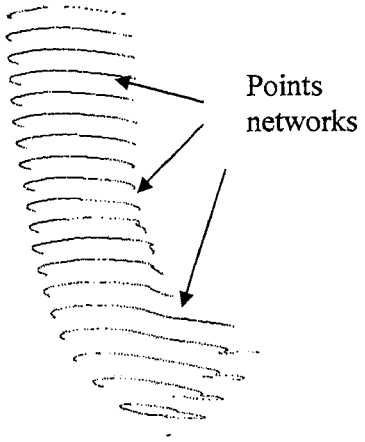

Figure 4.10: Network of points on clubfoot cloud

4.4.2.2 Curve modeling and analysis

After point cloud processing in section 4.4.2.1 the curves are created, in an interrogated way, which are modified and edited on point networks. Using the techniques discussed above, the curve network is built one by one in the 3-segmented area. The curves are then cleaned, reparameterized and edited so that they fit correctly. Some time curve stitching is needed, which is also done while maintaining proper continuity between different curves.

The curve fitting is done piecewise and the individual curves should satisfy the required constraints of tangency and position. For simplicity and accuracy we need normalized cubic spline curves. Provision is also made on the curves so that their tangency factor can be manipulated by the designer because the shape of a cubic curve is dependent to a large extent on the magnitude of tangent vectors at the end points. A step-by-step procedure of curve designing is given below.

1. Initially the bounding boxes of curves (boundary curve) are drawn at all the 3 segmented clouds, which will help in keeping the network of curves with in this boundary. Figure 4.11 (a) shows such boundary at three important regions of AFO.
2. The points in the previously created point's network are joined with cubic curves. The curve segments are such that they maintain position and tangent continuity at their intersection points. The shape of the segments can be varied by changing magnitude of tangent vector.
3. At lower foot position of AFO, 3D straight lines are drawn with in boundary curve and then these lines are offset downward depending upon deformity by an appropriate distance (6mm in this case).
4. These entire curves network in 3section of AFO, should be reparametrized by editing control point. These curves are then cleaned and make them twist free. Check their directions and confirm that all they are in same direction. Also see that their ends points should lies on the created curves boundary.
5. This give correct curves model, ready for next processing of surface fitting. Figure 4.11 (b) shows the final finish cure network ready for surface fitting.

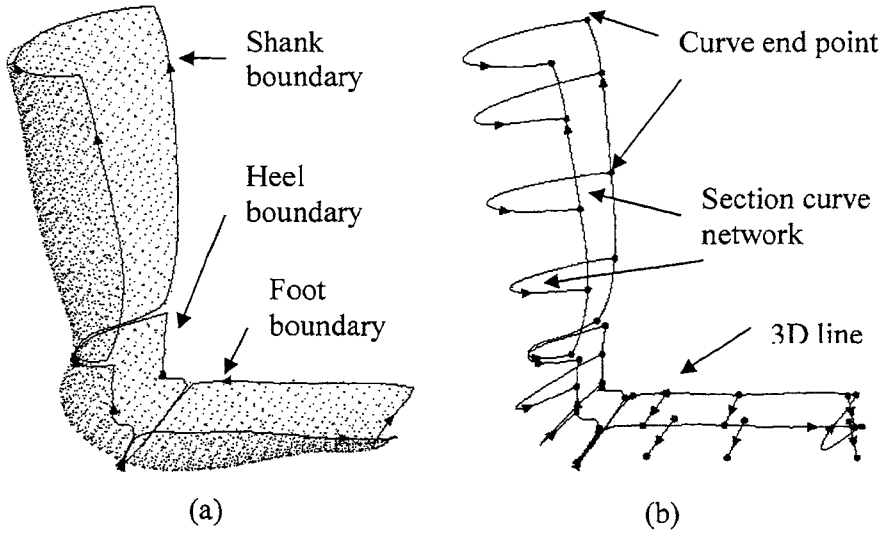

Figure 4.11: Curve network (a) boundary network (b) complete network

4.4.2.3 Surface modeling and analysis

After analyzing and processing the point cloud and curve fitting, the next task is to create a consistent and contiguous watertight surface model of AFO. This is possible when adjacency relationship between the constituent elements and mathematical equations of curves and surfaces are explicitly stored. A surface is defined as a mathematical function which describes the boundary of a three dimensional object. B-spline surface having two parametric dimensions, u and v, having maximum and minimum value. The surface edges are found at the extreme parameter values. As B-spline curve network have been used till now for the curve mesh, it is convenient to use B-spline surface [6].

There are many surfacing strategies to fit a surface. The decision is dependent on many criteria like downstream application (solid modeling, FEA, RP etc) requirements. A surface can be created in surfacer by fitting to

- Point data
- Lofting and blending
- Bounding with curves
- Revolving
- Offsetting and mirroring

Multiple surface patches can be joined along their boundaries with C^0 (position) and C^1 (Tangent) continuity. Coons (1967) and Mortenson (1985) provides the required conditions for joining together multiple bicubic patches in details.

A step-by-step surface fitting procedure for AFO is given below

1. On the shank and heel portion of AFO, the surface patches are created by curve lofting based on the created section curve network. At foot portion of AFO, the surface is also created by lofting on 3D line. Figure 4.12 (a).
2. In order to make watertight geometry of surface, the surface patches should meet the required position (C^0) and tangent (C^1) continuity. Therefore at common meeting edge, where the two surface patches meet should be constraint in a manner so that it satisfies position and tangent continuity for both the two patches. Three surface patches are meeting together on by one to make one complete patch, hence should satisfy above continuity at two meeting edges. These give one surface of designed AFO. Figure 4.12 (b).
3. This designed surface of AFO is check for form and fit with point clouds of clubfoot, in case if it satisfy, proceed ahead otherwise modify the surface model by curve and surface editing. Figure 4.12 (c).
4. Extend the foot region surface by suitable length, for keeping clearance between AFO boundaries and toe end point.
5. Clean and smooth the AFO surface, We can manipulate the AFO surface patches with the available degree of freedom by varying magnitude of twist and tangent vectors. This give final watertight surface model of AFO, ready for solid modeling application. Figure 4.13 (a) and Figure 4.13 (b) shows the side view and front view of final finish surface model of AFO.

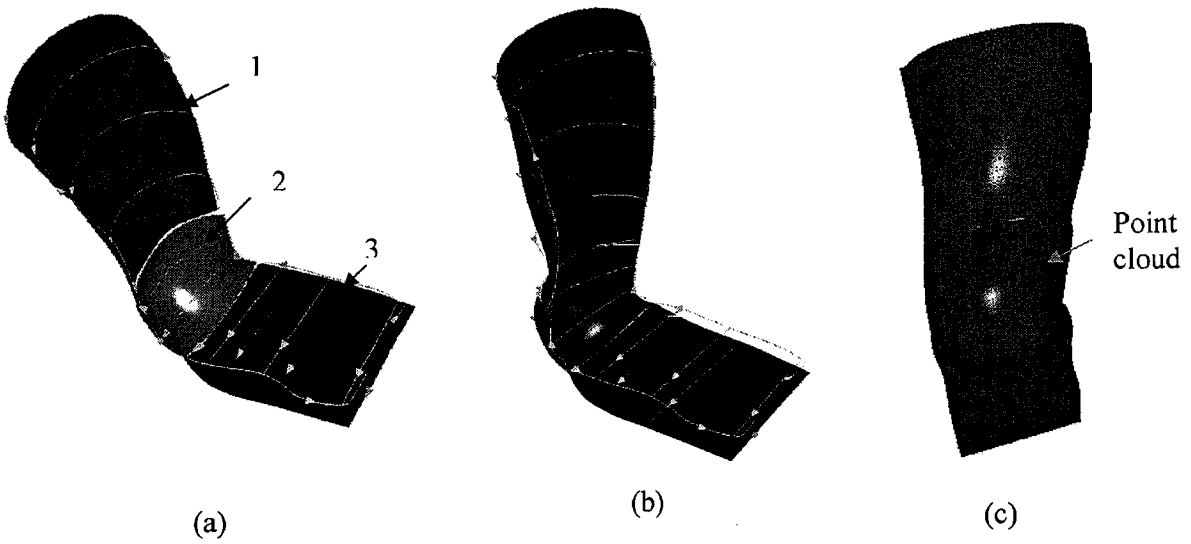

Figure 4.12: Surface models of AFO (a) three patches (b) matched single patch (c) form & fit check of AFO (**See color section**)

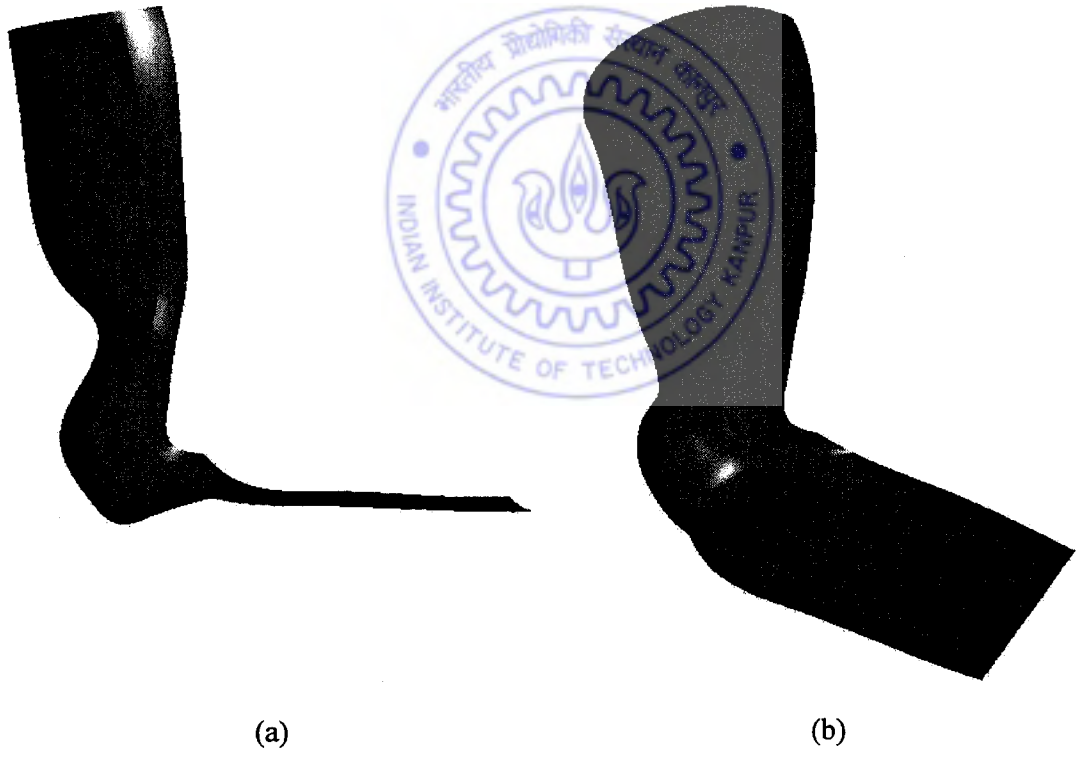

Figure 4.13: Final AFO surface model (a) side view (b) front view (**See color section**)

4.4.2.4 Solid modeling of AFO

The AFO design deals with conversion of ideas into reality and aims at fulfilling of AFO functional requirements. In this section a systemic approach has been discussed for design and development of its solid model. The solid modeling is done keeping into consideration of its functionality and strength. Our research is related to new born babies (up to the age of one month) and hence an ABS polymeric material which is tough plastic, is chosen for the design consideration. It is lighter in weight, non-toxic and having good look. Hence the chosen material fulfills the design requirements at this stage of research study.

From the literature survey [74] [82] it is observed that the center of the clubfoot deformity is lying at the heel (hindfoot) region. Hence we are interested to provide a mechanical joint of ball and socket type [11] at heel section of AFO, which behave as that of ankle joint for AFO. The design of the AFO solid model is done, with the provision of fixing this mechanism for its easy and smooth function.

Step-by-step procedures for solid modeling of AFO to fulfill the above design requirements are discussed below.

1. After making surface model of AFO in surfacer 8.1, it is exported in IGES format. The IGES surface model is imported in the I-DEAS-7 for the generation of its solid model. While opening the file in I-DEAS, it shows gaps across surface boundaries, although the surfaces were properly stitched with the position and tangent continuity in surfacer 8.1. These free edges are stitched in I-DEAS, which give watertight surface model of AFO, ready for processing in I-DEAS.
2. For accommodating cosmetic skin protection padding and sock of baby foot, a clearance is needed between foot and AFO surface, hence we offset the AFO surface by 5 mm, giving its modified surface model. By shell operation in I-DEAS and Keeping in mind, the strength of AFO for tender aged baby, a thickness of 5 mm is added to the above modified surface model of AFO. Check for any free edge and stitch if necessary. These give 5 mm thick, solid model of AFO. Figure 4.18 (b).
3. For providing an equivalent ankle joint in this AFO, we located an inclined sketch plane having appropriate angle with shank surface of AFO. Using this sketch plane as a reference plane, 5 more parallel sketch planes were drawn at distances as shown in Figure 4.14 (a), on either side of it. Intersection of this reference plane and AFO outer

surface, give 6 intersecting curves. With middle points of this intersecting curve, draw four, 3 D cubic curve of suitable length and radius, away from outer surface boundary of AFO. The radius of this curve is chosen such that, they easily accommodate the ball size of joints, giving enough wall thickness. Two 3D cubic curve of convenient length were also drawn on two extreme intersecting curves itself (Figure 4.14 a). Develop a loft surface on this six, 3D cubic curve and obtained a new part solid model of AFO rib as shown in Figure 4.14 (b).

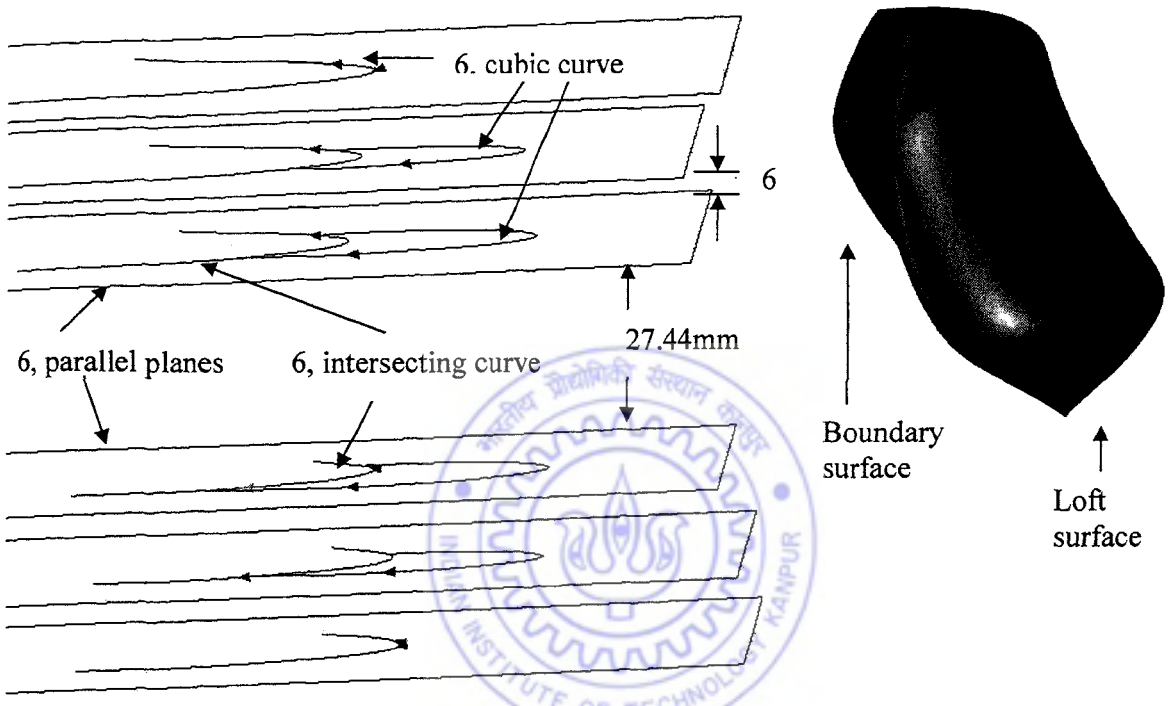

Figure 4.14: Designing of rib (a) curve modeling (b) lofted surface **(See color section)**

4. With Boolean operation join this new rib part with AFO solid model, giving new AFO solid model with rib as shown in Figure 4.20 (a). The ball of the joints is of 14mm diameter, considering 0.5mm clearance on either side, cut 2 hole of diameter 15 mm at 27.44 mm center distance by revolve cut operation at rib region of AFO (Figure 4.15). The centers of these holes are selected so that enough wall thickness is left for strength of the joint.

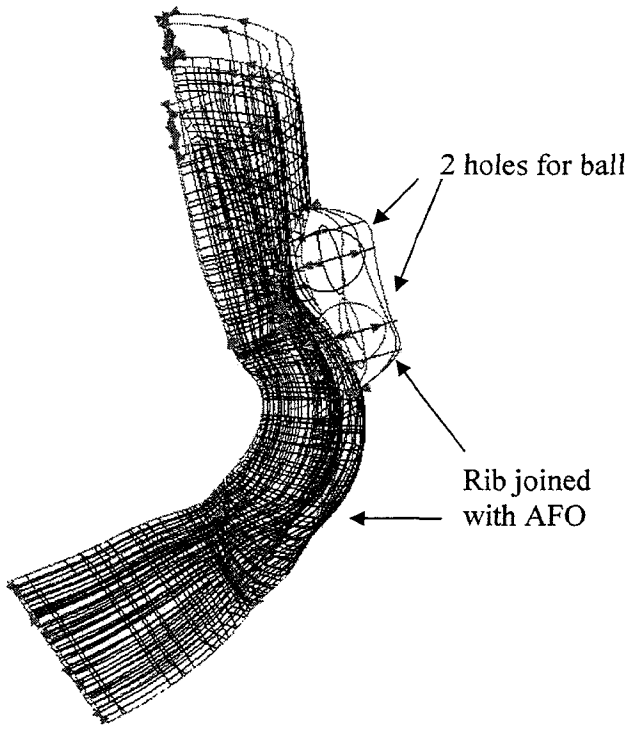

Figure 4.15: Ball & socket joint arrangement in AFO wire frame model

(See color section)

5. The rubber O-ring is of 16mm outside diameter and 2mm circular cross-section, hence develop two circular slots of 17mm diameter and 3mm depth by extrude cut operation, for housing O-ring on above two circular hole side. These O-ring prevent the ball to come outside from the socket of joint during functioning of mechanism. Figure 4.22 (a) and (b).
6. For fixing the cantilever of 4 bar link mechanism, a section as shown in Figure 4.16, is sweep along curve ae, this give additional new part chip on one side of AFO shank region. With Boolean operation this chips is joined with AFO Figure 4.22 (a). A slot of 7.05×13.2 mm rectangular section and of 20mm length, is cut, at this side shank top region of AFO, by extrude cut operation. This gives the slot for fixing the fix end of cantilever. Three holes (2 on one side and 1 on back side) on this slot are also cut, to tighten the cantilever link (Figure 4.22 a).

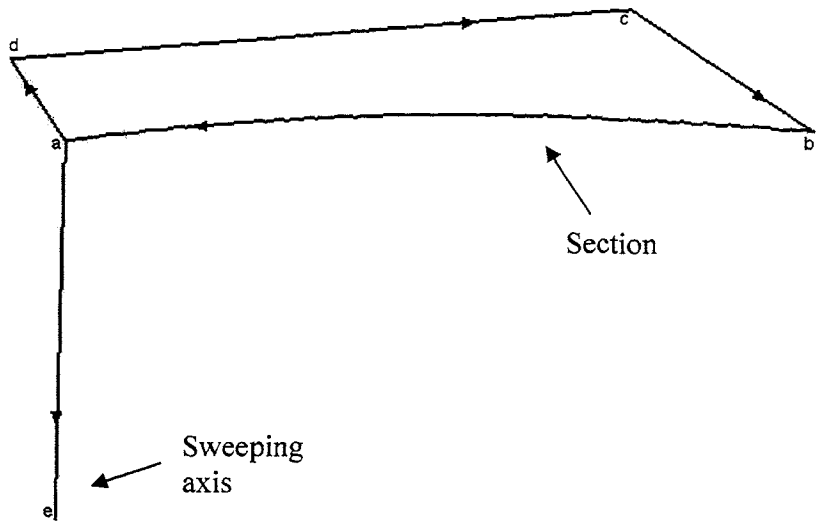

Figure 4.16: Sweep section along an axis (**See color section**)

7. Cut 2 holes with slot at a distance from toes profile on lower portion of AFO by extrude cut operation. These holes provide Pin hinge joint, for attaching the mechanism, see Figure 4.21 (a) and (b)
8. Cut this AFO by 2 parallel cutting plane, parallel to reference sketch plane between joint at a separation distance of 2mm, giving 2 pieces of AFO. Check these two pieces of AFO for any free edge and stitch if needed, this give final two –piece solid model of AFO ready for next process of prototyping. These are shown in Figure 4.20 (b).

Various solid models develop for this research study from beginning to this stage of research, are shown in following Figures.

Figure 4.17: Simple one piece AFO (**See color section**)

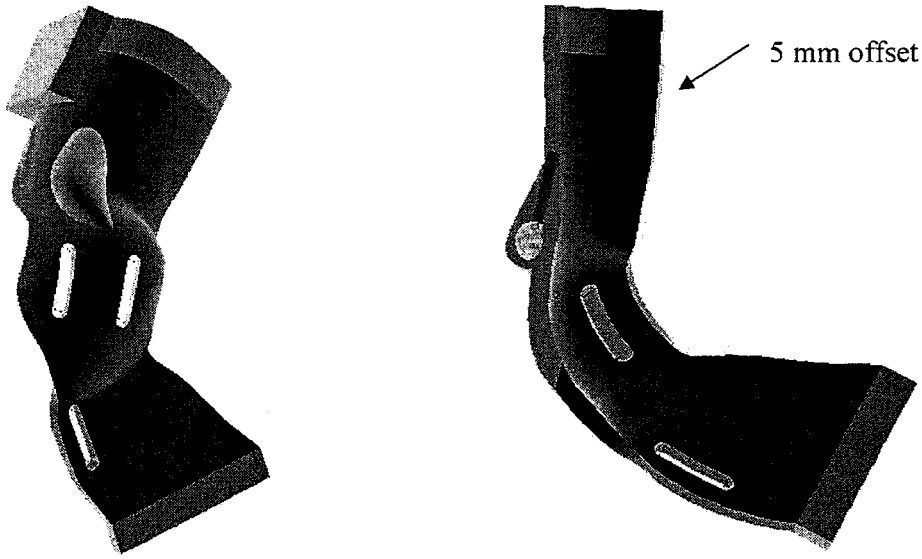

Figure 4.18: AFO having integrated arrangement for fixing single spherical ball & socket joint (a) back view (b) sectional side view (**See color section**)

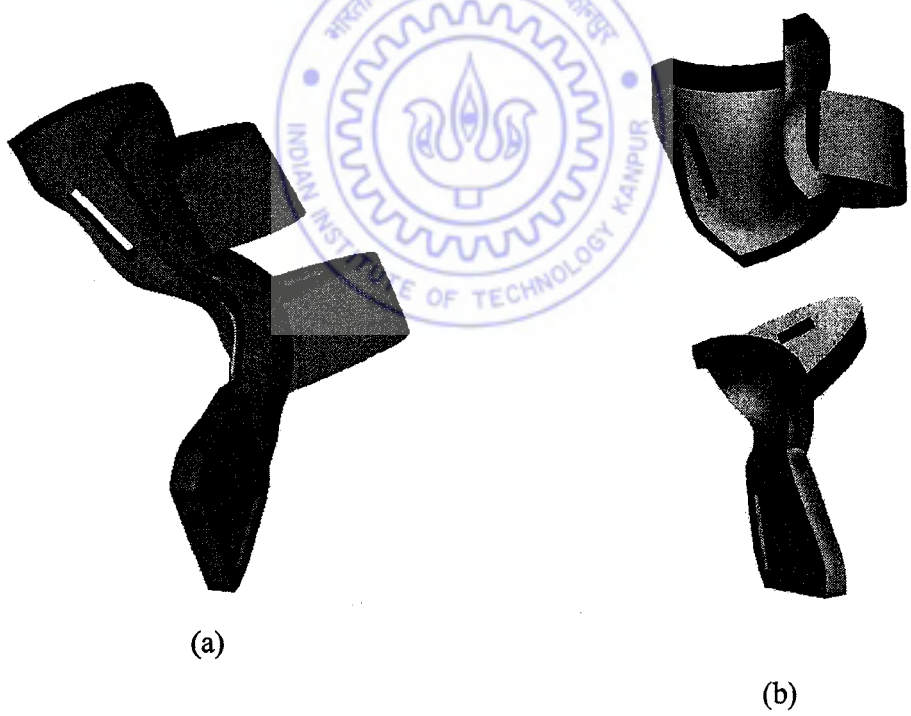

Figure 4.19: AFO having arrangement for externally fixing single hemispherical ball & socket joint (a) one piece (b) two piece (**See color section**)

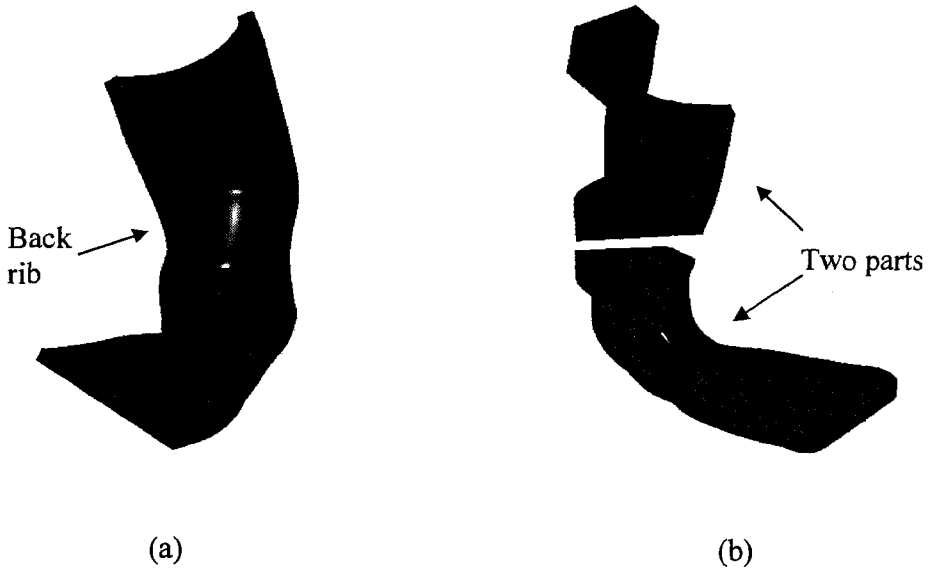

Figure 4.20: AFO with integrated arrangement for fixing double ball & socket joint (a) back view of designed rib (b) two piece front view (**See color section**)

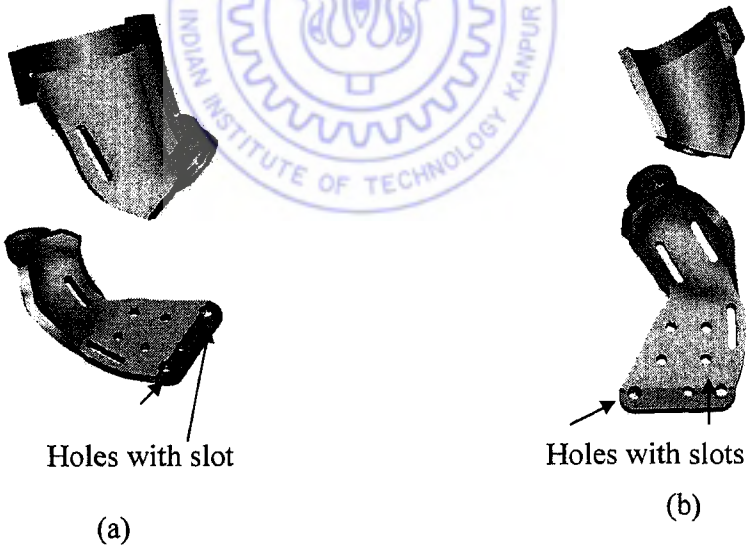

Figure 4.21: Two piece AFO having integrated arrangement for externally fixing double spherical ball & socket joint (a) AFO for right clubfoot (b) AFO for left clubfoot (**See color section**)

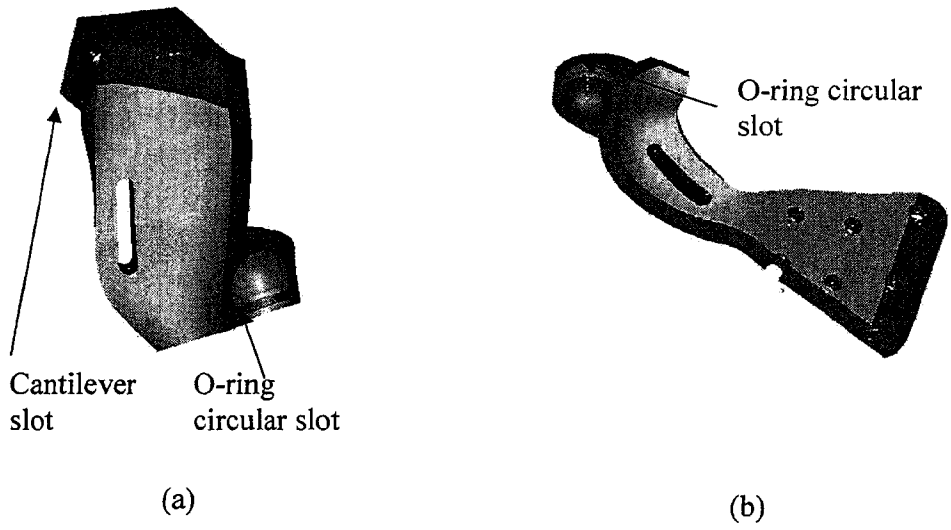

Figure 4.22: Sectional view of above right clubfoot AFO showing arrangement for fixing mechanical elements (a) upper part (b) lower part (**See color section**)

4.4.2.5 Prototyping of AFO

After CAD modeling of AFO, the next step is to create its STL file. Two STL file of lower and upper part of an AFO are shown in Figure 4.23 (a) and (b).

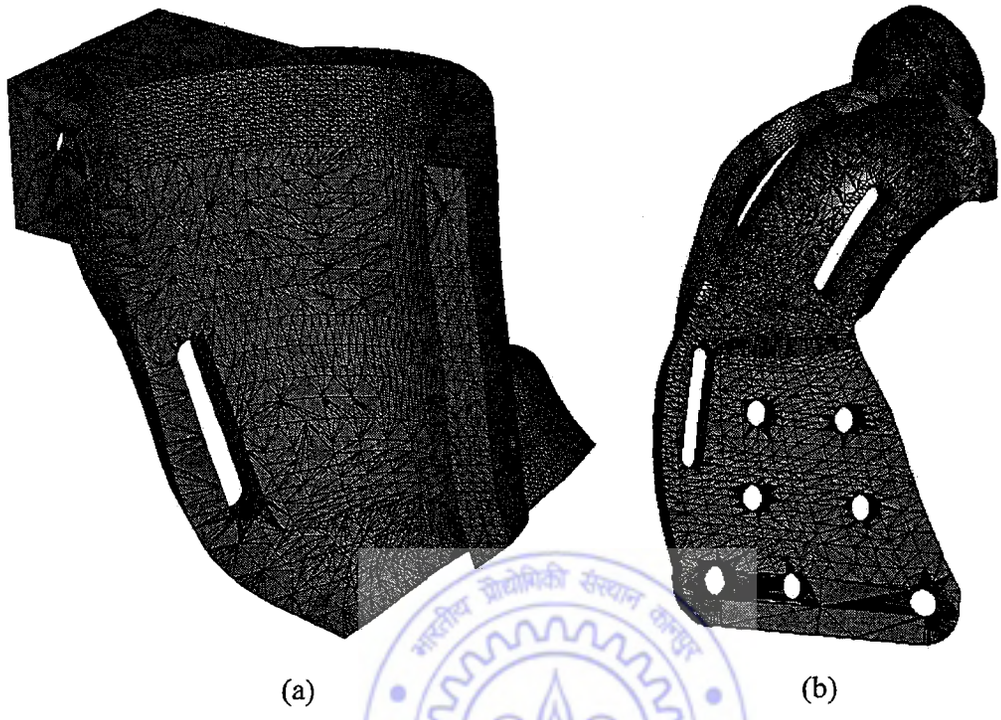

(a) (b)

Figure 4.23: STL views of AFO (a) upper part STL (b) lower part STL

These STL file is processed in INSIGHT software of Stratasys Inc., where SSL (Stratasys Slice Language) file and SML (Stratasys Machine Language) file are created.

In SSL file, the STL model is mathematically sectioned (sliced) into a series of parallel cross-section pieces by intersecting it with a set of horizontal planes. After creation of slices, base and support are created. Base is needed to hold the job, while support is needed to hold the overhanging part geometry, during part building process. Figure 4.24 show two parts of AFO (isometric view of upper part and front view of lower part), sectioned into thin slices having base and support.

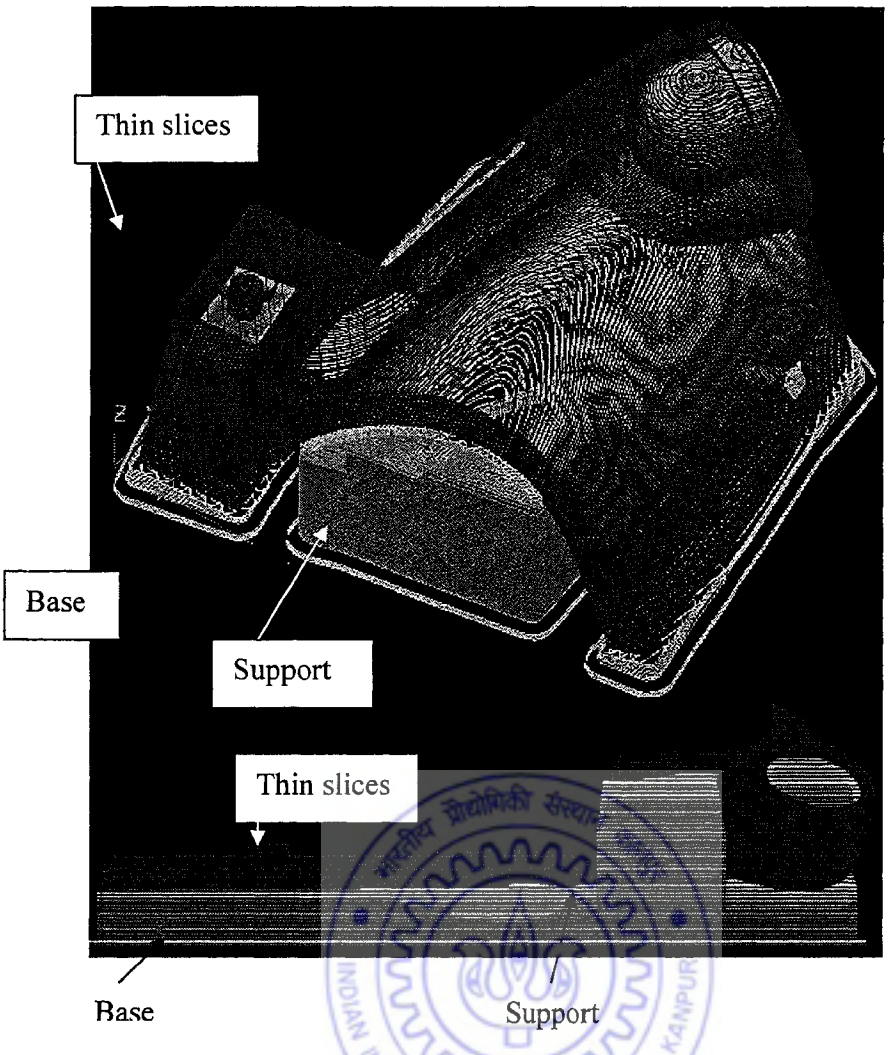

Figure 4.24: SSL file showing slices, base and support of AFO **(See color section)**

The SML file contains the actual instruction code for FDM hardware. SML file orders the FDM to take a specific tool path at each Z level. The file also has information about model and support material consumption and build time of the job.

The created SML file is sent to FDM-1650 hardware where it built the part with ABS (Acrylonitrile Butadiene Styrene), which is non-toxic and tough plastic having following properties.

S. No.	Particular	Value
1.	Tensile Strength	34.5MPa
2.	Flexural Strength	65.5 MPa
3.	Tensile Modulus	2482.8Mpa
4.	Flexural Modulus	2620.7Mpa
5.	Melting Point	270°C
6.	Softening Point	104.4°C
7.	Specific Gravity	1.05gm/cc

Table 4.2 Properties of P400-ABS Plastic

After built up of AFO its post processing i.e. finalizing the part is done, which mainly involves removal of support material from the model and its surface finishing by mechanical means.

4.4.2.5.1 Assembly of AFO

We have prototyped many AFO, during early stage of research, whose solid models were shown in previous section of this chapter. Those AFO are of two types rigid and flexible. The rigid AFO (fix shape & size) have the provision of holding and keeping the foot statically, as equivalent to normal foot. This AFO does not have any provision of dynamically quantitative load applying arrangements and hence does not meet the requirements of AFO. The designing and prototyping of this type of AFO give a feedback to proceed ahead. One such prototype is shown in Figure 4.25. After prototyping of this rigid AFO, in next step, a flexible AFO is prototyped, by providing a rubber joint of double dowel section as shown in Figure 4.26. This AFO does not give enough degree of freedom for correction and both this rigid and flexible AFO fails in form, fit and function test.

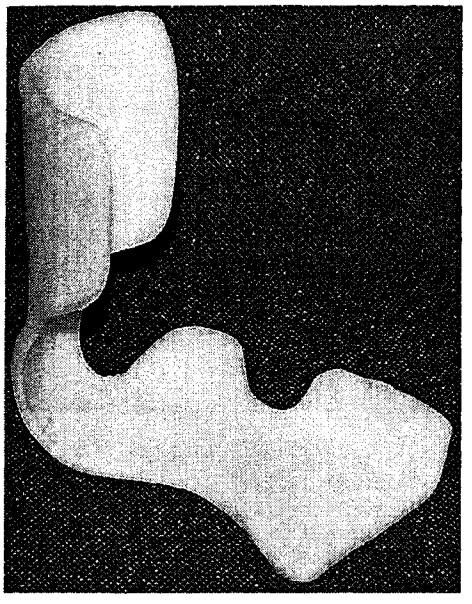

Figure 4.25: Prototype of rigid AFO

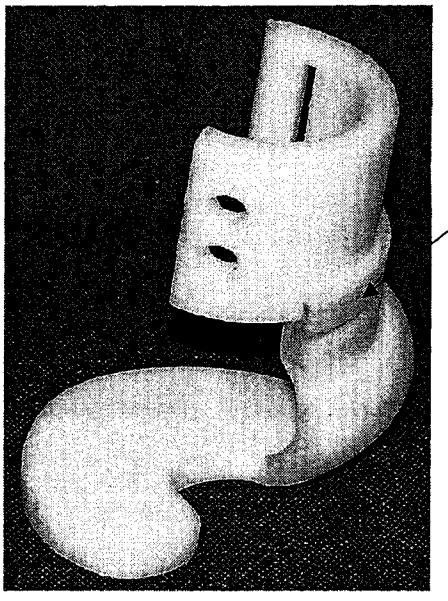

Figure 4.26: Prototype of flexible AFO

Hence the latest AFO whose solid modeling procedure was explained in previous section, and it full fill the mechanical design consideration of AFO is prototyped and assembled. The assembly involves different mechanical elements given in table 4.1. These elements needed some machining operations, before assembly and they are briefed as follows.

The tapping operation is done across balls diameter and at one end of cantilever, as per stud and fastening screw size. For passing the screw link and fixing the U-pin, holes of different size are also drilled on other end of cantilever acrylic strip. Drilling through holes, in nylon bar across its diameter at its two ends, as per pin size is done. The head end of screw link is completely machined and at this end, one through hole of 1.5 mm diameter is drilled for hooking the spring end. One end of spring is made circular and its other end is hooked to the screw link. Cosmetic padding is cut with scissor as per required shape and size.

After performing all above machining operations, the mechanical elements are ready for assembling. The two parts of the AFO is taken, and 2 balls are housed in sockets and locked with rubber O-ring, these develop the ball & socket joint. Using pins, cantilever, screw, spring and nylon bar attach the 4 bar mechanism with these 2 parts of AFO. Glued the cosmetic padding piece on internal surface of AFO with instant adhesive. These give final finish assembly of AFO. Its three views are shown in Figure 4.27 (a) (b) (c).

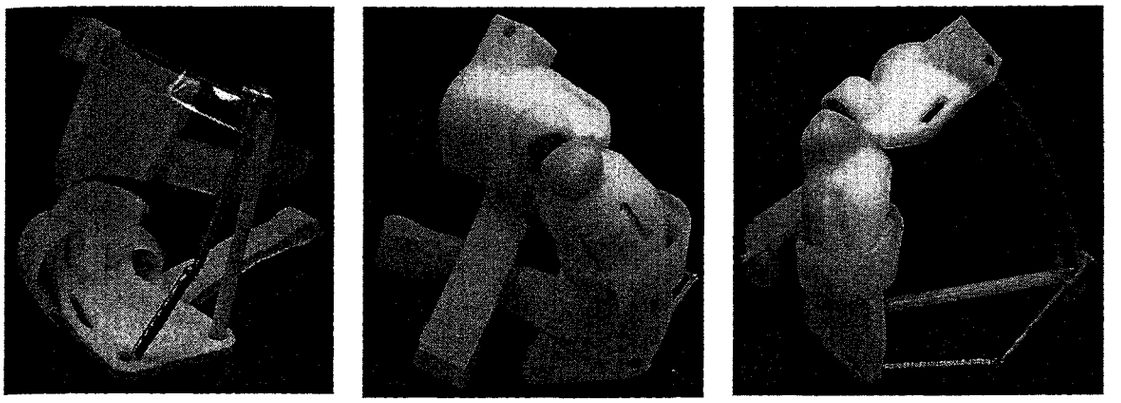

(a) (b) (c)

Figure 4.27: Prototype of developed AFO (a) front view (b) back view (c) left side view (**See color section**)

4.4.2.5.2 Form fit and function checking

Figure 4.28 Shows the prototype of an AFO made up of an ABS material and is very much like the final working product. It give the feel, how it looks, grips the foot and function. The completeness of this prototype meets the requirements of AFO by its shape, color, design, feel and overall look. It is tested on silicone rubber foot and it is observed that the required degree of rotation for correction of foot is obtained. This can be use for actual clinical test.

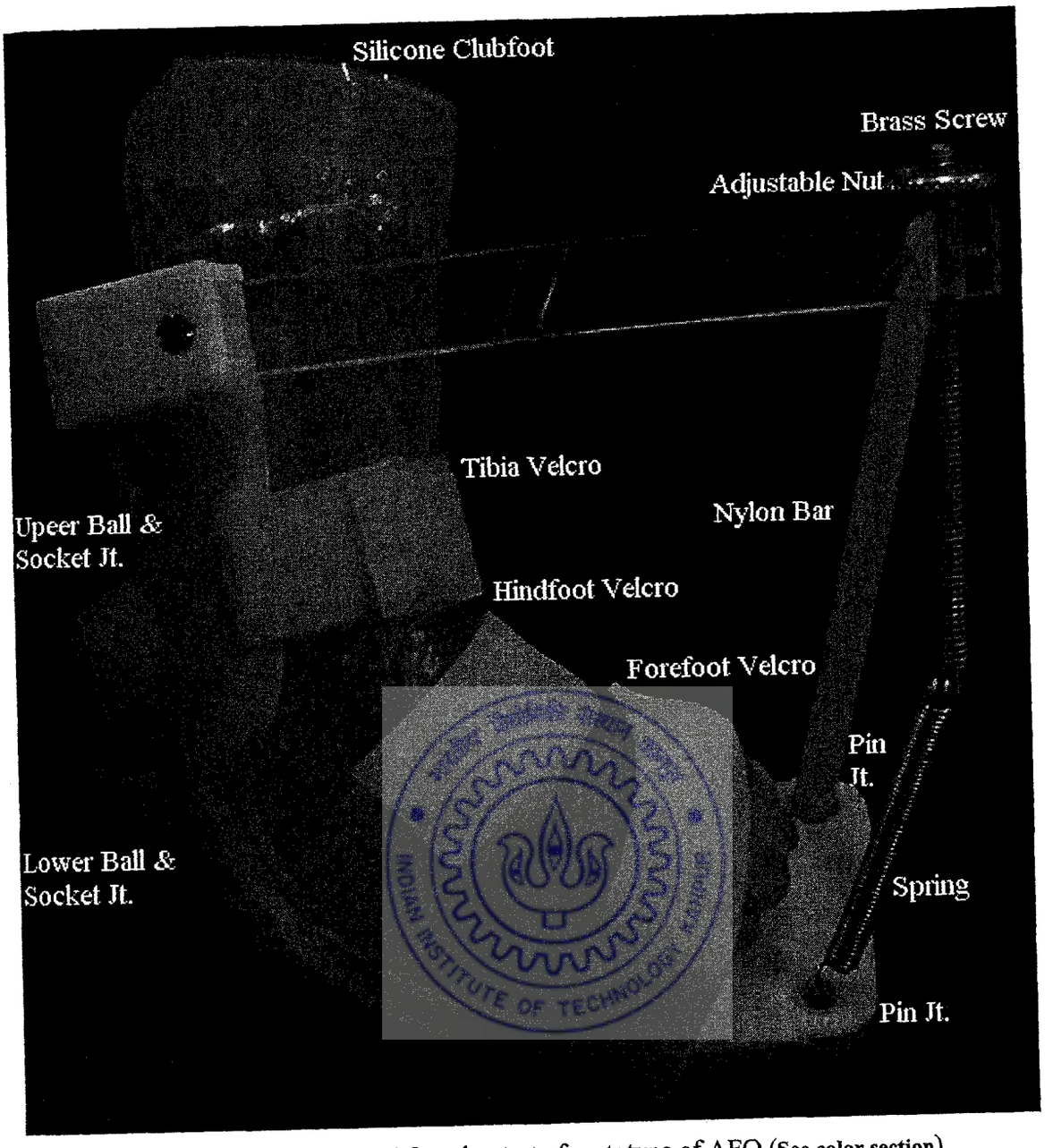

Figure 4.28: Form, fit and function test of prototype of AFO (**See color section**)

Chapter 5

CASE STUDY

Integration of medical imaging to CAD, RP and vacuum casting process, helps in 3D reconstruction and manufacturing of realistic anatomic models. These models and prototypes play a significant role in the reduction of risk and cost for both the patient and physician. Although it is a relatively new practice, case studies and applications prove the potentials and importance of this phenomenon. Figure 5.1 shows the relationship of different case studies, which was conducted, in order to achieve the targeted goal of clubfoot correction.

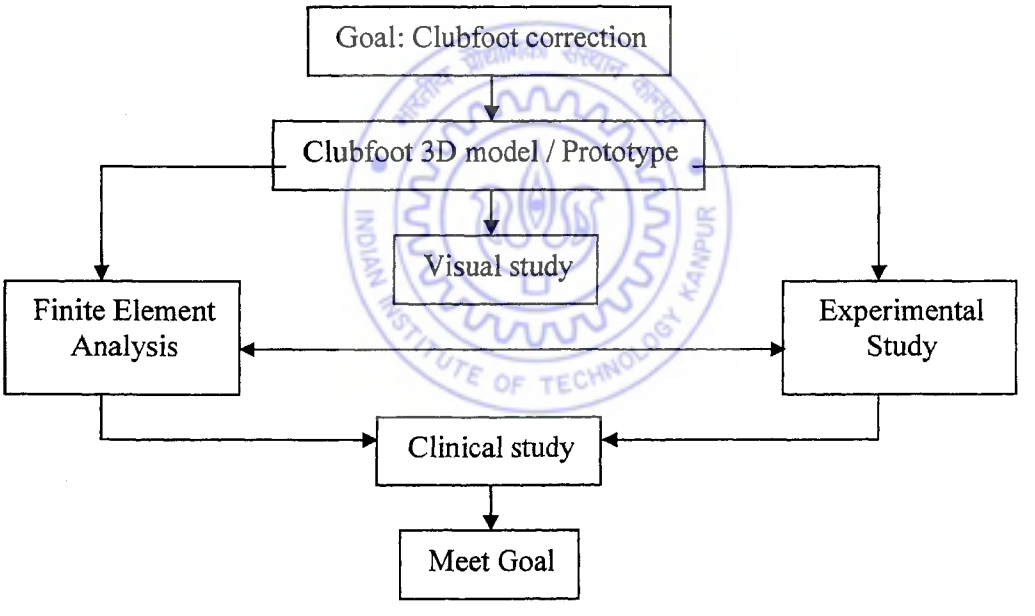

Figure 5.1: Relationship of different study for clubfoot correction

This chapter, present the finite element case study of clubfoot, experimental case study of silicon clubfoot, visual case study of RP clubfoot model and a clinical case study of a clubfoot patient.

5.1 Finite element case study of clubfoot

Finite element analysis has a significant role in soft tissue mechanics, particularly when it is coordinated with experimental research. One important new emphasis in finite element modeling is to consider its applications in very small dimensions where mechanical electrical, and biochemical responses must be simultaneously considered. One important role of finite element analysis in soft tissue mechanics in the immediate future is to enable us to obtain certain quantitative input to facilitate continued research effort [31].

Several 3D finite element models of the human adult foot have been developed, but most have been uniquely tailored to study the loading that a lower limit may undergo in automobile accidents, while others have studied the effects of Hanse's disease, Some finite element foot model was used to analyze sports injury and footwear design [16] [12] [8] [4].

Finite element analysis in soft tissue mechanics must be viewed somewhat differently from its application in traditional structural mechanics research, this is mainly because the "normal response" of soft tissue cannot be uniquely defined. There is always a range in the magnitude of pressure or deformation of the tissue that is considered to be normal. This contributes to the difficulty in assessing accuracy in analytical solution procedures. Additionally, the experimental data available on soft tissue are generally limited. Even for those tissues where data are available, there are often more questions than answers in the conditions and limitation of the data [31].

In present study, a finite element analysis of a 3-D realistic clubfoot model, which incorporates the actual geometry and appropriate material property data, is done. This analysis helps in exploring the model's applicability in predicting the biomechanical response. The method involves the creation of a finite element model by subdividing the clubfoot continuum into a finite number of regions called elements. These elements are connected at finite number of points called nodes. Finally an approximate admissible solution is constructed over the assemblage of elements, and the solution continuity is maintained at the inter – element boundary. The deformation and stress analysis of the clubfoot model is carried out using, Patran 2002 r2a version (section 1.4.1 chapter1) software. Before proceeding further, the following assumptions are made, for simplicity of the problem

I. As the present study is restricted to foot of the newborn babies, which is under growing stage and the bone tissue are of spongy nature, whose ossifications is not achieved. The foot is very soft and almost behaves like rubber. Hence, to avoid complexity in analysis because of composite material (bone, tendons, cartilage, ligament, blood vessels, nerves, skin etc.), we assume that, the foot is made up of homogeneous isotropic material of soft tissue. The Young's modulus of elasticity and poisson's ratio of soft tissue is taken as 1.0 MPa and 0.49 respectively [44].

II. No material transport takes place in the system and the material is considered to be incompressible.

III. Elastin and collagen fibers whose analytical model made by finite element analysis and other analytical process as shown in Figure 5.2, are considered to be the force bearing element components in soft tissue [30].

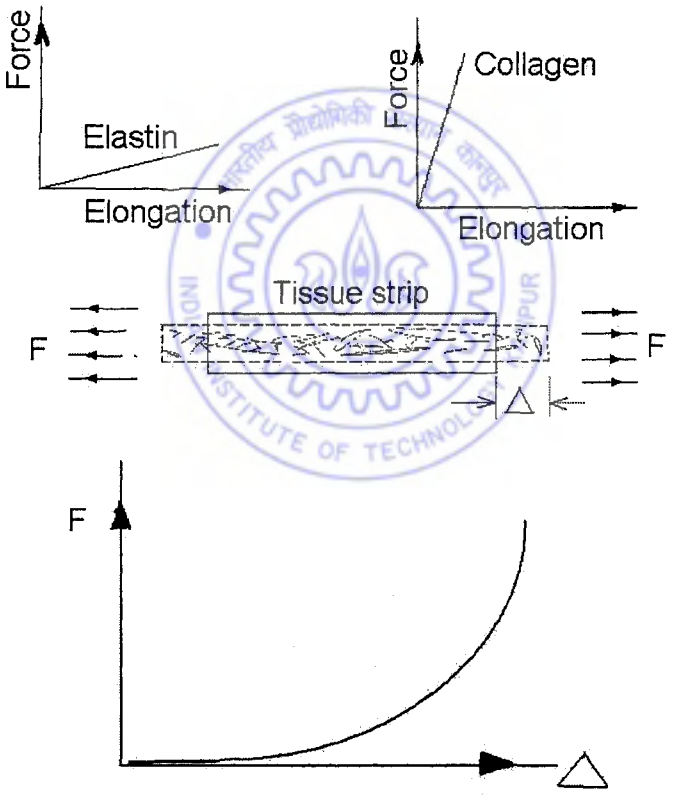

Figure 5.2: Schematic illustration of the analytical model of the force – elongation relationship of soft tissue strips.

IV. The foot is considered, like cantilever beam whose upper end (i.e. top cross section of tibia) is fixed and corrective loads are applied at lower free foot end.

V. The elements of the foot are considered to be of three dimensional, 10-noded, tetrahedron solid elements as shown in Figure 5.3.

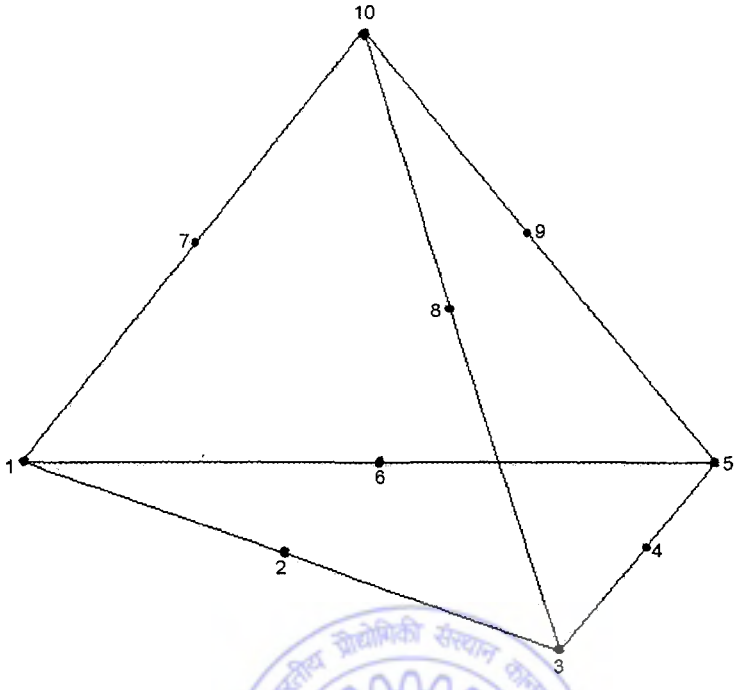

Figure 5.3: A, 3D solid, 10 node Tetrahedron element

VI. The corrective loads (bending) are applied, at regions of interest on foot, in consultation with orthopeadic surgeons to avoid any other anatomic joints problems of foot.

VII. The model geometry shown in figure 3.9 (d) of chapter 3 is used for simulation.

5.1.1 Finite element modeling

In order to convert the clubfoot shape to the normal foot shape by non – surgical correction, some exact external loading arrangement is needed. Before proceeding for the direct external loading arrangement to the realistic baby clubfoot, some predetermined theoretical foot analysis is needed. The deformation and stress induced in the clubfoot can be predicted by using appropriate mathematical or numerical model of clubfoot acted upon by important corrective load. Hence it is necessary to model the clubfoot to establish the corrective deformation and stress distribution in it before directly applying the corrective load to the realistic newborn baby clubfoot.

After making the above assumptions, the 3-D realistic geometry of the clubfoot (solid model) developed by using medical imaging scans data in section 3.4.1 of chapter 3, Figure 3.25 and Figure 3.26 is used for analysis. The model in I-DEAS is exported in IGES format and is imported in patran software.

In geometry toolbox of Patran, the imported geometry is verified, where it shows 5 surface patches only. With the helps of B-rep method (section 3.4.1.1 of chapter 3), a solid of clubfoot is created with these surface patches, this give a valid solid, suitable for finite element analysis in this software. With finite element toolbox this valid solid is discretized into 3D, 10-nodded tetrahedron element as shown in Figure 5.4. The discretization gives:

Total number of elements	= 2315
Total number of nodes	= 3780
Numbers of degrees of freedom/node	= 3

The various elements are assigned the properties of soft tissue as per assumption number I above, using elements properties toolbox of the software.

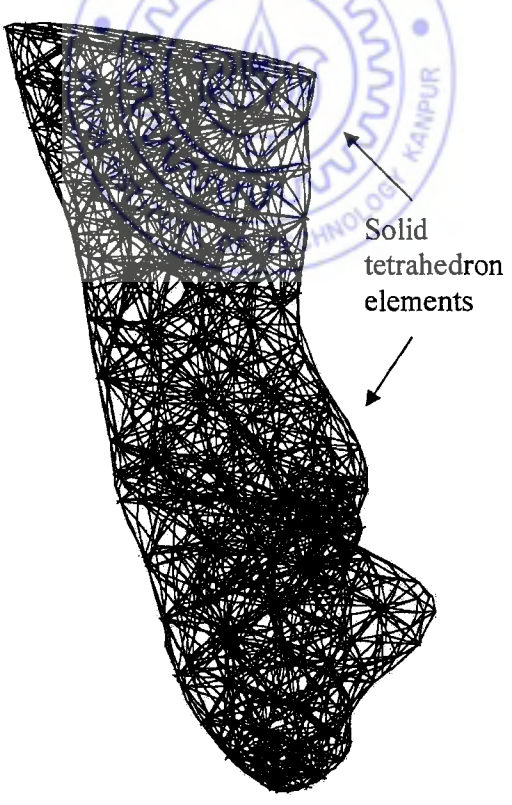

Figure 5.4: Finite element model of clubfoot.

5.1.2 Loads and boundary conditions

In Loads / BCs toolbox, as per assumption no IV above, the upper face of the clubfoot (tibia top face) is fixed. Hence, this part of the clubfoot does not have any translations or rotations, so all *x*, *y*, *z*, translations are zero for this upper fixed face of clubfoot. The 4 different corrective bending loads at 4 regions of interest, as per assumptions number VI above are applied to the clubfoot. The boundary conditions and various corrective bending loads are shown in Figure 5.5. The details of the applied corrective bending loads are as follows

a. Corrective bending loads F1= 20.0 N, in downward direction is applied at point A, having node number 660, located at upper side of 1st metatarsal region (big toe). This force is applied for correcting equines of forefoot.
b. Corrective bending loads F2= 20.0 N, in upward direction (-ve) is applied at point B, having node number 1237, located at lower side of 5th metatarsal region (small toe). This force is applied for correcting equines of forefoot.
c. Corrective bending loads F3= 7.0 N, in lateral direction is applied at point C, having node number 2642, located at heel region. This force is applied for correcting varus of heel.
d. Corrective bending loads F4= 5.66 N, in medial direction is applied at point D, having node number 325, located at upper surface of cuboid region. This force is applied for correcting adduction of fore foot.

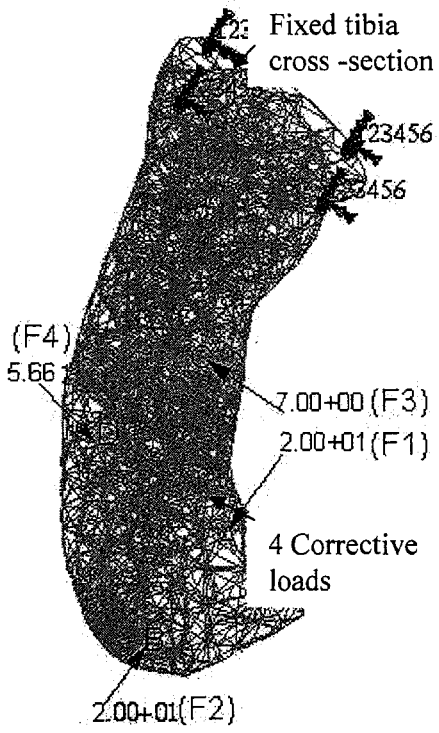

Figure 5.5: Boundary conditions with corrective loads on clubfoot finite element model (**See color section**)

After creating the geometry, assigning the element properties, assigning the boundary condition and applying the corrective bending loads on finite element clubfoot model, the analysis of clubfoot model is started, using analysis toolbox of software.

5.1.3 Results

Under linear static analysis, the various obtained results are presented here.

Fig.5.6 represents the average displacement of the clubfoot because of applied corrective bending loads. The contour plots show the behaviors of foot due to applied corrective loads. The maximum value of the deformation is found to be 1.44×10^{1} mm at node number 2642, while its minimum value is 0.0 mm at node number 2548. The simulation shows that the medial heel regions of the clubfoot, displaced in lateral direction, which is necessary for removing the varus of heel. Hence this type of loading arrangements at heel, helps in minimizing or removing the varus of heel in deformed foot. However the magnitude of applied corrective force and deformation of clubfoot depends upon nature of deformity (light, moderate, severe) and properties of individual tissue.

The forces applied at A and B are equal in magnitude but opposite in directions, hence they constitutes the moment and because of this, the simulation shows that the small toe region of fore foot is displaced upward. This displacement reduces the equines of fore foot in clubfoot.

The simulation also shows the minor displacement of midfoot in lateral direction because of the combined applied corrective load at point D of cuboid region and at point A and B. This displacement minimizes the adduction of fore foot in clubfoot.

In conclusion the contour plots of simulation shows the corrective deformation of clubfoot, as per gray scale, given on right side of clubfoot in Figure 5.6.

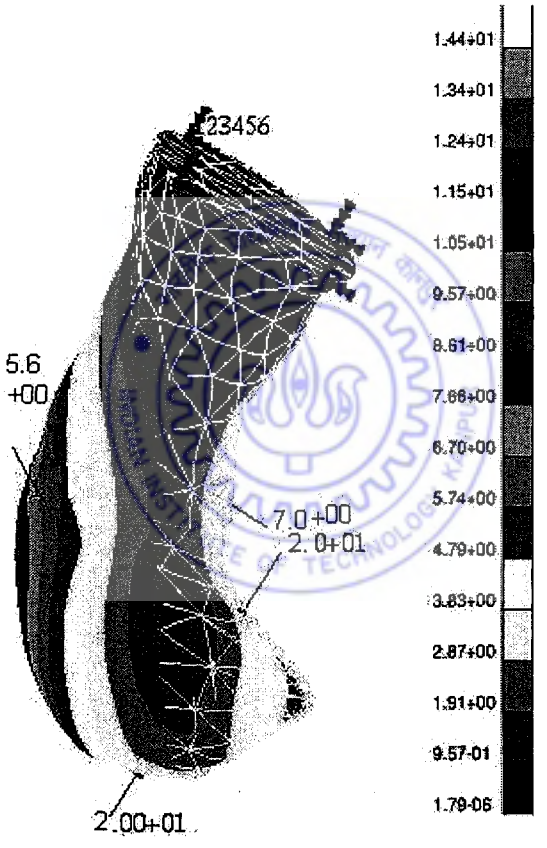

Figure 5.6: Deformation of clubfoot model (**See color section**)

Figure 5.7 represents the maximum principal stress along with displacement due to point corrective bending loads. The contour plots show the foot average behaviors due to applied corrective load. The maximum principle stress is found to be 7.52×10^{-1} MPa (tensile) at node number 3228, while its minimum value is found to be -3.79×10^{-1} MPa (compressive) at node

number 2705. Both these value are obtained at maximum deformation of 1.44×10^{1} mm at node number 2642. The simulation, shows the variation of principle stress along with displacement, higher the displacement more is the principle stress and vice versa. The contour plots shows that the principle stress is found to be more, particularly at the location where the forces are applied, which is confirmed because of the stress occurred during simulation, at F1, F2, F3 and F4 acting points. The contour plots show the maximum principle stress variation, whose value is given in the gray scale of Figure 5.7. This contour plots is taken at a particular deformation of 1.44×10^{1} mm at node number 2642 and the plots is different at different deformation.

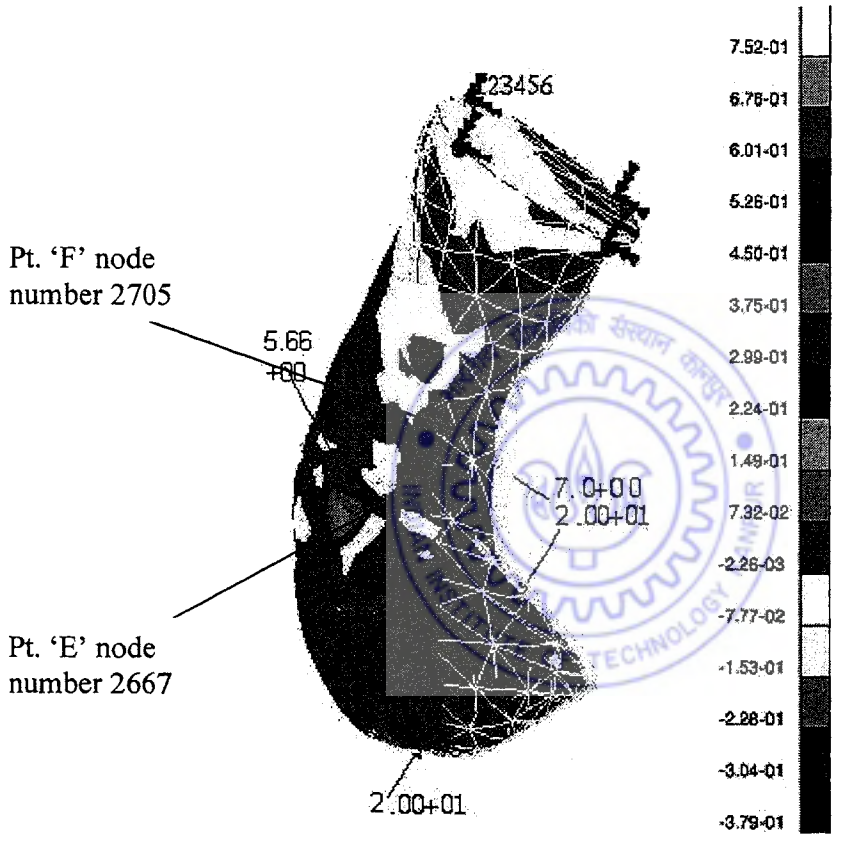

Figure 5.7: Maximum principal stress & displacement of clubfoot model (**See color section**)

Figure 5.8 represents the von Mises stress distributions because of applied corrective bending point loads. The contour plots show the average behaviors of foot due to applied corrective loads. The maximum value of von Mises stress is 6.76×10^{-1} MPa found at node number 2667 (Point 'G', near the force F3 at C), while its minimum value is 1.12×10^{-3} MPa is found at node number 3517 (at point 'H', near force F3 at C, but at bottom portion of foot). This stress found when maximum deformation of 1.44×10^{1} mm is occurred at node number 2642. The

contour plots shows the von Mises stress is more particularly at the region where corrective loads are applied. The variations of this stress are proportional to deformation. The stress contour plots of both maximum principle stress and von Mises stress are different. More stresses are found to be at the lateral side of tibia parts. Both principle stress and von Mises stress are maximum at different node. Their minimum value is differing at different node number. The result also shows that the calculated von Mises stress does not exceed the yield stress of soft tissue.

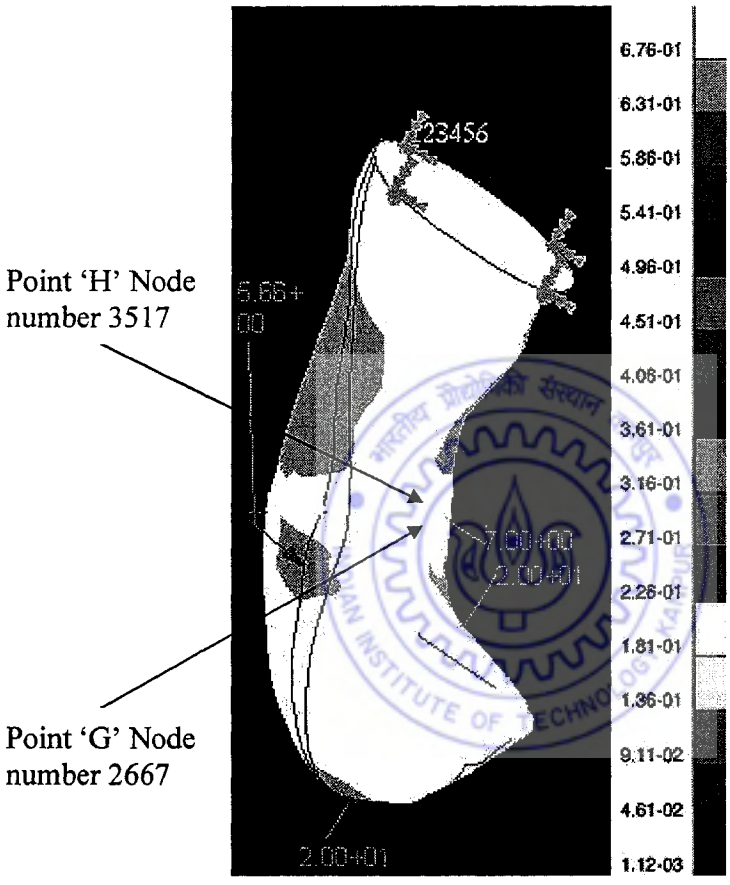

Figure 5.8: von Mises stress distributions in clubfoot model **(See color section)**

5.1.4 Discussion

The present three-dimensional analysis allowing the description of the 3D clubfoot deformity and from this observation one should get a clear idea about the development of stress with deformation. The results of the stress analysis show that the von mises stress are high at the applied load region and on lower posterior region of tibia. These areas of high von mises stress

are important since these are the regions where major anatomical ankle joints are located. This stress distribution is useful for orthopedician who applied plaster of Paris bandage for correcting the clubfoot.

While applying the forces the tissues structures is changes, which vary the blood flow and other tissues characteristics [45]. It is also observed that as the magnitude of F3 is increased the displacement is increased, but in order to maintain the upper and lower anatomic ankle joint position, this force cannot be increased beyond a specific limit and this limit is depends on the nature of deformity. Hence while applying the gradual distraction forces the deformation should not be increases suddenly at the ankle joint regions, otherwise the ankle joint will start growing in an abnormal direction which is not suitable for correcting the clubfoot and will increases the deformity in other direction.

The method allowed to analyze the 3D motion of the clubfoot and to get a better comprehension of this deformity. The simulation of the motion of clubfoot should be of interest as a tool for preoperative surgical planning of orthopedic surgeons for better result. These investigations provide an insight into the development of a Splint / Orthosis for non – surgical correction of clubfoot deformity in newborn babies.

The finite element model of the clubfoot will serve as a base for its mechanical studies and the analysis helps in the conversation of clubfoot geometry to the normal foot geometry. The stress developed in the foot depends upon geometry of the foot, magnitude and insertion points of the corrective force. By studying the descriptions of 3D clubfoot's motion, three dimensional finite element analysis provide an excellent tool for evaluating the potential of AFO design.

5.2 Experimental case study of clubfoot

All materials deform to some extent when subjected to a stress. Elastic materials have internal forces, which restore the size and shape of the object when the stress is removed. If the deformation, or strain, is directly proportional to the applied stress and if it is completely reversible so that the deformation disappears when the stress does, then the material is said to be perfectly elastic. All elastic materials follow the basic law of elasticity known as Hook's law.

This case study gives an idea about deformation of silicone clubfoot at some region of interest, when corrective loads are applied. The case study is performed using LabVIEW experimentation, which is a graphical programming language. The LabVIEW uses icons instead of text to create applications. In contrast to text based programming languages where instructions determine program execution, LabVIEW uses data flow programming, where the flow of data determine execution. The programs of the LabVIEW are called virtual instruments, or VIs, because their appearance and operation imitate physical instruments, such as oscilloscopes and multimeters. A VIs mainly contains Front panel, block diagram and icon and connector pan. Data can be transferred on block diagram through wires. LabVIEW supports data flow programming. A block diagram nodes execute, if data is available on its entire node. When the node completes execution, data is passed to the output terminal.

5.2.1 Experimental set-up and procedure

Silicone, in comparison to metal, is made up of very long chain polymer molecules. They are tangled and intertwined in a very disordered state, when stretched, they become slightly ordered and aligned. When it is heated the vibrations of the molecules become more intense, the molecules become more tangled and it contracts. In case of metal when it is heated, the atomic vibrations increases, the inter atomic distances open up and the metal expands. The Young's modulus of rubber and other "soft" elastic material is about 10^6 MPa units.

The Lab view instrumentation system, having 8 channels for measurement, is used for the experiment. The various components of the set up is shown in Figure 5.9 (a). Figure 5.9 (b) below left shows the silicone clubfoot used for the experimental study is fixed in an AFO (Figure 4.28) for applying the loads. It also shows the various strain gauge leads connected to the VIs instrumentation. Figure 5.9 (c) shows the corrective load application by rotating the flynut through hand and the corresponding output signal on the display unit

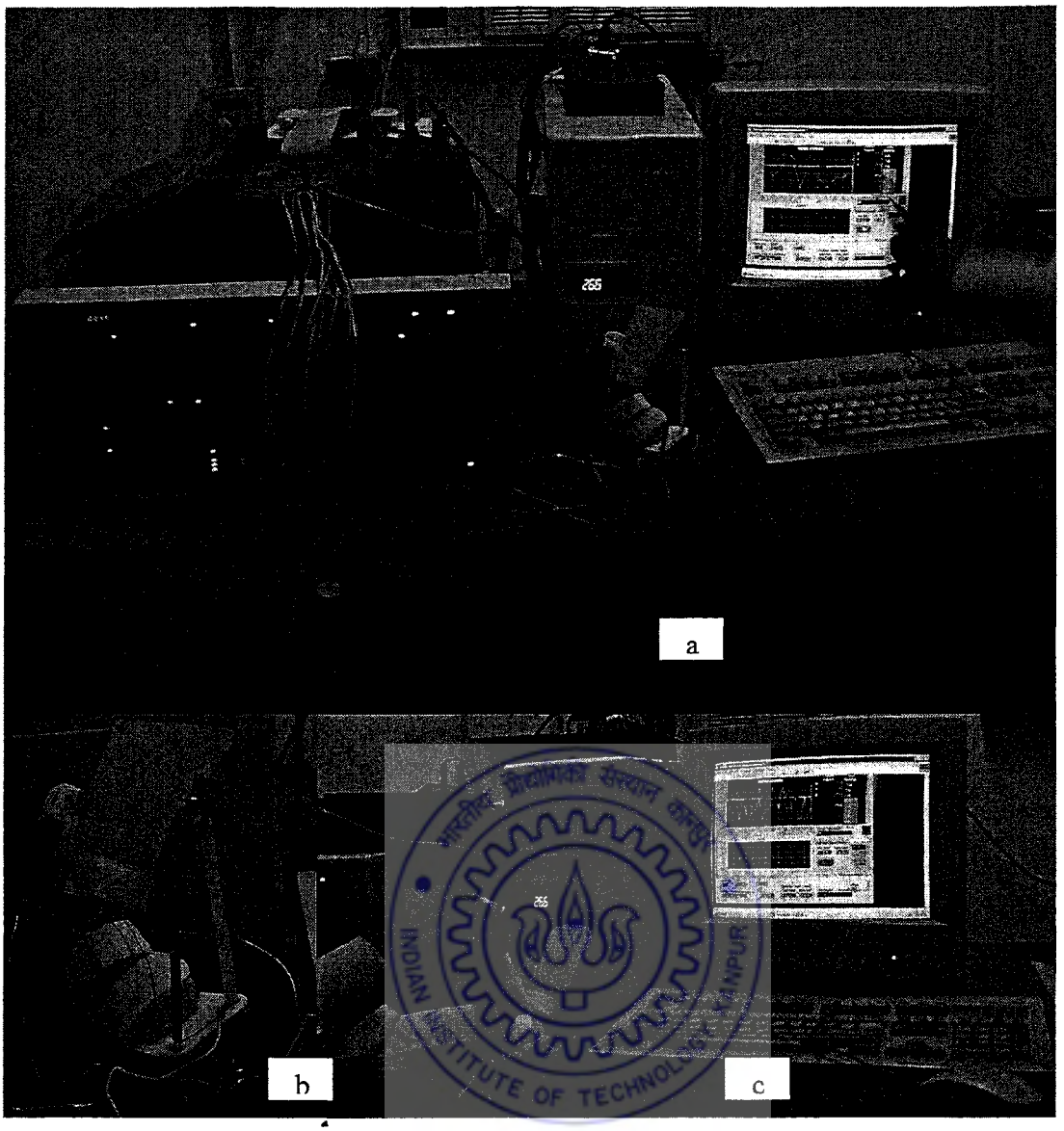

Figure 5.9: Experimentation on silicone clubfoot model

Three electrical resistance strain gauge (Made in Japan, having gauge factor 2.11) are fixed in the silicone clubfoot during its casting process (section 3.6.2, chapter 3). These are fixed at region of interest in the hindfoot and midfoot as represented in Figure 5.10 (b) and (a) as per following details.

a. Strain gauge "1" is fixed longitudinally, approximately parallel to axis of shaft (tibia), at posterior (back) medial side of heel (hindfoot).
b. Strain gauge "2" is fixed at talocalcaneo joint region, longitudinally parallel to articulated joint surface on lateral side of hindfoot.

c. Strain gauge "3" is fixed at talonavicular joint region, longitudinally parallel to articulated joint surface on anterior (front) side of midfoot.

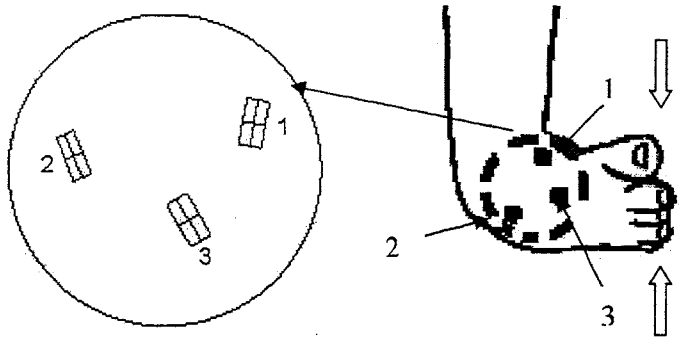

(a) (b)

Figure 5.10: Strain gauge fixing in clubfoot model (a) arrangement of strain gauge (b) placement of strain gauge (**See color section**)

With the help of Velcro strip the foot is fixed on the AFO and various leads of the strain gauge are connected to the instrument system as shown in Figure 5.9 (b). While connecting the strain gauge leads, care should be taken that each leads must be connected at a particular channel only. After making all connections, check it and start the experiments as follows.

i. Hold the AFO on the table along with, foot and connections so that no movements take place, Figure 5.9 (c).
ii. Turn the flynut (tightening) with hand for applying compressive loads, without any jerks Figure 5.9 (c) and observe the live reading of applied load on the computer display.
iii. Continue applying compressive load at uniform rate upto 170.00 seconds (30 turns), observing the shape of the computer – generated load vs. strain graph throughout the loading. The time should be selected so that maximum travel of the screw is possible.
iv. As a precautionary measure, initially perform some trail experiment for checking the repeatability and, then proceed for the final experiment. It should be remember that the load must be applied smoothly without any jerks.
v. Stop the experiment and the output data is recorded and processed in Microsoft excel for plotting the result.

5.2.2 Spring stiffness and calculations for result

Spring stiffness

A universal testing machine of INSTRON make is used for determining the stiffness of spring through tensile test. The spring specimen is fastened between two grips of machine as shown in Figure 5.11.

Figure 5.11: Spring stiffness determination on universal testing machine

The upper grip attached to the load cell, which is fitted in the fixed upper crosshead. The lower grip is fitted into an adaptor mounted on top of the moving crosshead. The test is carried out, above the moving crosshead. The moving crosshead is operated vertically by a servomechanism drive system. During the test the results are plotted and recorded on a graph paper. After the test the output is taken from the machine and is presented as shown in Figure 5.12.

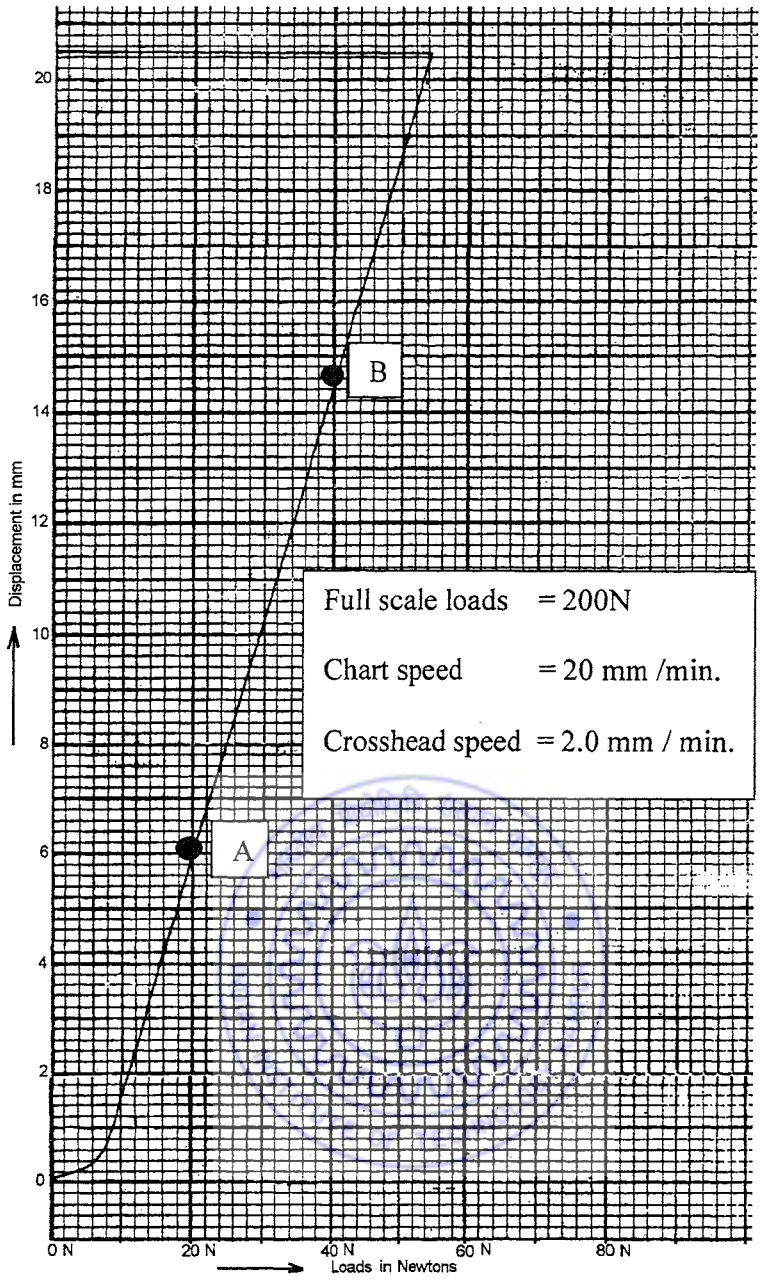

Figure 5.12: Graph showing loads vs. deformation of spring

The graph shows that the spring behaves linearly except for an initial loads upto 8.0 N for which the deflections is 0.8 mm. For calculating spring stiffness of spring, two points ***A*** and ***B***, as shown in Figure 5.12 are taken on the graph. These points will gives:

Loads along X - axis $\delta F = 20.00$ N

Displacements along Y- axis $\delta Y = 8.40$ mm

The stiffness, K of the used spring, which is defined as the ratio of force per unit deformation, can be calculated as

$$\text{Stiffness } (K) = \frac{Force(\delta F)}{Displacement(\delta Y)}$$

$$\text{Stiffness } (K) = \frac{20}{8.4} = 2.439$$

Hence the stiffness (K) of the spring for loads applying arrangement is found to be 2.439 N / mm

Conversion of time unit into load unit

The pitch of the used screw.

= 1.4 mm.

Total time for turning the flynut at uniform rate for covering maximum travel of the screw.

= 170 seconds

Total number of turn of flynut for covering maximum travel of screw.

= 30

Total deformation of the spring for these 30 turns

= 30 × 1.4

= 42.00 mm.

Hence, total uniform load on spring, applied in 170 seconds.

= Spring deformation × Spring stiffness

= 42.00 × 2.439 N

So, the load applied per seconds.

= (42.00 × 2.439) / 170

= 0.6026 N / second

Assuming ψ to be a constant factor, defined as the load per unit time, then we have

$$\psi = 0.6026 \text{ N / second}$$

The experiment was performed by applying load in a fixed time, hence we got the observation of time along with strain in all the three strain gauge. The time column of the observation in Microsoft excel is multiplied by this constant factor of ψ. This convert time scale into an approximate equivalent load (N) scale, of the whole observation.

5.2.3 Result

The result of the experiment observation (Loads Vs. Strain) are plotted using Microsoft excel and are shown in Figure 5.13 with legends on the bottom. Here Y – axis represent the strain in micrometer per meter (μ m / m or mm/m), while X – axis represents loads in newtons (N).

As the clubfoot geometry is highly variable, the graph shows its elastic behaviors under applied corrective loads at room temperature. The natures of the graph in all the three region of foot are nonlinear and are polynomial of degree three.

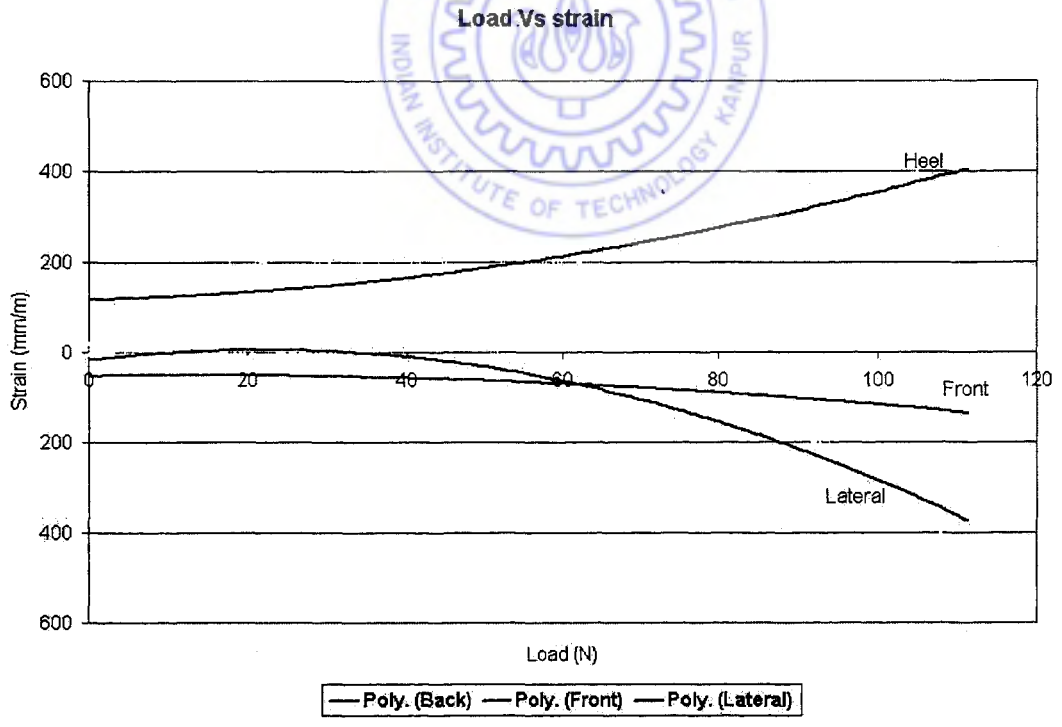

Figure 5.13: Graph showing load vs. strain for a silicone clubfoot model (**See color section**)

From this graph, at applied corrective compressive load of 110.00 N, we observe that:

The maximum strain at heel regions (where strain gauge "1" is located), is found to be tensile (+ve) 400 μm / m, while its minimum value tensile (+ve) 110 μm/m at 0.0 N, in longitudinal direction of strain gauge

The maximum strain at front region (where strain gauge "3" is located), is found to be compressive (–ve) 125 μm / m, while its minimum value is compressive (–ve) 40.0 μm / m.

The maximum strain at lateral region (where strain gauge "2" is located) is found to be compressive (–ve) 375 μm / m and its minimum value is zero.

5.2.4 Discussion

If a weight is hung on a sample of rubber material, it stretches almost immediately to a new length, but then continue to stretch slowly and exponentially in time to a final length. This is called creep. If the weights are now removed and the new contracted lengths plotted, a "return" stress – strain diagram is obtained. The two curves are not the same and this effect is called hysteresis. Rubber and rubber like substance always creep and show the hysteresis. The tissue of the clubfoot, as already assumed, is also behaved like elastic material. The graphs include only the loading parts of the experiment and hence do not account for the hysteresis effect.

From the graph it is observed that the initial strain is not zero, even when there is zero applied load. This is because of the residual stress of the silicone during casting process at which the strain gauge is deformed because of silicone curing. As most materials expand when heated and contract when cooled, but silicone is different because of its polymeric makeup.

The graph at heel increases uniformly from its minimum to maximum value, while graph at front region having almost constant tensile (+ve) strain upto 50N and then increases marginally to maximum compressive (–ve) value. Also the graph at lateral region having almost constant tensile (+ve) strain upto 30N and then increases exponentially to a maximum compressive (–ve) value. This represent that correct strains are induced at proper region due to applied deform loads.

5.3 Visual case study of RP clubfoot model

Today, medical modeling is used by various experts throughout the world as a means for diagnosis and other purposes. But till this dissertation, none of them have developed the RP model of baby's clubfoot as well as its internal bony structure. This study aimed to examine the various RP – model of clubfoot developed in chapter 3 and shown in Figure 3.32 and Figure 3.8 (b). The study was carried out in consultation with noted orthopaedic surgeons of Kanpur city (India). In this study, the overall clubfoot geometry influences by some parameters have been examined. During the study we assume that the RP model represent true real anatomical geometry.

The various parameters to be measured are, maximum length (L_{max}), maximum width (W_{max}) and maximum perimeter (S_{max}). These parameters are shown below with the help of Figure 5.14.

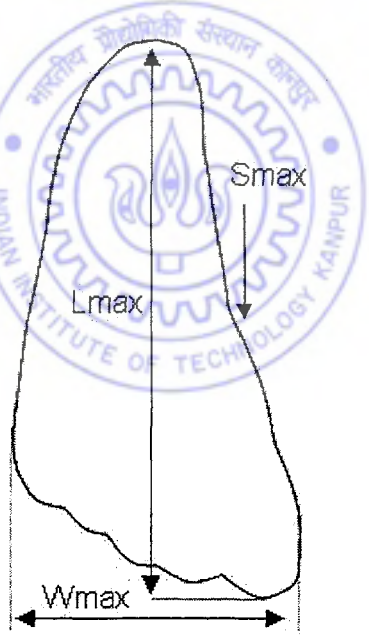

Figure 5.14: Parameters of foot for measurements

Two types of patients, unilateral and bilateral clubfoot are considered for this study. In case of unilateral clubfoot, the normal foot and deformed foot's RP models geometrical parameters are measured and compared. Similarly the bilateral clubfoot RP models geometrical parameters are measured and compared.

Unilateral clubfoot study

The measurements are done on four unilateral clubfoot, shown in Figure 3.32 (b), (c), (d) and (g) of chapter 3, having age 1 Month, 3 Month, 4 Month and 4 Years. The measured parameters are tabulated below

S. No.	Particulars	Clubfoot				Normal foot			
		Patient				Patient			
		I	II	III	IV	I	II	III	IV
1.	L_{max} (mm)	76.00	81.50	78.00	105.00	85.50	94.50	89.00	125.00
2.	W_{max} (mm)	41.00	43.50	39.00	53.00	41.50	40.50	37.50	50.00
3.	S_{max} (mm)	196.00	210.00	206.00	280.00	206.00	220.40	236.00	300.00
4.	Position of heel	Turn medially in all four patients				Parallel to transverse plane			
5.	Tibia axis	Turn medially in all four patients.				Parallel to foot axis in all four cases			

Table 5.1 Showing measured parameters of unilateral clubfoot

Bilateral clubfoot study

Two bilateral clubfoot shown in Figure 3.32 (a) and (f), having age 6 days and 5 months are considered for measurement. The measured parameters are tabulated below

S. No.	Particulars	Clubfoot of Patient I		Clubfoot of patient II	
		Left foot	Right foot	Left foot	Right foot
1.	L_{max}	63.30	66.00	91.50	88.00
2.	W_{max}	38.00	38.50	48.80	48.00
3.	S_{max}	180.00	183.00	245.00	243.00
4.	Heel position	Turn medially more than right foot	Turn medially	Turn medially	Turn medially more than left foot
5.	Tibia axis	Turn medially more than right foot	Turn medially	Turn medially	Turn medially more than left foot

Table 5.2 Showing measured parameters of bilateral clubfoot

Bony structures study of clubfoot

As the bone of the foot at tender age of the baby is under development stage, the full connectivity of the bone is not observed in foot. The RP model of normal and clubfoot's internal bony structure of hindfoot of two unilateral clubfoot patients of age 4 Month and 4 Years is developed. The model support is not removed for maintaining the position and orientation of bones. They are shown in Figure 5.15 and Figure 5.16. The shape of the bony structure is observed and compared.

(a) (b)

Figure 5.15: Ankle skeletal of foot of Patient V (a) normal foot (b) clubfoot (**See color section**)

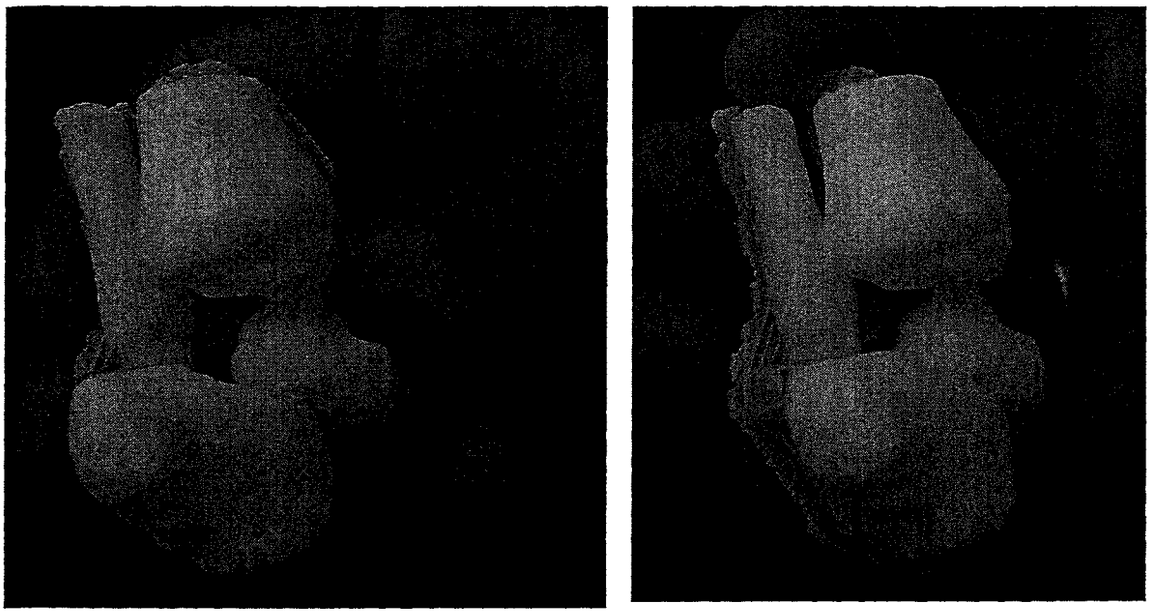

(a) (b)

Figure 5. 16: Ankle skeletal of foot of Patient VII (a) normal foot (b) clubfoot (**See color section**)

5.3.1 Result of visual study

(a) Unilateral clubfoot

After careful observation and study of table 5.1, comparison between normal foot and Clubfoot were made and following conclusions are drawn.

i. The maximum length of deformed foot (hind foot to forefoot) is shorter than the normal foot in clubfoot
ii. The maximum width of forefoot in deformed foot is more as compared to normal foot in clubfoot
iii. In clubfoot, the heal and toe is twisted inwardly as compared to normal foot.
iv. It is observed that, in clubfoot, the infant's foot point downward and turns inward while the forefoot curls towards the heel.
v. Tibia is rotated medially in clubfoot as compared to normal foot.
vi. The lateral malleolus is displaced posterior in clubfoot as compared to normal foot.

(b) Bilateral clubfoot result

From table 5.2 study and visual look of bilateral clubfoot following observations are inferred

a. On close comparisons of patients I foot, it is observed that the left foot is more deformed then the right foot.
b. Similarly it is observed that in patients II, that right foot is more deformed than the left foot.
c. In both the case the deformity is of severe nature.
d. The tendons and ligaments on lateral side are more elongated and are much shorter on medial side in both cases.
e. On touching the real foot of patient it was observed that the foot is much stiffer than the normal foot in both patients

(c) Bone observation

On observing closely, Figure 3.15 and Figure 3.16, following results are concluded.

It is observed that the talus is underdeveloped; the talar neck is shortened and deviated in the medial and plantar direction. The abnormal position of the talus causes the calcaneus to fall into the equinus. Similarly from Figure 3.15 (b), the navicular is smaller than normal and articulates with the medial aspect of the neck of the talus, which forces the forefoot into adductus. The generalized hypoplasia of the major bones of the foot causes it to be smaller than normal. The abnormal positioning of the foot creates a deep medial foot crease on the plantar aspect of the foot.

5.3.2 Discussion

This study has produced numerous results and comparing the findings of the different parts of the study can draw interesting conclusions. The results of the study indicate that, built RP model of clubfoot have good result and agreeing with discussed geometrical details in medical literatures. The study helps in understanding the ankle joint anatomy of clubfoot. The models increase their clinical importance, as it depicts the true geometry of the clubfoot.

From this study, it can be concluded that 3D-RP clubfoot models developed from FDM – 1650 by CT / MRI scan data, can help Orthopaedic surgeons for better operative treatment and hence for better patients care. We believe our study advances the understanding of clubfoot.

5.4 Clinical case study of a clubfoot patient

Under special treatment protocol, a male patient of age 1M, having unilateral deformity, who was initially treated by Ponseti method at the age of 2 weeks, was considered for treatment with AFO. The patient having the moderate deformity and his first cast was removed after 2 weeks. The cast was taken off because the patient was feeling uncomfortable in holding the cast. Also the parent was not happy with cast, as the baby was unable to perform his routine activities. He was not able to sleep at nights because of a particular fixed posture of cast. A similar AFO, like the one shown in Figure 4.27, but was a preliminary version (Figure 4.19), was fixed to the right clubfoot of patient at one month age and initially 10 mm spring displacement was given. After one week, the spring displacement was increased to 5 mm followed by another 5 mm in the next week. After 3 weeks the AFO was taken off and thrice a day (morning, evening & night) physiotherapy was performed. The AFO was again fixed in the night and a total 30 mm spring displacement was given and the patient was observed after 2 weeks followed by this, a 10 mm spring displacement was again given. After 3 weeks the AFO was taken off and physiotherapy procedure was adopted again as earlier. The AFO was again fixed in the night and a total 50 mm spring displacement was adjusted, the patient was called after 3 weeks, the AFO was removed and it was observed that the patient's foot had almost got corrected. Later on the parent was advised to see the patient wearing the AFO, only at nights and physiotherapy was prescribed twice (morning & evening) a day. The patient was kept under observation till the age of 2 years 9 months. During these periods, his foot's geometrical measurements (maximum length, maximum width and maximum circumference) were periodically noted down. The details of measurement are given in table 5.3.

S. No.	Particular	Clubfoot			Normal foot		
	Age	L_{max} (mm)	W_{max} (mm)	S_{max} (mm)	L_{max} (mm)	W_{max} (mm)	S_{max} (mm)
1.	1M	76	41.5	190	85	41	195
2.	1M 3week	80	42	194	87	41.5	199
3.	2M 1week	82	43	200	89.5	43.5	204
4.	3M	85	44.2	205	91	45.7	209
5.	1Yr.	110	49	255	112	51	256
6.	2Yr.	132	56	310	133.5	57	320
7.	2Yr. 9M	150	61	355	154	62.5	367

Table 5.3 Measured clinical parameters of unilateral clubfoot patients

5.4.1 Result

From the clinical parameters of unilateral clubfoot of table 5.3 it is observed that the clubfoot geometry gradually changes towards normal foot geometry. With the increase in time, the length and width of the foot becomes almost equal to that of the normal foot. This is probably because of the changes in growth resulting from the changes in mechanical loading on fast-growing tissues during early age of the baby growth [45].

The walking pattern of the patient is closely observed, at the age of 2 Years 9 Months. The subject is walking (forward, backward) and even jumping successfully. His walking GAIT cycle, during his walking was found to be satisfactory. He was dancing as shown in Figure 5.17 without any problem. The patient was discharged in good condition.

Figure 5.17: Corrected foot of a subject in dancing position **(See color section)**

5.4.2 Discussion

From the data of clubfoot measurements of patient in table 5.3 it is observed that, good corrective results had been observed and the treatment had resulted in correction of the abnormal relationships of the tarsal bones, as well as the abnormal shapes of the tarsal bones.

Chapter 6

CONCLUSIONS

This chapter presents the technical summery of the research, done in this thesis on AFO developing procedures for clubfoot patients. It also presents a short note on the scope for future work.

6.1 Technical summery

The main objective of this research has been to develop the prototype of an AFO using rapid prototyping. A system architecture combining computer software and mechanical hardware has been designed and demonstrated through a case study in the medical arena. Contributions of this work and significant findings from this study are summarized as follows.

By studying anatomy of foot, biomechanics of foot and clubfoot, a new technique for correcting clubfoot is proposed in consultation with medical professionals. The technique is based on interdisciplinary bridge between engineer, surgeon, patient and radiologist. Hence this research undergoes inputs and evaluations from different parties, thus integrating knowledge from each. Such a highly interactive feedback loop is crucial in the successful treatment of clubfoot. The treatment performs following corrections.

- Removing varus of heel
- Removing adduction of forefoot and
- Removing equines of forefoot

One important contribution of this thesis work is the realization of clubfoot model of newborn babies. By integrating medical imaging modality and rapid prototyping, a technique to produce solid model and prototypes of clubfoot is proposed and developed. The replica is extremely accurate in dimension and geometrical shape. Due to the successful creation of replicas, a

surgeon is able to prepare, for performing exploratory surgery to restore normal foot. Experience gained from pre-operatives planning and procedural practicing of such non-routine procedures will play critical roles in surgical considerations, and could lead to minimization of risks and potential loss of life. The prototypes obtained from this thesis work, strongly demonstrate the importance of information technology in the development of new products. The developed system architecture characterizes the unique contribution of the presence of a virtual manufacturing environment. In order to create functional prototypes, CAD software is required to initiate the 3D solid modeling process. However, in the medical arena, it is the image data, which plays a crucial role for physicians. Processing this image data for prototyping, represents a new challenge, which is well beyond problem solving in a traditional mechanical engineering domain. Thus as a pioneer effort, an image software system is incorporated in the process of designing the integrated system. The selected MIMICS software packages, developed by Materialise USA, have recorded an excellent performance in the process of creating 3D solid models of clubfoot from CT or MRI image data. The created solid model of clubfoot can be used for many downstream applications such as FEM analysis, prototyping, CNC etc.

By integrating rapid prototyping and vacuum casting, a method to produce silicone prototypes of clubfoot is proposed and developed in this research. A batch of functional prototypes of clubfoot is fabricated by this integration. Due to the versatility of vacuum casting, the integrated approach is unique as it creates opportunities to use materials with properties resembling those of the final products, additionally; the use of an integrated process reduces the high costs, often associated with using rapid prototyping alone.

The finite element case study done in the present work reveals that the analysis in soft-tissue mechanics must be viewed somewhat differently from its application in traditional structural mechanics research. This is basically because of the "normal response" of soft tissue cannot be uniquely defined. There is always a range in the magnitude of pressure or deformation of the tissue that is considered to be normal. This contributes to the difficulty in assessing accuracy in analytical solution procedures. Additionally, the experimental data available on soft tissue are generally limited. Even for those tissues where data is available, there are often more questions than answers in the conditions and limitations of the data. An important contribution of this case study in the immediate future is to enable us to obtain quantitative inputs to facilitate continued experimental and numerical research efforts.

For quantitative dynamic load applying arrangement to clubfoot, a mechanical mechanism, having different types of joints is proposed and developed. The mechanism consists of 6-linkage system having 9 degree of freedom (DOF). The mechanism successfully applies the deforming mechanical load to the clubfoot and helps in restoring the normal foot geometry.

Another major significant contribution of this thesis is the product realization of AFO for clubfoot correction by mechanical design consideration. From the point cloud data of clubfoot, a solid model of the AFO is designed and developed. A conventional manufacturing strategy is proposed which considers point cloud processing, curve modeling, surface modeling and solid modeling. An equivalent ankle joint of ball and socket type in this AFO is designed and developed The designed equivalent ankle joint seems to be an important contribution in this AFO, as it helps in deforming the foot with enough DOF for correction of clubfoot of any severity. In other words, this joint, replaces the ankle joint of foot in AFO. The form, fit and function of created AFO is quite satisfactory. The joints are working well and the patient feels comfort by wearing it.

Our preliminary results of case study, suggest that the reproduction of complex anatomic structures by RP technique are ultimate tools for all the steps in the process of treating patients with complex pathologies: visualization of the problem, communication in a team, diagnosis, orthosis design, planning of the surgery and rehearsal of the surgery. The RP clubfoot models will increase quality of life as the patient improves the surgical result and reduce overall treatment costs. We believe that in the near future the clubfoot prototype and AFO will play the central role in medical research, and will become a crucial part of clinical routine.

6.2 Scope for Future Work

As in any research work, there are certain areas for continuous improvement and expansion. For making AFO manufacturing more user-friendly and flexible, several recommendations for this integrated manufacturing system are listed as follows.

Clinical test

The created AFO is more successful, when clinical test with AFO has to be carried out on more number of patients. At least four numbers of patients should be considered at early stage. The

success rate can be more conveniently judged if the test is performed on at least fifty numbers of patients.

Instrumentation

The present AFO design does not have any instrumentation for display units that can display magnitude of applied load, and displacement / rotation of foot's deformity during normal foot geometry restoration. The design should be modified so that it will display all suitable parameters for doctors to make decision more confidently.

Costing

In the present work, the AFO of ABS material is created from FDM – 1650 rapid prototyping system that makes more initial cost of the AFO. In near future this cost should be reduced by optimizing cost parameters, so that poor patients can also avail the technology. Hence, using different suitable materials like polyethylene, polypropylene, cork or foamed plastic for making the AFO will decrease the cost of AFO.

Flexible manufacturing

The present methodology leads to establishment of a standard computer-aided product development process. An application program (interactive CAD / CAM) interface has to be developed and is taken into CAD / CAM environment. These give a good tool in design, analysis and manufacturing of AFO. While scanning the foot, instead of using MRI, one may use the optical scanning by placing the cameras at certain fixed locations with respect to baby foot. The critical points of the foot can then be obtained directly from the scanned data by making use of appropriate algorithms. This then assists in building the AFO automatically from FDM. This will increase the customization and will be suitable for any parts of the world, like African, Europeans, Asian, American patients etc.

References

[1] A Biomechanics-based model for the animation of human locomotion, *Ankle and foot*, Web Site, http://www.cgg.ru/BIOMECHANICS/BIOMECHANICS.htm

[2] adam.com, *Clubfoot repair*, Web Site, http://www.uscuh.com/CWS/ADAM/Surgery/Clubfootrepair_2.html

[3] Akkas Nuri, *Progress in Biomechanics*, 1979, Sijthoff & noordhoff International Publishers B. V., Alphen aan den Rijn, The Nietherlands.

[4] Alexander, R. McN., Bennet-Clark, A. C., 1977, *Storage of elastic strain energy in muscle and other tissues*, Volume 265, Nature, pp. 114 – 117.

[5] Amas Libermann, 2003, *Objet's Rapid Prototyping Biomodel used to separate Conjoined twins*, International Conference on 3D Modeling-2003, Paris, Proceedings, pp. 1 – 6.

[6] AICTE – ISTE Winter School, *Lecture Note*, December 2003, Volume 1 & 2, Rapid Design & Manufacturing: CAD/CAM/RP/RT/CE/RE, Department of Mechanical Engineering, BHU, Varanasi, India.

[7] American academy of orthopaedic surgeon, *Footwear Guide*, Web Site, http://orthoinfo.aaos.org/fact/thr_report.cfm?Thread_ID=101&topcategory=Foot

[8] Asai, T. and Murakami, H., 2001, *Development and evaluation of a finite element foot model*, Proceeing of 5th Symposium on Footwear Biomechanics, Zuerich / Switzerland, pp. 10 –11.

[9] American academy of orthopaedic surgeon, *Shoe*, Web Site, http://orthoinfo.aaos.org/brochure/thr_report.cfm?thread_id=15&topcategory=shoes

[10] Athearn, J. N., Case, J. S., Roberts, J. M., 1995, *Impression techniques and model modification of a custom – molded Ankle – Foot Orthosis for idiopathic clubfoot*, Journal of Prosthetics and Orthotics (JPO), Volume 7, Number 3, pp 91 – 95.

[11] Baerlocher, P., Boulic, R., 2000, Parametrization and range of motion of the ball-and-socket joint, Web Site, http://vrlab.epfl.ch/Publications/pdf/Baerlocher_Boulic_Deformable_Avatars_01.pdf.

[12] Beaugonin, M., Haug, E., 1996, *A numerical model of the human ankle/foot under impact loading in inversion and eversion*, International conference on high performance computing in automotive design, Engineering and manufacturing cray research silicon graphics Inc. Enghien France, Oct.7-10, 1996, 1 – 13.

[13] Bibb, R. and Sisias, G., 2002, Bone structure models using stereolithography: a technical note, Rapid Prototyping Journal, Volume 8, Number 1, pp. 25 – 29.

[14] Blesser William B., *A System Approach to Biomechanics*, 1969, McGraw-Hill Book Company, USA.

[15] Bradish, C. F., Noor, S., 2000, *The Ilizarov method in the management of relapsed club feet*, The Journal of Bone and Joint Surgery, Volume 82 – B, Number 3, pp 387 – 391.

[16] Camacho, D. L. L., Ledoux, W. R., Rohr, E. S., Sangeorzan, B. J., Ching, R. P., 2002, *A three-dimensional, anatomically detailed foot model: A foundation for a finite element simulation and means of quantifying foot-bone position*, Journal of Rehabilitation Research and Development, Volume 39, Number 3, pp. 401 – 410.

[17] Chakradeo, A. and Kulkarni, 2002, M. A., *Rapid Prototyping – A tool for presurgical planning*, International Conference, MACT Bhopal, India.

[18] Children's Hospital, St. Louis, *Orthopaedic Surgeon Specializes in Nonsurgical Treatment of Clubfoot*, Web Site, http://www.stlouischildrens.org/articles/professional.asp?ID=719

[19] Chivate, Promod N. and Jablokow, Andrei G.,1993, *Solid – model generation from measured point data*, Computer – Aided Design, Volume 25, Number 9, pp.587 – 600.

[20] Chu, T.-M., Feng, R., 1998, Determination of stress distribution in various Ankle-Foot Orthosis: Experimental stress analysis, Volume 10, Number 1, Journal of Prosthetics & Orthotics, pp. 11 – 16.

[21] Dhande, S. G., August 1998, Lecture note, Computer Aided Design & Rapid Prototyping for Footwear and Leather Industries, Department of Mechanical Engineering, CAD-P Laboratory, I.I.T., Kanpur India.

[22] Dhande S. G., 2001, *CAD and Rapid Prototyping*, Lecture Notes, CAD-Project Lab, IIT Kanpur, India.

[23] Dhande, S. G., 2001, *Engineering Graphics using Auto CAD*, TA 101, Lecture Notes, CAD-Project Lab, IIT Kanpur, India.

[24] Downey, D. J., Drennan, J. C. and Garcia, J. F., 1992, *Magnetic resonance image findings in congenital talipes equinovarus*, Journal of Pediatric Orthopaedics, Volume 12, Number 2, pp. 224 – 228.

[25] Downey, D. J., Drennam, J. C., Garcia, J. F., 1992, *Magnetic resonance imaging finding in congenital talipes equinovarus*, Journal of Pediatric Orthopaedics, Volume 12, Number 2 pp 224 – 228.

[26] Faux, I. D., and Pratt, M. J., 1979, *Computational geometry for design and manufacturing*, Ellis, Horwood Limited, West Sussex, England.

[27] Ferreira, J. C., Alves, N. F., Bartolo, P. J. S., Gouveia, D., Janeiro, J., 2003, *Computed tomography for reverse engineering of anatomic models and ergonomic studies*, International Conference on Advance Research in Virtual and Rapid Prototyping, VR@P 2003, pp.683 – 689.

[28] FootCareMD.com, The foot clinic, *A guide to children's shoes*, Web Site, http://www.footcaremd.com/fc_a_childrensshoes.html

[29] Frankel, V. H., Docent, Burstein, A. H., *Orthopaedic Biomechanics*, 1970, Lea & Febiger, Philadelphia, Published in Great Britain.

[30] Fung, Y. C, Perrone, N. and Anliker M., 1972, Biomechanics its foundation and objectives, Prentice-Hall, Inc. Englewood cliffs, New Jersey.

[31] Gallagher, R. H., Simon, B. R., Gross, J. F., 1982, *Finite elements in BIOMECHANICS*, John Wiley & Sons.

[32] Ghosh, A., 1997, *Rapid Prototyping: A brief Introduction*, Affiliated East West Press Private Limited, New Delhi, India.

[33] Gluesing, N., Haw, L-G., Chen, X.-Y., 2000, SIEMENS, *Somatom Esprit Application Guide of Spiral CT.*

[34] HEK GmbH, Germany, *MCP Vacuum casting Techniques: a Guide for new users.*

[35] HEK Germany, 1997, *Operation manual of MCP Vacuum casting Machine*

[36] Henning, E. M., *The Human Foot During Locomotion – Applied Research for Footwear*, Lecture note, October 10, 2002, University of Hong Kong.

[37] Herzenberg, J. E. Carroll, N. C., Christofersen, M. R., Lee, E. H., White, S. and Munroe, R., 1988, *Clubfoot analysis with three – dimensional computer modeling*, Journal of Pediatric Orthopaedics, Volume 8, Number 3, pp 257 – 262.

[38] Huang Yih-ping, Huang Patrick and Chang, D. J. H., 1989, *Scaling of Sport Shoes and Computer Graphics*, Computer in Industry, Volume 13, pp. 23 – 35.

[39] Hobatho, M. C., Estivalezes, L. E., Baunin, C., Cahyzac, J. P., 1998, *Simulation of the 3D motion of the clubfoot bones using helical axes theory*, Journal of Biomechanics, Volume 31, pp. 107 –108.

[40] Indegene, *Feature Article on Congenital Clubfoot*, Dr. Ramani, N., Web Site, http://www.indegene.com/Ort/FeatArt/prn_indOrt_Fet_13-10-2000_1.asp

[41] INSIGHT, version 3.3, 2003, Stratasys Inc.

[42] Jahss, Melvin H., Disorders of the Foot and Ankle – Medical and Surgical management, Volume I, Second Edition, 1991, W. B. Saunders Company, Philadelphia, USA.

[43] Jacobs, Paul F., 1992, *Rapid Prototyping & manufacturing: Fundamentals of Stereolithography*, SME, Doarborn, MI.

[44] Jacob, S., Patil, M. K., 1999, *Three-dimensional foot modeling and analysis of stresses in normal and early stage hansen's disease with muscle paralysis*, Journal of Rehabilitation Research and Development, Web Site, http://www.vard.org/jour/99/36/3/jacob363.htm.

[45] Jain, Manak, L., 1997, *Imaging of tissue structural variation in the sole of human foot by laser back scattering*, M. Tech. Thesis, IIT Madras, India.

[46] Jamieson, R., Holmer, B. and Ashby, A., 1995, *How rapid prototyping can assist in the development of new orthopaedic products – a case study*, Rapid Prototyping Journal, Volume 1, Number 4, pp 38 – 41.

[47] Johns Hopkins Department of Orthopaedic Surgery, *Patient Guide to Clubfoot*, Web Site, http://www.hopkinsmedicine.org/orthopedicsurgery/peds/clubfoot.html

[48] Kai, Chua Chee & Fai, Leong Kah, 1997, *Rapid Prototyping: Principles & Applications in manufacturing*, John Wiley & Sons, N. Y., USA.

[49] Kamegaya, M., Shinohara, Y., Kuniyoshi, K., Moriya, H., 2001, *MRI study of talonavicular alignment in clubfoot*, The Journal of Bone and Joint Surgery, Volume 83, B.Number 5, pp. 726 – 730.

[50] Kang, Y., Engelke, K., Kalender, W. A., 2004, *Interactive 3D editing tools for image segmentation*, Medical Image Analysis, Volume 8, pp. 35 – 46.

[51] Kim, Wangdo and Voloshin, A. S., 1995, *Role of Plantar Fascia in the load bearing capacity of the human foot*, Journal of Biomechanics, Volume 28, Number 9, pp. 1025 – 1033.

[52] Kinesiology Department of Michigan State University, *Biomechanics*, Web Site, http://www.msu.edu/course/kin/830/definition.htm

[53] Kotajarvi, BR. PT., Jouve, JL, Shaughnessy, WJ., Kitaoka, HB., Kaufiman, KR., *Dynamic foot biomechanics of children with clubfoot*, Web Site http://www.indiana.edu/~hperk500/gcma01a/a034kota.pdf., pp. 1 – 2.

[54] Krek, J., Duhovnik, J., 2002, *Model generation and application in medical domain*, International Design Conference – DESIGN 2002, pp. 1 – 6.

[55] Leardini, A., Connor, J. J., Catani, F., Giannini, S., 1999, *Kinematics of the human ankle complex in passive flexion; a single degree of freedom system*, Journal of Biomechanics, Volume 32, pp. 111 – 118.

[56] Leardini, A. J., Connor, J. J., Catani, F., Giannini, S., 1999, *A geometrical model of the human ankle joint*, Journal of Biomechanics, Volume 32, pp 585 – 591.

[57] Lopez, S. M. and Wright, P. K., 2002, The role of rapid prototyping in the product development process: A case study on the ergonomic factors of handheld video games, Rapid Prototyping Journal, Volume 8, Number 2, pp. 116 – 125.

[58] Mantyla, M., 1988, *An introduction to solid modeling*, Computer Science Press, M. D.

[59] Marieb Elaine, R. N., *Human Anatomy and Physiology*, 1998, Fourth Edition, An imprint of Addison Wesley Longman, Inc., Benjamin/Cummings Science Publishing, Menlo Park, California.

[60] Materialise Software, 2001, *MIMICS Reference Guide*, B – 3001, Leuven Belgium. {3.9, chap3}

[61] Mermet, J., 1982, The introduction of CAD in the shoe industry, Computer in Industry, Volume 3, pp. 181 – 186.

[62] Matey, M. A., Meritt, S. M., 1998, Article, *Custom Foot Orthotics: Theory, Indications, and Utilization*, pp. 1 – 5, Web Site, http://www.dcmsonline.org/jax-medicine/1998journals/april1998/Custom%20Foot%20Orthotics.htm

[63] Mortenson, M. E., 1985, *Geometrical Modeling*, John Wiley & Sons, New York.

[64] Moritani, T., Aihara, T., Oguma, E., Shimanuki, Y., Takano, H., Sato, M., 2000, *MR evaluation of talonavicular angle in congenital talipes equinovarus*, Journal of Clinical Imaging, Volume 24, pp. 243 – 247.

[65] Ng, P., Lee, P. S. V. and Goh, J. C. H., 2002, *Prosthetic sockets fabrication using rapid prototyping technology*, Rapid Prototyping Journal, Volume 8, Number 1, pp 53 – 59.

[66] Olabarriaga, S. D., Smeulders, A. W. M., 2001, *Interaction in the segmentation of medical images: A survey, Medical Image Analysis*, Volume 5, pp. 127 – 142.

[67] Orphanoudakis, Stelios C., 1988, *Supercomputing in Medical Imaging,* IEEE Engineering in Medicine and Biology Magazine, December 1988, pp. 16 – 20.

[68] Pediatric Oncology Resource Center, Association of Cancer Online Resources, *MRI-scan: A diagnostic procedure*, Web Site, http://www.acor.org/ped-onc/treatment/MRI/MRI.html.

[69] Pekindil, G., Aktas, S., Saridogan, K., Pekindil, Y., 2000, *Magnetic resonance imaging in follow-up of treated clubfoot during childhood*, European Journal of Radiology, Accepted paper, Web Site, http://www.elsevier.nl/locate/ejrad

[70] Petzold, R., Zeilhofer, H.-F., Kalender, W. A., 1999, *Rapid prototyping technology in medicine – basics and applications*, Computerized Medical Imaging and Graphics, Volume 23, pp. 277 – 284.

[71] Pham, D. T., Gault, R. S., 1998, *A comparison of rapid prototyping technologies*, International Journal of Machine Tool & Manufacturing, Volume 38, pp. 1257 – 1287.

[72] Pirani, S., Zeznik, L. and Hodges, D., 2001, *Magnetic Resonance Imaging Study of the Congenital Clubfoot Treated With the Ponseti Method*, Journal of Pediatric Orthopaedics, Volume 21, Number 6, pp. 719 – 726.

[73] Podiatry Forum, Web Site, http://www.podiatrychannel.com/achillestendinitis, *Achilles Tendinitis*.

[74] Ponseti, Ignacio V., *Congenital Clubfoot - Fundamentals of treatment*, 1996, Oxford University Press, Oxford.

[75] POSNA, The Pediatric Orthopaedic Society of North America, *Gait*, Web Site, http://www.posna.org / resources / coreCurriculum / walkingGait.html

[76] Precision Intricast, Inc., *Defination of Foot Orthosis*, Web Site, http://www.dpmlab.com/html/newsletter01.html

[77] Procter, P. and Paul, J. P., *Ankle joint Biomechanics*, 1982, Journal of Biomechanics, Volume 15, Number 9, pp. 627 – 634.

[78] Progress 2002, *UI's Ponseti developed way to cure clubfoot*, Kathryn Howe, Web Site, http://www.press-citizen.com, Iowa City Press-Citizen.

[79] Sanghera, B. Naique, S., Papaharilaous, Y. and Amis, A., 2001, *Preliminary study of rapid prototype medical models*, Rapid Prototyping Journal, Volume 7, Number 5, pp 275 – 284.

[80] Shigley, J. E., and Uicker, J. J., 1980, *Theory of Machines and Mechanisms*, McGrah-Hill Book Company, New York.

[81] Simons, G. W., 1986, *Seattle Clubfoot Orthosis*, Journal of the Association of Children's Prosthetic-Orthotic Clinic, JACPOC, Volume 21, Number 2, pp. 27.

[82] Simon, George W., 1993, *The Clubfoot – The Present and a view of the future*, Springer – Verlag, New York.

[83] Smith, M. A., 1985, *The technology of Magnetic Resonance Imaging*, Clinical Radiology, Volume 36, pp. 553 – 559.

[84] Snell, Richard S., *Clinical Anatomy for Medical Students*, 1981, Third Edition, Little, Brown and Company Boston/Toronto.

[85] Song, H. R., Carroll, N. C., Neyt, J., Carter, J. M., Han, J., Amato, C. R., 1999, *Clubfoot analysis with three – dimensional foot models*, Journal of Pediatric Orthopaedics, Volume 8, Number 1, pp 5 – 11.

[86] Staats, T. B., Kriechbaum, C. P. M. P., 1989, *Computer aided manufacturing of foot orthosis*, Journal of Prosthetics and Orthotics, Volume 1, Number 3, pp 182 – 186.

[87] Stratasys Inc., 1996, *FDM system Documentation*, 14940 Martin Drive, Eden Prairie, Minneapolis, USA.

[88] Stratasys Inc., 2000, Web Site, http://www.Stratasys.com

[89] Suetens, Paul, 2002, Fundamentals of medical imaging, Cambridge University Press. USA, pp. 66 – 98.

[90] Swann, S., 1996, *Integration of MRI and Stereolithography to build medical models. A case study*. Rapid Prototyping Journal, Volume 2, Number 4, pp 41 – 46.

[91] Takahashi, 1983, Illustrated Computer Tomography, Springer – Verlag Berlin Heidelberg, New York, pp. 4 – 19.

[92] Tay, F. E. H., Manna, M. A. and Liu, L. X., 2002, *CASE STUDY – a CASD / CASM method for prosthetic socket fabrication using the F. D. M. technology*, Rapid Prototyping Journal, Volume 8, Number 4, pp 258 – 262.

[93] Udupa, J. K., Bauer, G. R. and Kneeland, J. B., 1998, *Analysis of in vivo 3-D internal kinematics of the joints of the foot*, IEEE Transactions of biomedical engineering, Volume 45, Number 11, pp. 1387 – 1396.

[94] Uglow, M. G., Clarke, N. M. P., 2000, *Relapse in staged surgery for congenital talipes equinovarus*, The Journal of Bone and Joint Surgery, Volume 82-B, Number 5, pp. 739 – 743.

[95] Urso'D, P. S., Atkinson, R. L., Weidmann, M. J., Redmond, M. J., Hall, B. I., Earwaker, W. J. S., Thompson, R. G., Effeney, D. J., 1999, Biomodelling of skull base tumours, Journal of Clinical Neuroscience, Volume 6, Number 1, pp. 31 – 35.

[96] Virtual Hospital, *Treatment of Congenital Clubfoot*, Web Site, http://www.vh.org/pediatric/provider/orthopaedics/Clubfoot/Fig1.html

[97] Web Site, http://www.eorthopod.com/eorthopodV2/index.php, *A Patient's Guide to Foot anatomy*

[98] Web Site, http://www.jointhealing.com/pages/foot/foot_anatomy.html, *Foot And Ankle Anatomy*

[99] Web Site, http://www.vard.org/mono/gait/soutas.htm, *Motion Analysis and Biomechanics*, Chapter Two.

[100] Woo, Savio L-V., 2002, *Contribution of Biomechanics to clinical practice in Orthopaedics*, ICBME 2002, Singapore.

[101] Wynarsky, G. T. and Greenwald, A. S., 1983, *Mathematical model of the human ankle joint*, Journal of Biomechanics, Volume 16, Number 4, pp 241 – 251.

[102] Xu, E., Loh, H. T. and Wong, Y. S., 1999, *Considerations and selection of optimal orientation for different rapid prototyping systems*, Volume 5, Number 2, pp. 54 – 60.

[103] Yamada, H., *Strenght of biologica materials*, 1970, Williams & Wilkins, Baltimore, Maryland.

[104] Ying, N., Kim, W. and Wang, Y. S., 2002, *Mathematical model of the ankle joint complex*, ICBME Singapore.

[105] Ying, Y., Kim, W., 2002, *Use of dual Euler angles to quantify the three – dimensional joint motion and its application to the ankle joint complex, Journal of Biomechanics*, Volume 35, pp. 1647 – 1657.

[106] Zeid, I., 1991, *CAD / CAM Theory and Practice*, McGraw Hill Publishing, N. Y.

[107] Zeid, I., 1991, *CAD / CAM Theory and Practice*, McGraw Hill Publishing, N. Y. Chapter 6.

[108] Zeid, I., 1991, *CAD / CAM Theory & Practice*, McGraw Hill Publishing, N. Y., pp. 930.

[109] Zhang, G., Tsou, Y.-C. and Rosenberger, A. L., 2000, Reconstruction of the Homunculus skull using a combined scanning and stereolithography process, Rapid Prototyping Journal, Volume 6, Number 4, pp. 267 – 275.

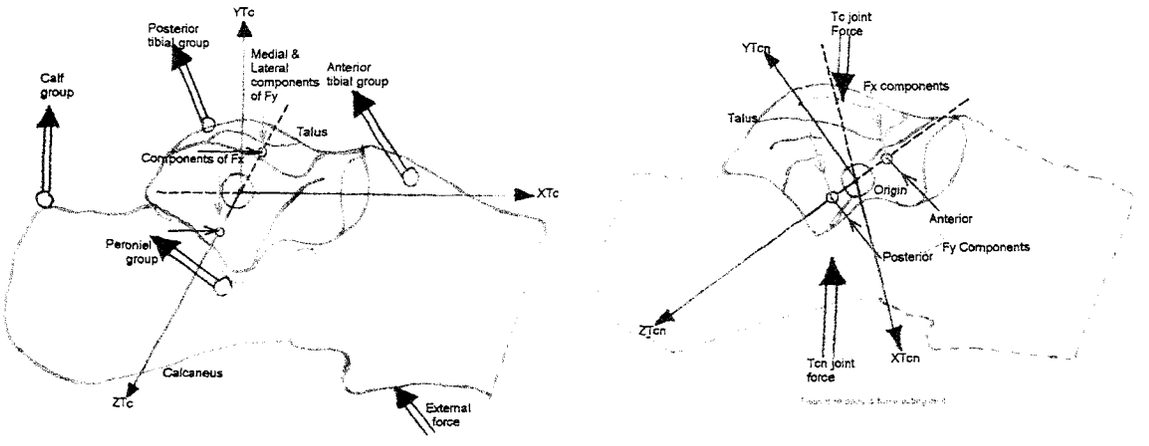

(a) (b)

Figure 2.5: Forces acting on free body of (a) talus and calcaneus of foot (b) talus of foot

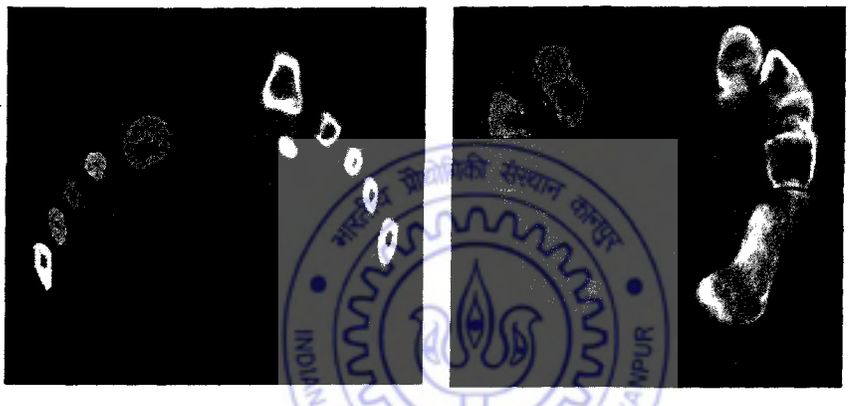

(a) (b)

Figure 3.13: Region grew segmented image of two slices (a) section at metatarsal region (b) section at tarsal region

Figure 3.14: Skeletal of an adult normal foot

Figure 3.15: Skeletal of unilateral clubfoot of Patient VII

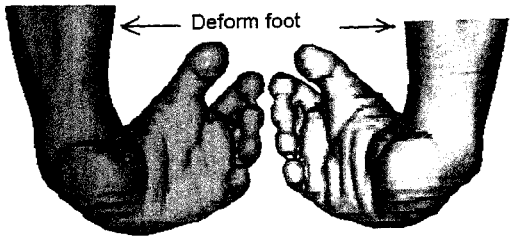

Figure 3.16: Bilateral clubfoot model of Patient I

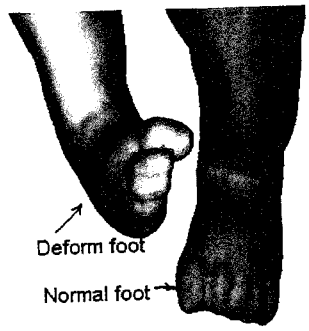

Figure 3.17: Unilateral clubfoot model of Patient II

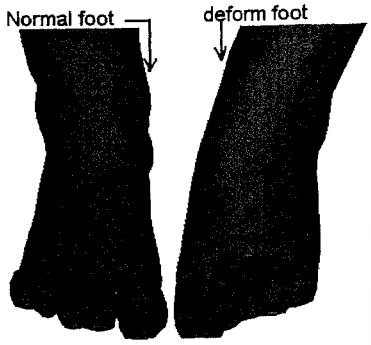

Figure 3.18: Unilateral clubfoot model of Patient III

Figure 3.19: Unilateral clubfoot model of Patient IV

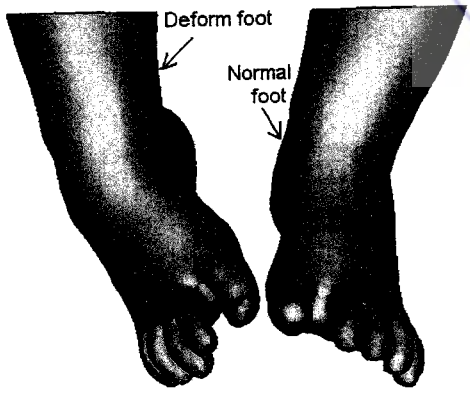

Figure 3.20: Unilateral clubfoot model of Patient V

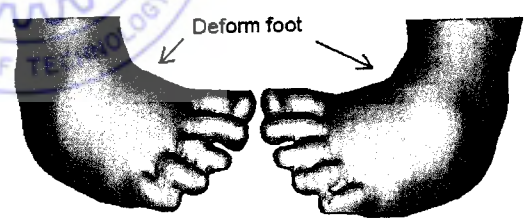

Figure 3.21: Bilateral clubfoot model of Patient VI

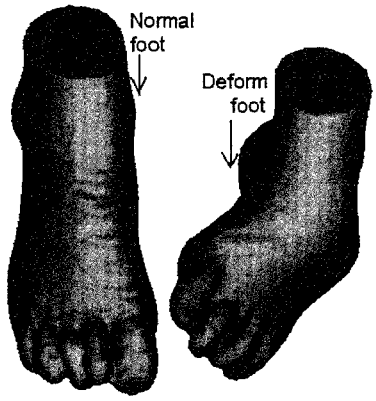

Figure 3.22: Unilateral clubfoot model of Patient VII

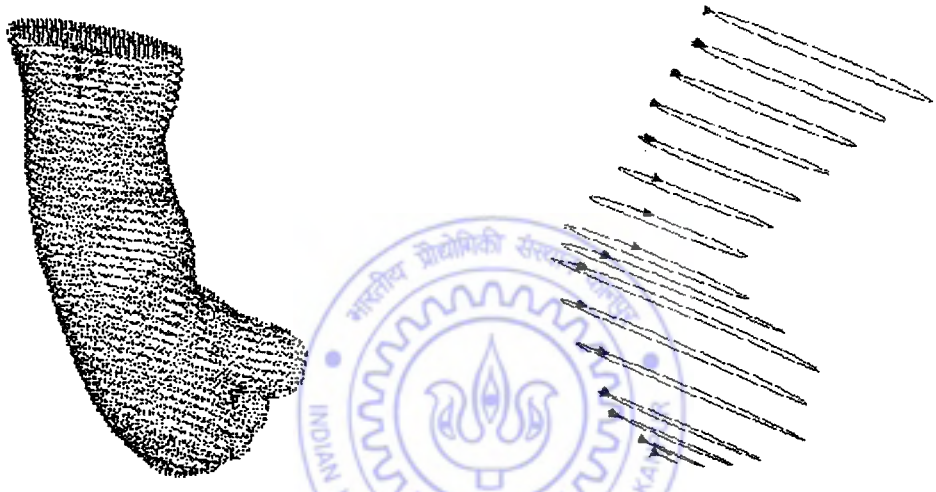

(a) (b)

Figure 3.25: Curve modeling (a) point cloud data of clubfoot (b) curve model of clubfoot

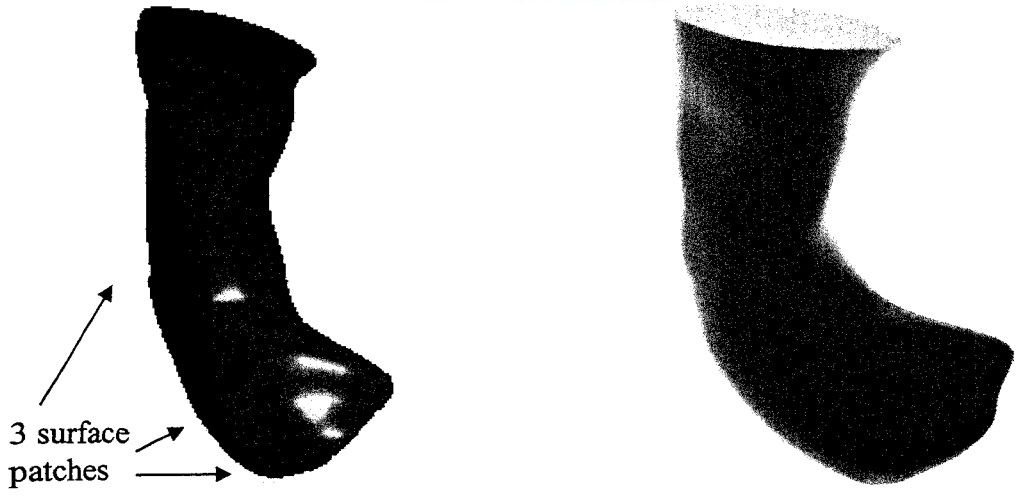

(a) (b)

Figure 3.26: Solid modeling (a) surface model of clubfoot (b) solid model of clubfoot

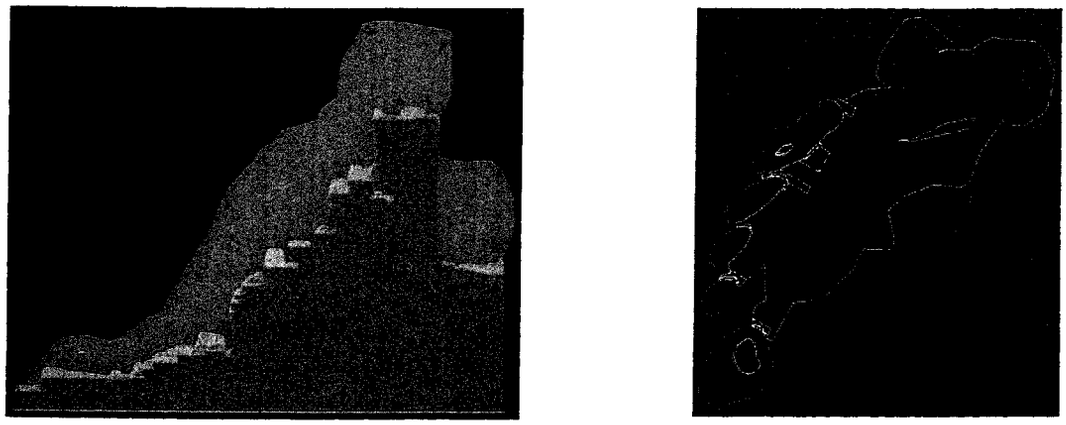

(a) (b)

Figure 3.30: Support generation for foot RP modeling (a) generated support (b) one slice at typical foot-support section

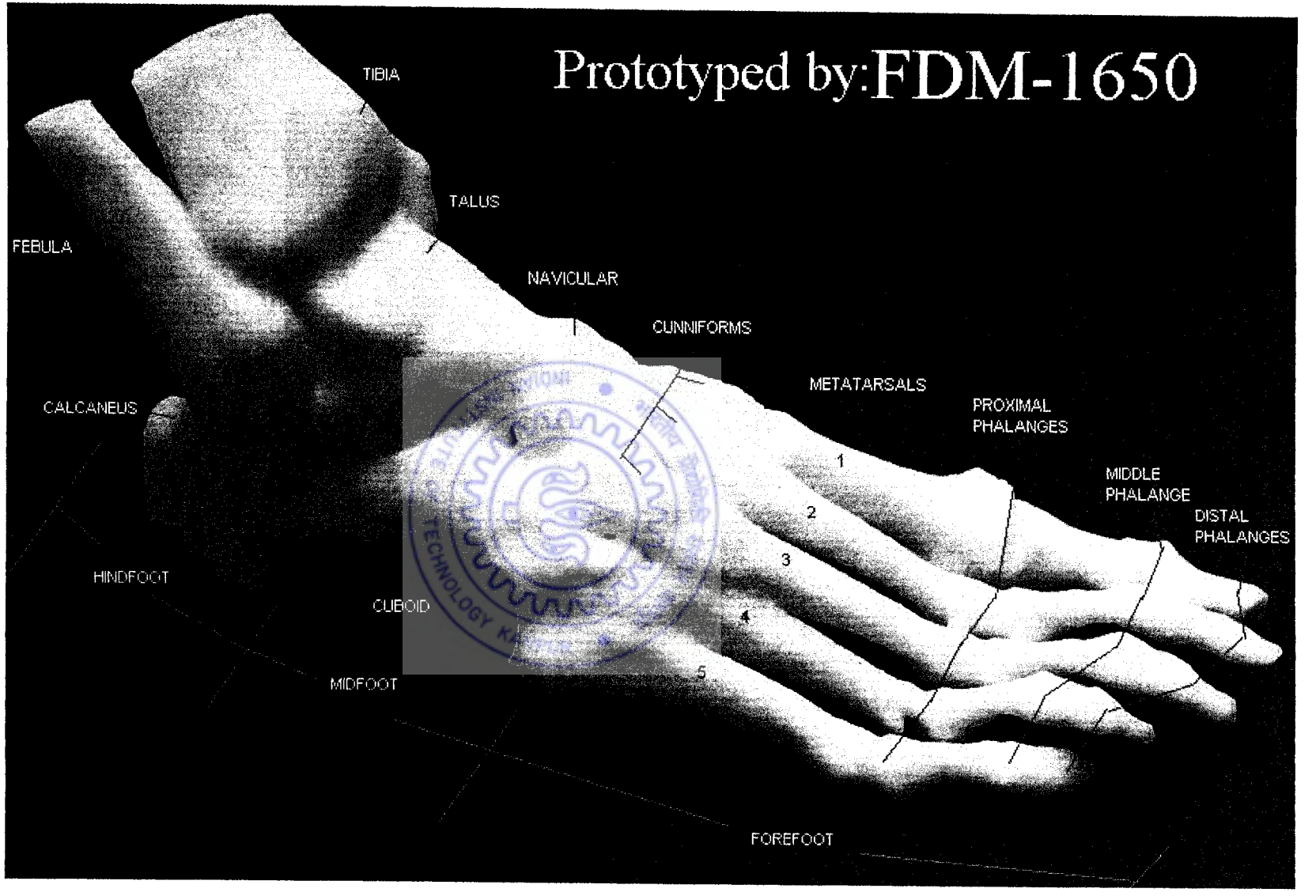

Figure 3.31: RP model of skeletal of foot

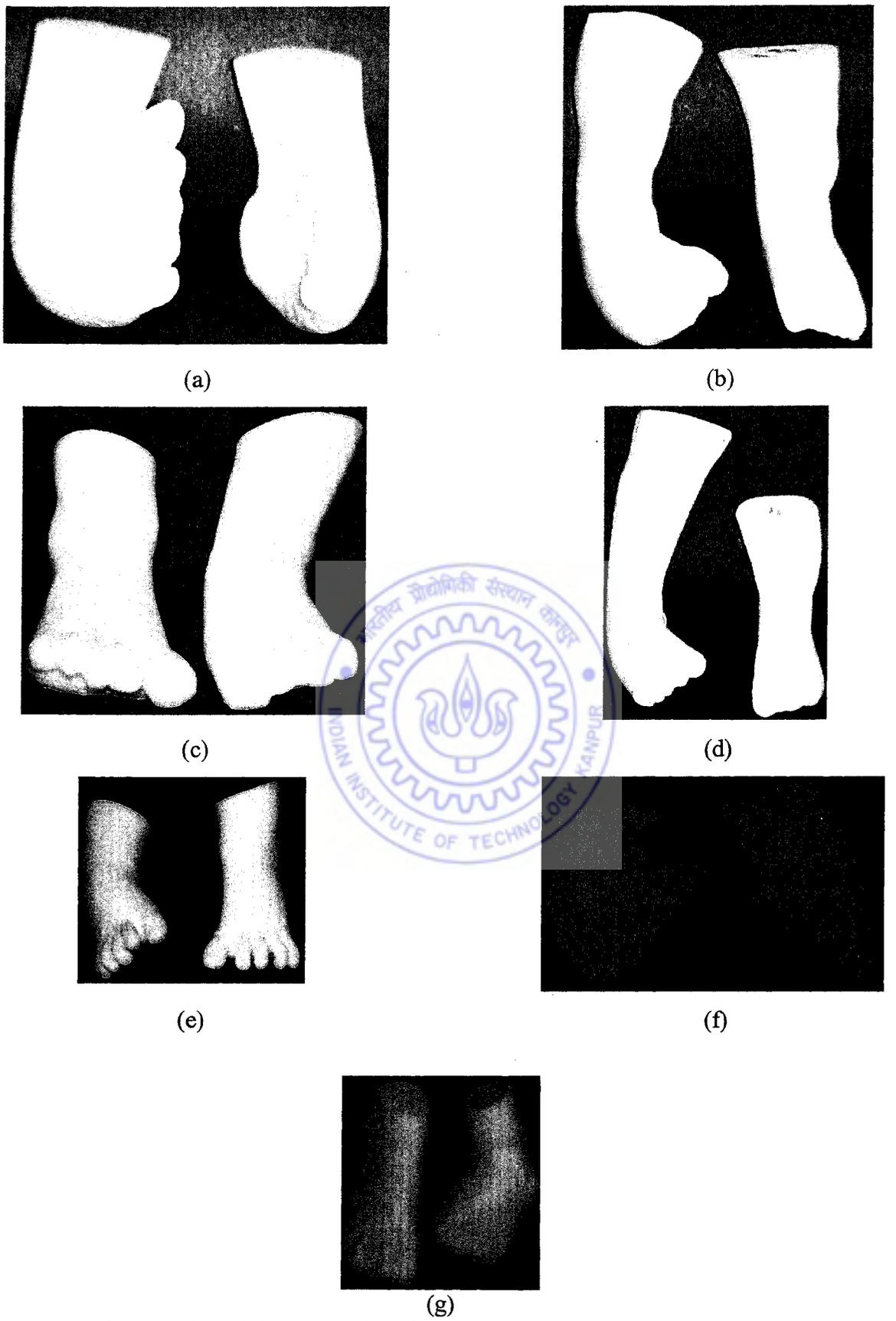

(a) (b) (c) (d) (e) (f) (g)

Figure 3.32: RP model of clubfoot of (a) Patient I (b) Patient II (c) Patient III (d) Patient IV (e) Patient V (f) Patient VI and (g) Patient VII

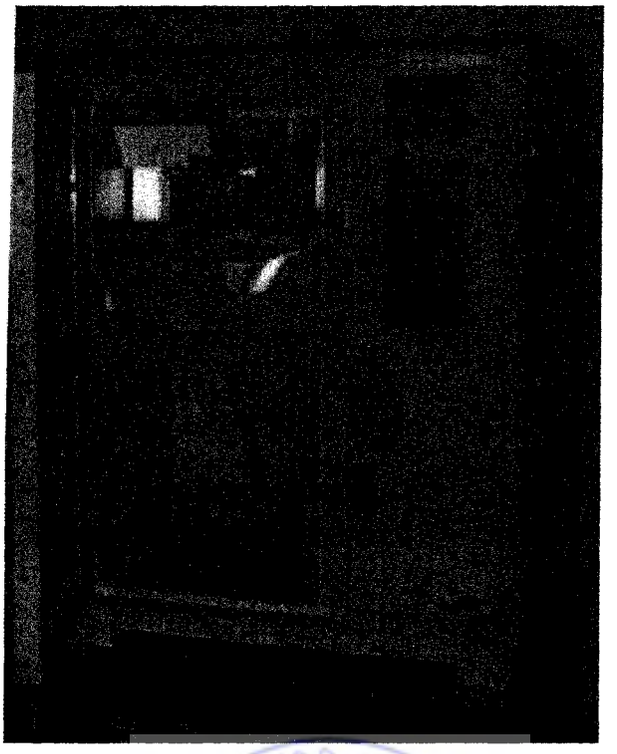

Figure 3.34: MCP vacuum casting machine

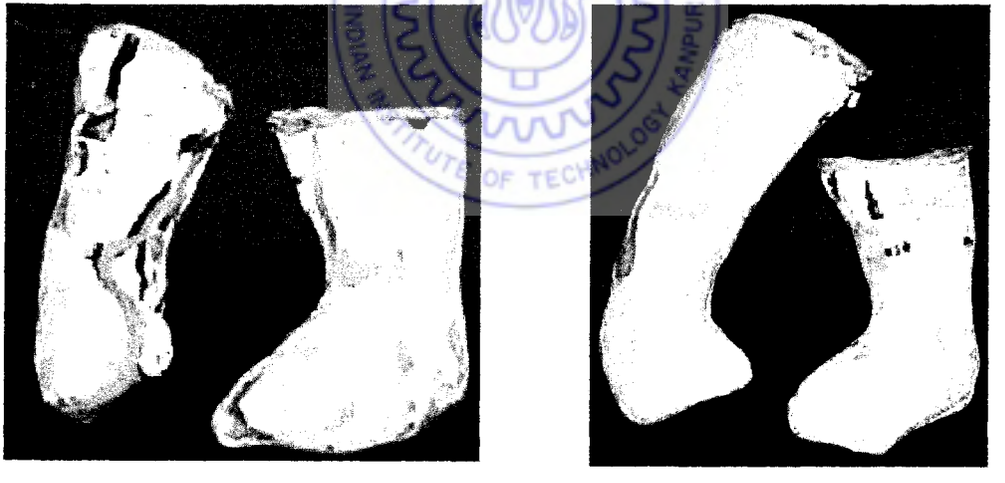

(a) (b)

Figure 3.35: POP mold of feet (a) patient II feet (b) patient IV feet

Figure 3.36: Process of Silicone casting

Figure 3.37: Silicone clubfoot model of patient VII

(a) (b)

Figure 3.38: Instrumented silicone foot manufacturing (a) mold with strain gauge fixing arrangement (b) silicone foot with strain gauge

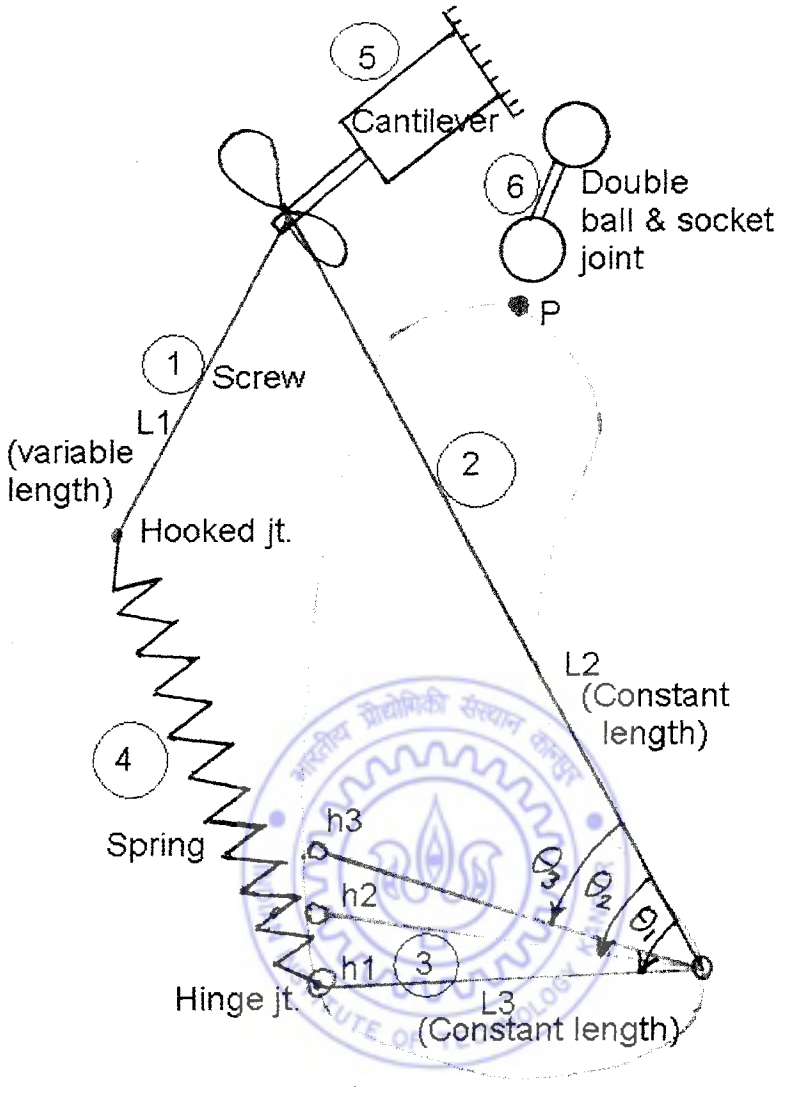

(a)

Figure 4.1: Proposed mechanism of AFO (a) mechanical elements

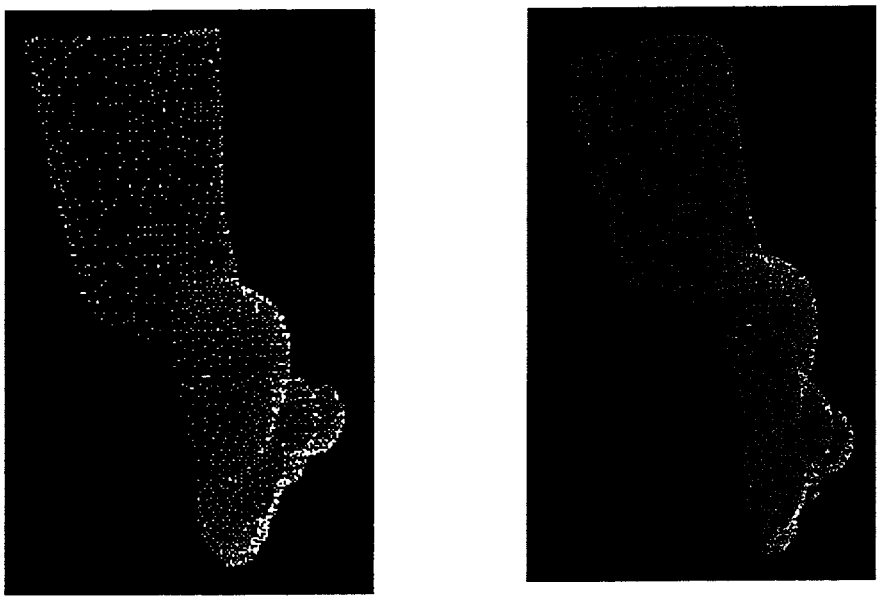

(a) (b)

Figure 4.9: Segmentation of point cloud (a) single segment (b) three segments

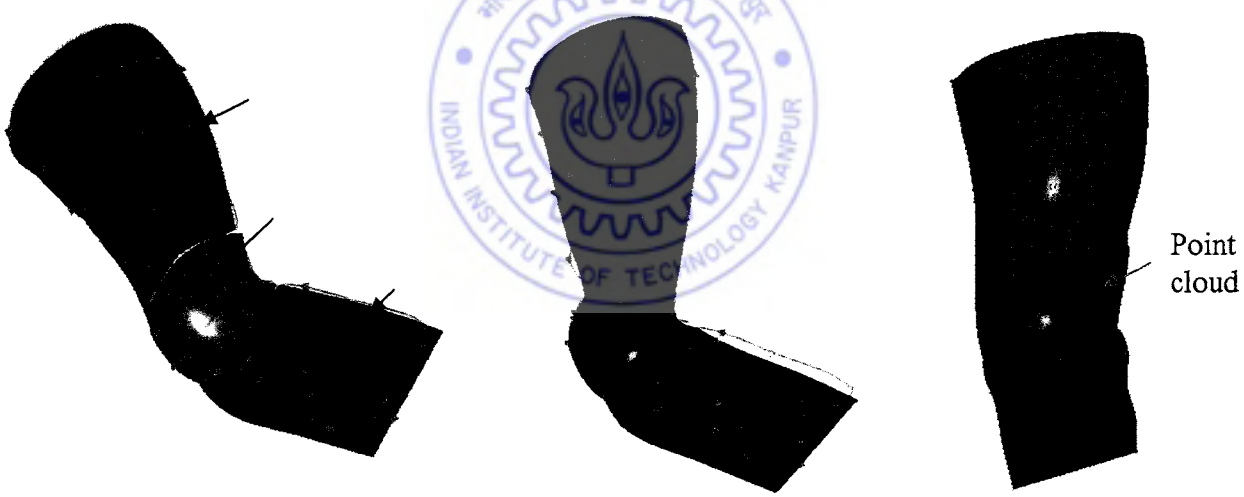

(a) (b) (c)

Figure 4.12: Surface models of AFO (a) three patches (b) matched single patch (c) form & fit check of AFO

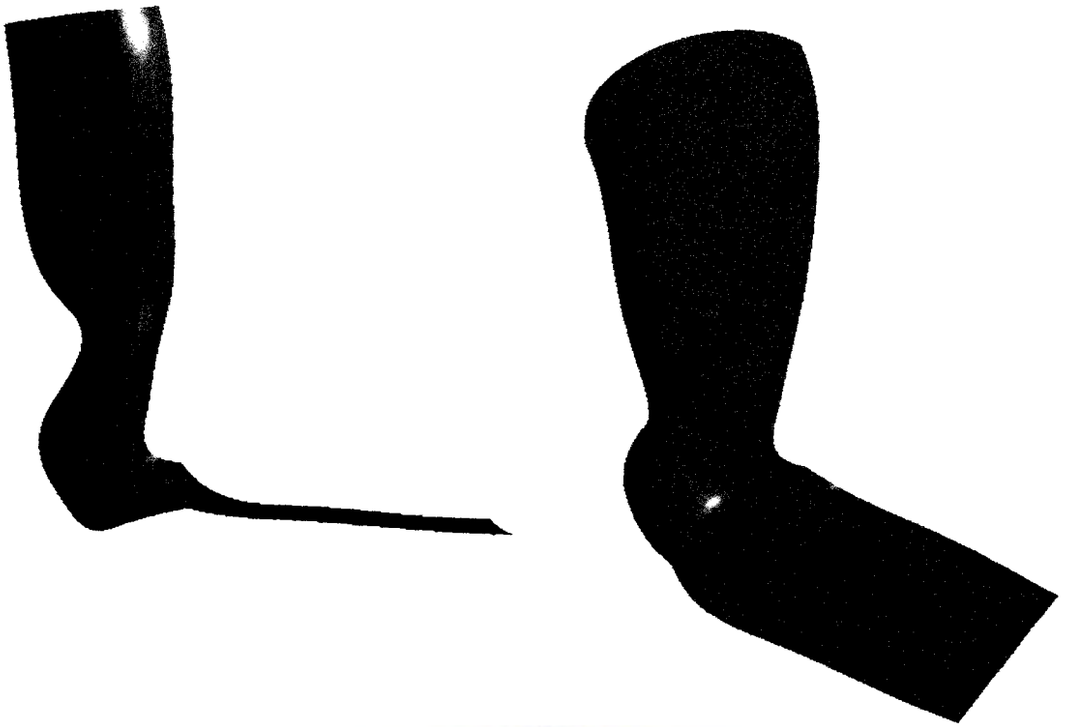

(a) (b)

Figure 4.13: Final AFO surface model (a) side view (b) front view

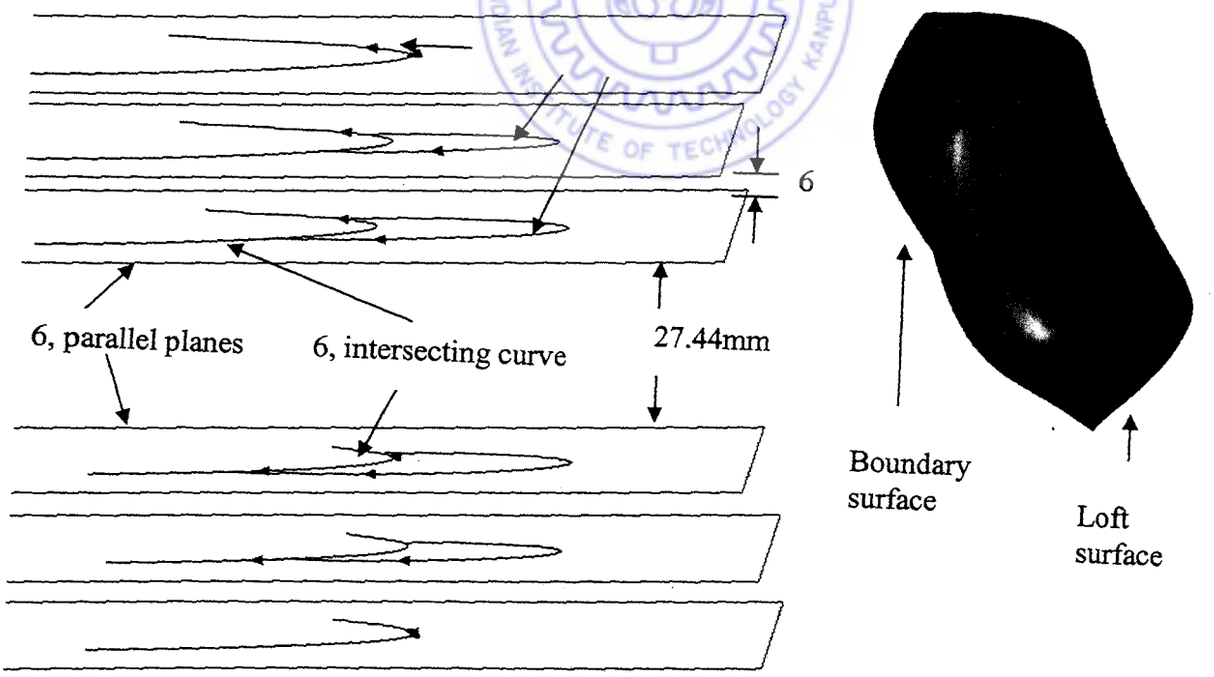

(a) (b)

Figure 4.14: Designing of rib (a) curve modeling (b) lofted surface

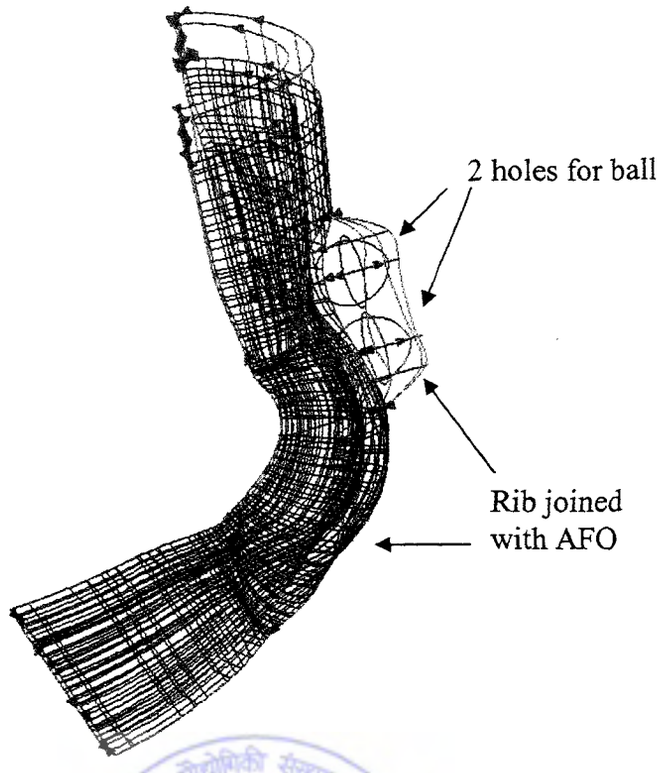

Figure 4.15: Ball & socket joint arrangement in AFO wire frame model

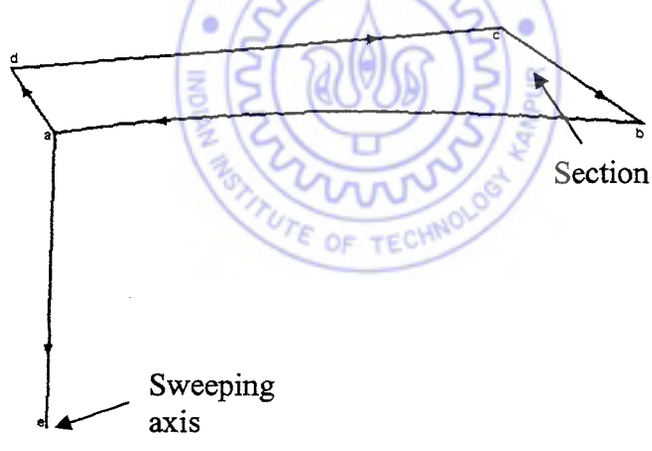

Figure 4.16: Sweep section along an axis

Figure 4.17: Simple one piece AFO

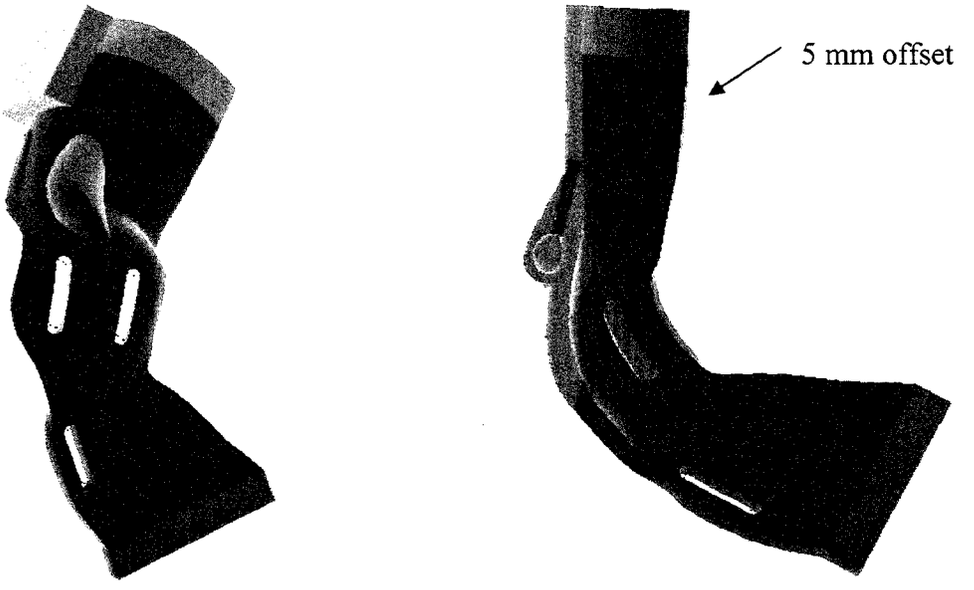

(a) (b)

Figure 4.18: AFO having integrated arrangement for fixing single spherical ball & socket joint (a) back view (b) sectional side view

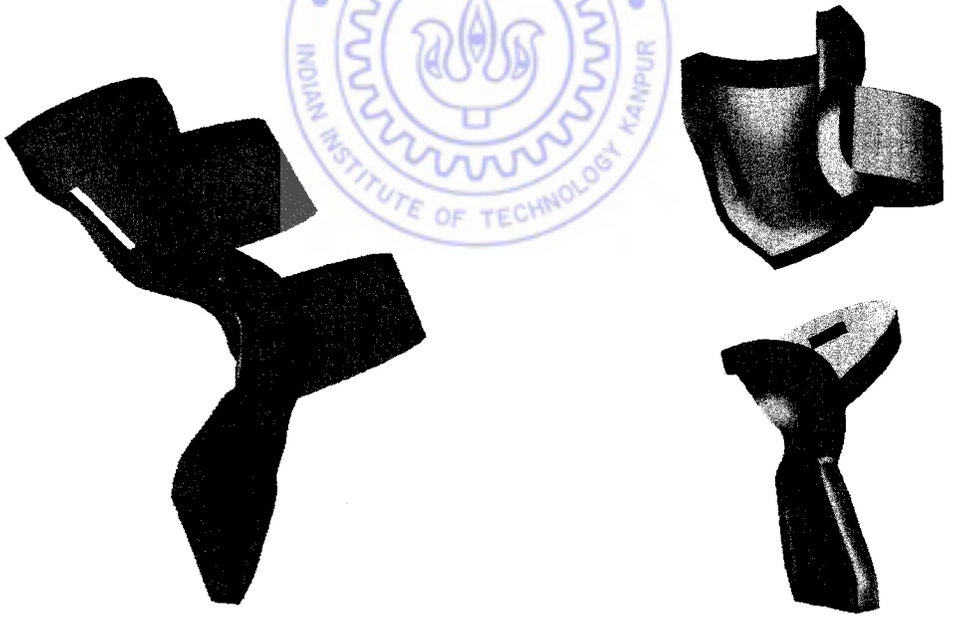

(a) (b)

Figure 4.19: AFO having arrangement for externally fixing single hemispherical ball & socket joint (a) one piece (b) two piece

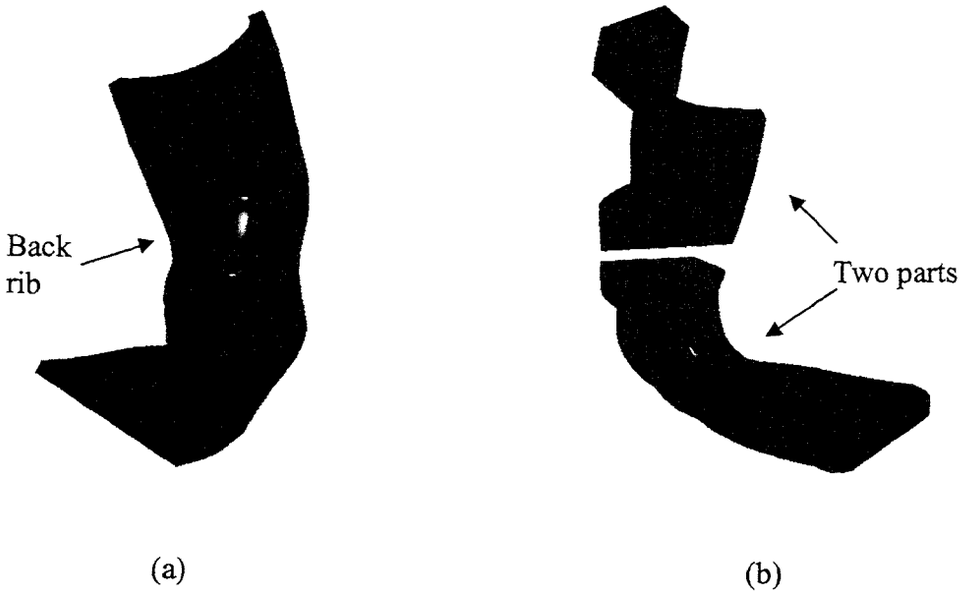

Figure 4.20: AFO with integrated arrangement for fixing double ball & socket joint (a) back view of designed rib (b) two piece front view

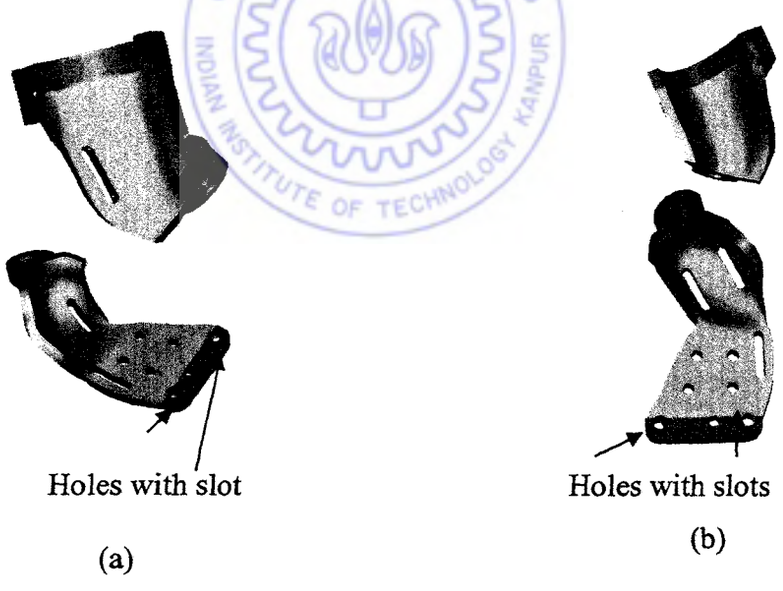

Figure 4.21: Two piece AFO having integrated arrangement for externally fixing double spherical ball & socket joint (a) AFO for right clubfoot (b) AFO for left clubfoot

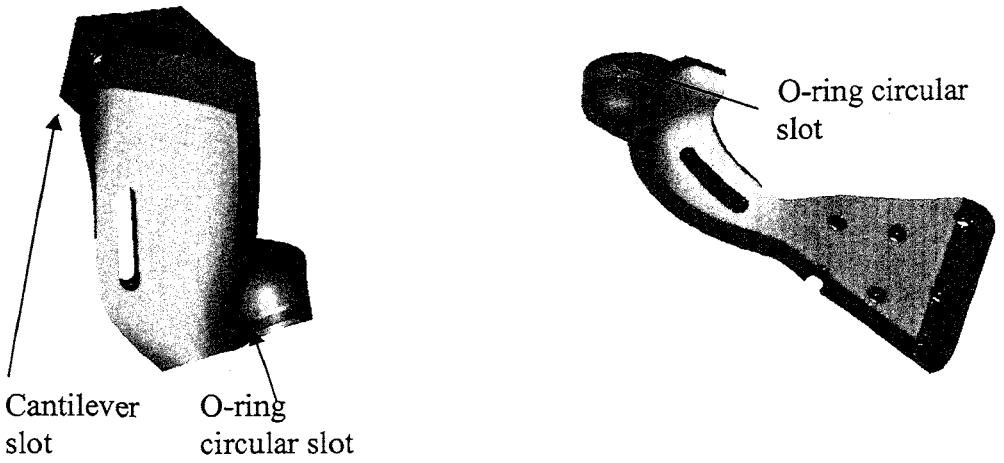

Figure 4.22: Sectional view of above right clubfoot AFO showing arrangement for fixing mechanical elements (a) upper part (b) lower part

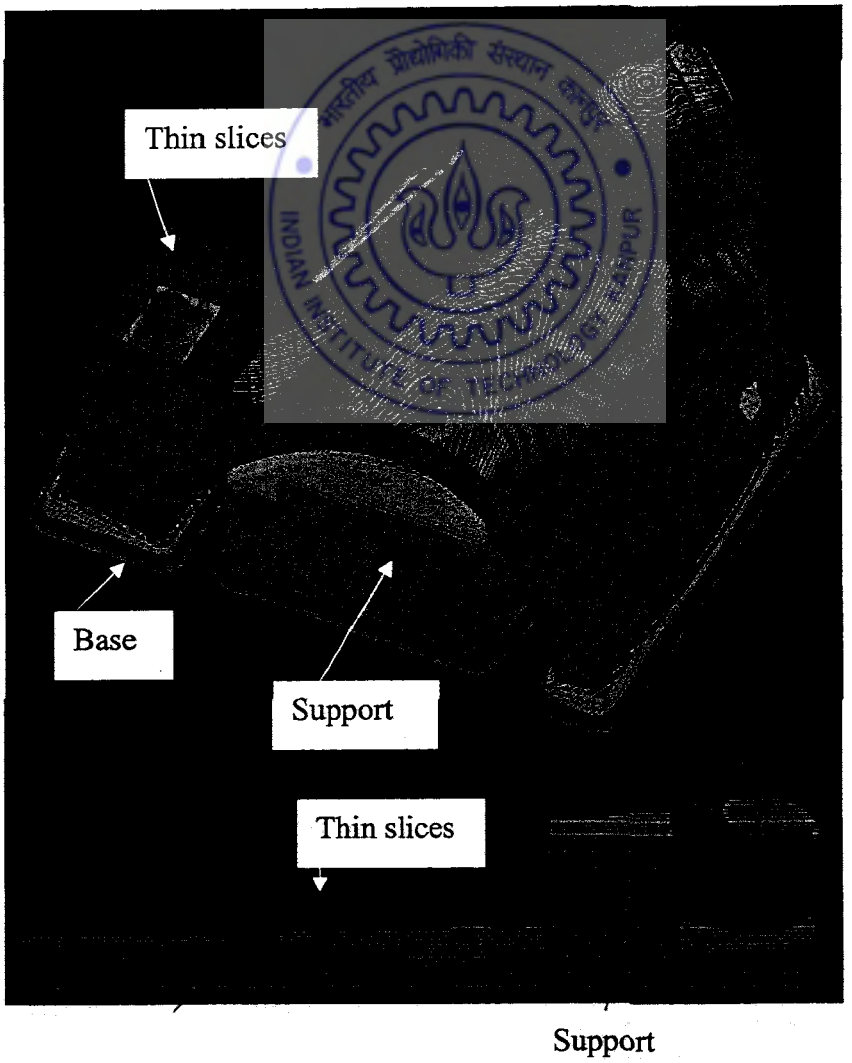

Figure 4.24: SSL file showing slices, base and support of AFO

(a) (b) (c)

Figure 4.27: Prototype of developed AFO (a) front view (b) back view (c) left side view

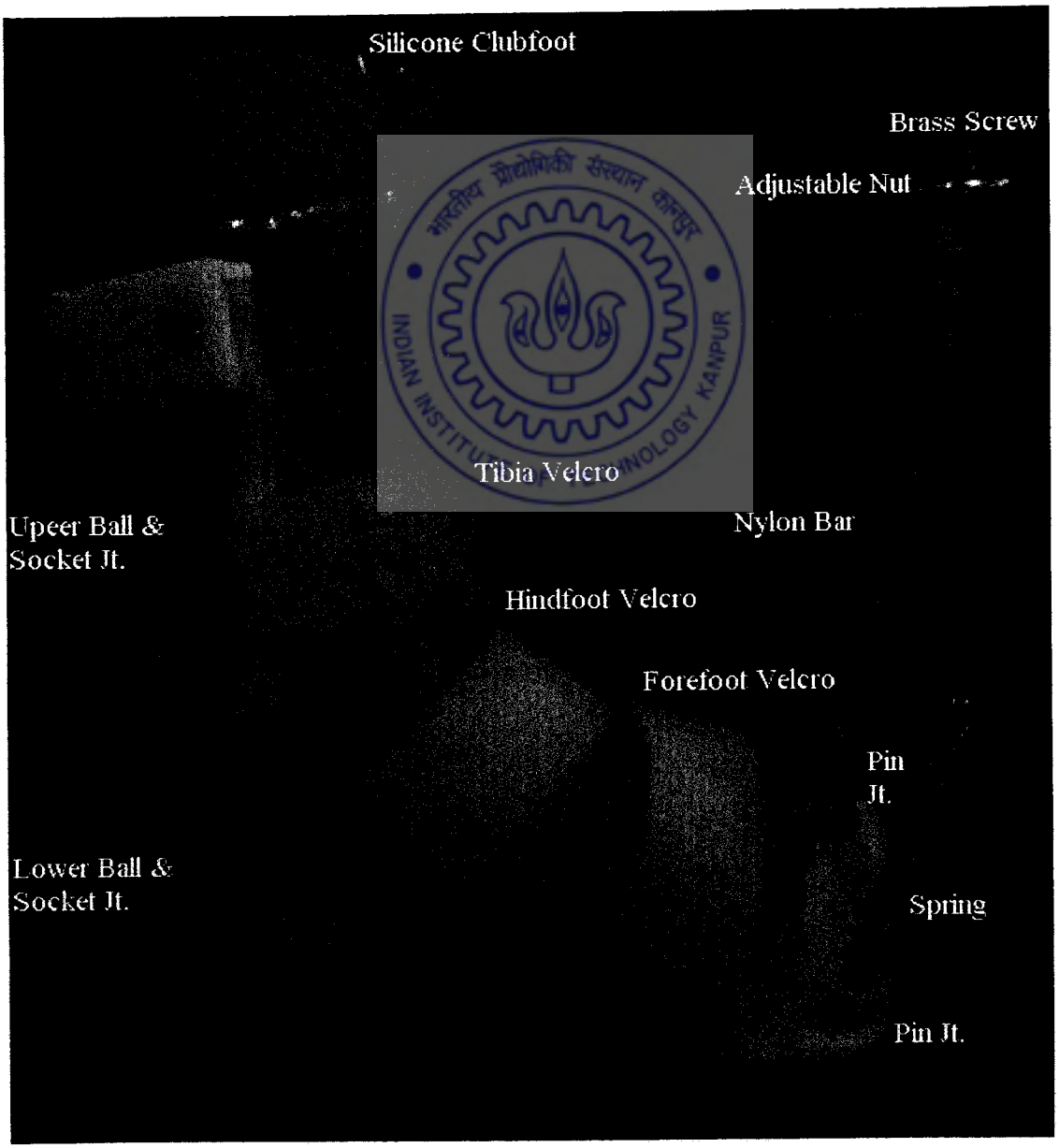

Figure 4.28: Form, fit and function test of prototype of AFO

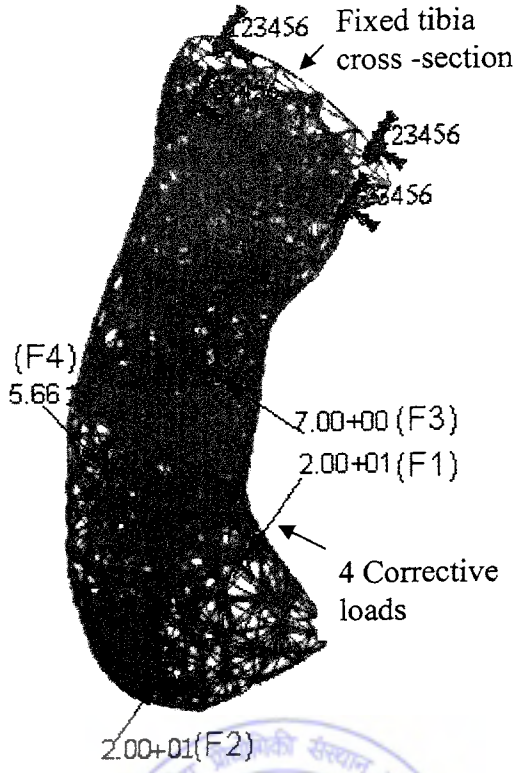

Figure 5.5: Boundary conditions with corrective loads on clubfoot finite element model

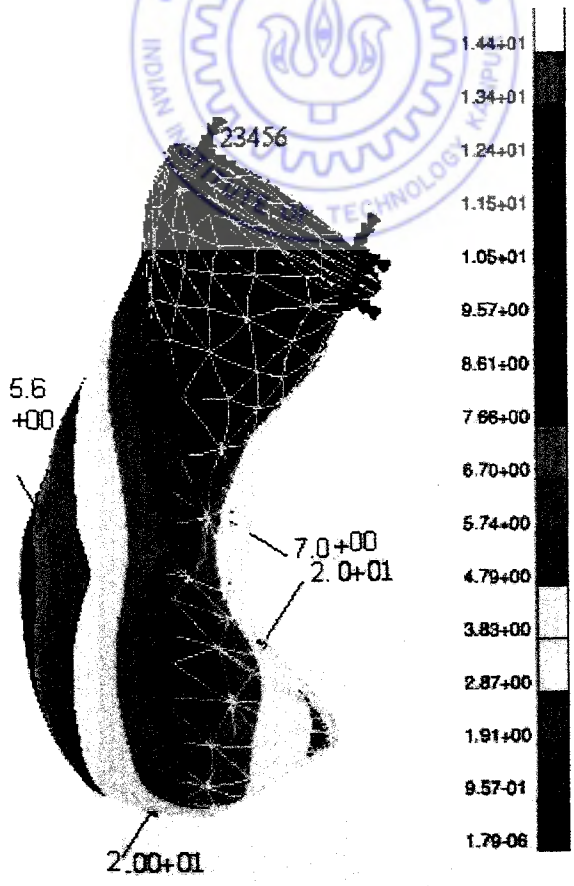

Figure 5.6: Deformation of clubfoot model

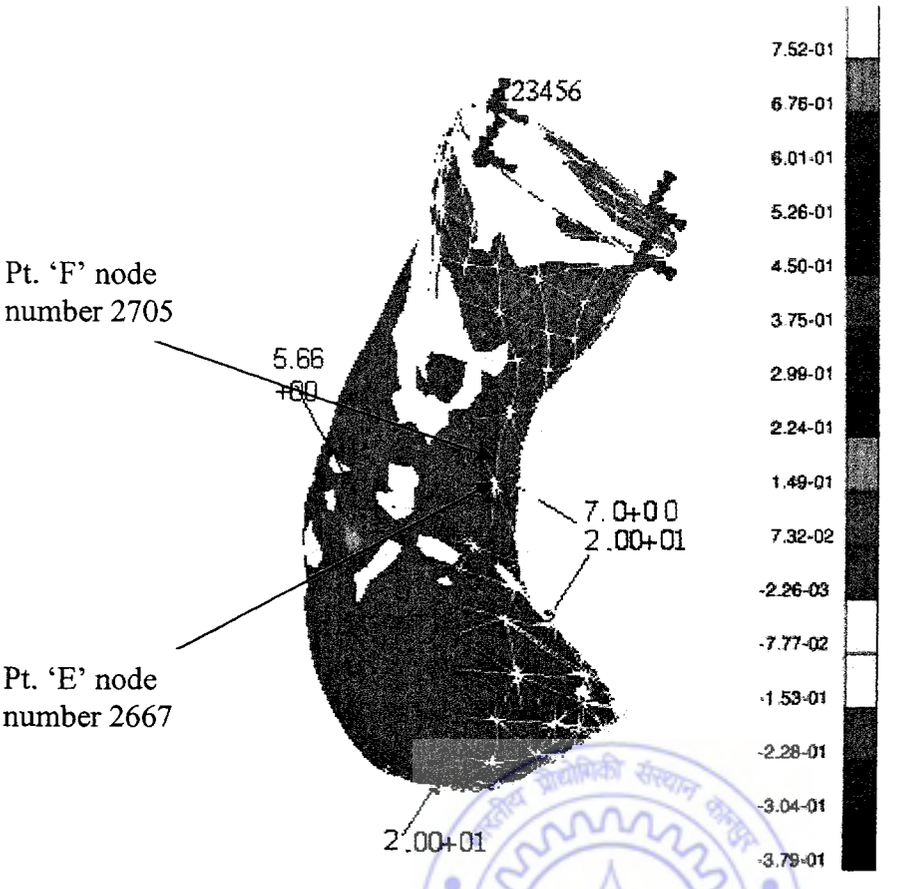

Figure 5.7: Maximum principal stress & displacement of clubfoot model

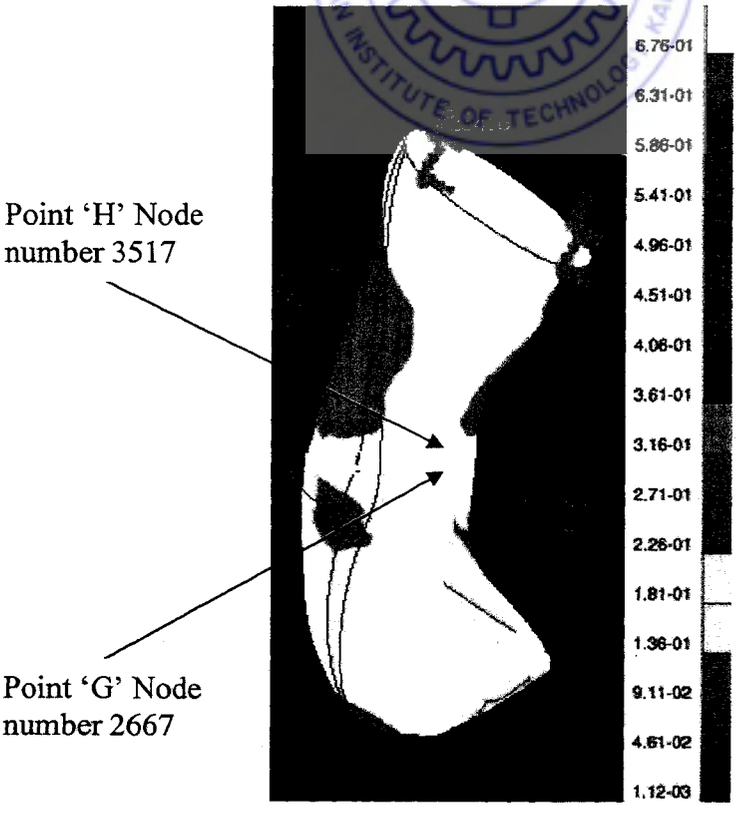

Figure 5.8: von Mises stress distributions in clubfoot model

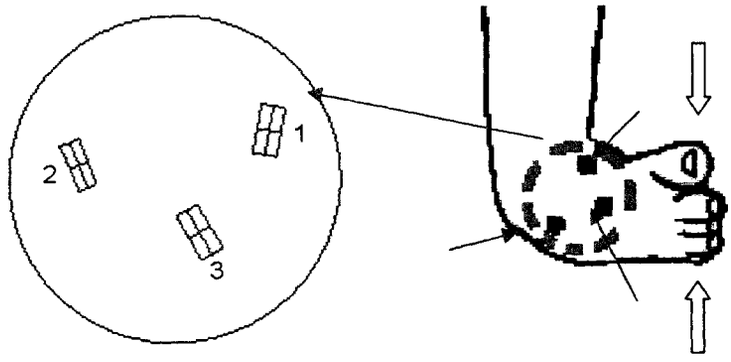

(a) (b)

Figure 5.10: Strain gauge fixing in clubfoot model (a) arrangement of strain gauge (b) placement of strain gauge

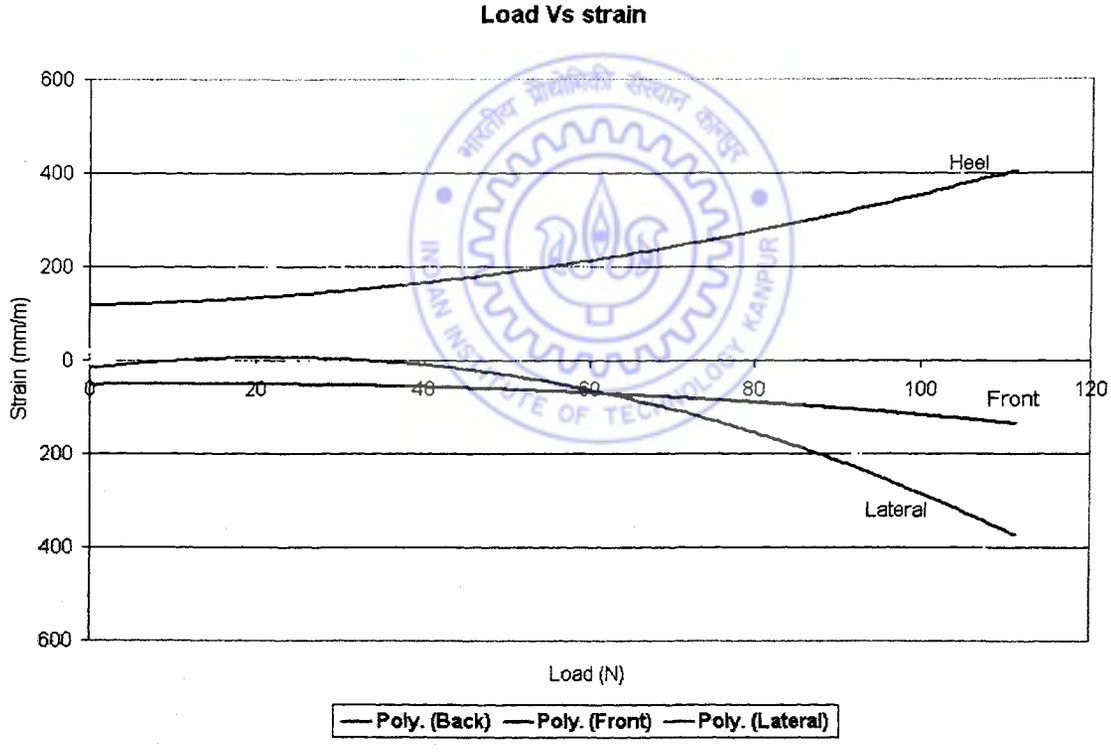

Figure 5.13: Graph showing load vs. strain for a silicone clubfoot model

(a) (b)

Figure 5.15: Ankle skeletal of foot of Patient V (a) normal foot (b) clubfoot

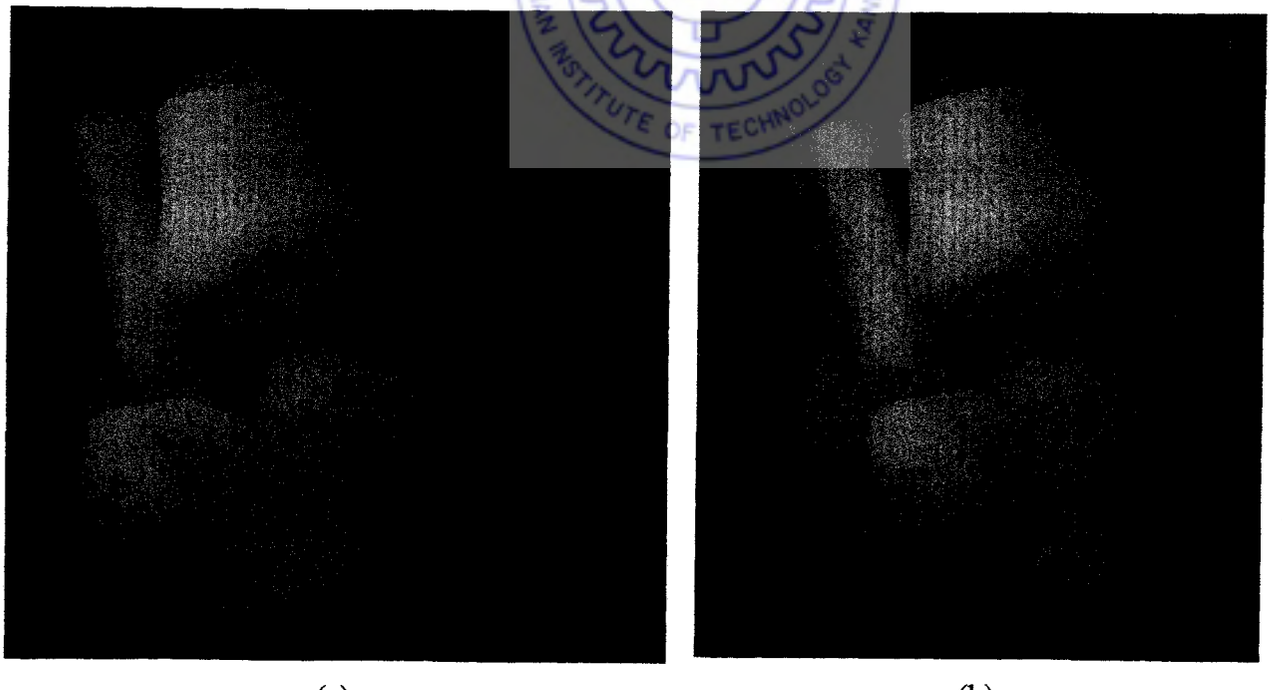

(a) (b)

Figure 5. 16: Ankle skeletal of foot of Patient VII (a) normal foot (b) clubfoot

Figure 5.17: Corrected foot of a subject in dancing position